DAA/Langley

158p.

ELECTROMAGNETIC BACKSCATTERING BY CORNER REFLECTORS

IN-31460

Semiannual Report

Constantine A. Balanis and Timothy Griesser

August 1, 1985-January 31, 1986

Department of Electrical and Computer Engineering
Arizona State University
Tempe, AZ 85287

Grant No. NAG-1-562
National Aeronautics and Space Administration
Langley Research Center
Hampton, VA 23665

ABSTRACT

The Geometrical Theory of Diffraction (GTD), which supplements Geometrical Optics (GO), and the Physical Theory of Diffraction (PTD), which supplements Physical Optics (PO), are used to predict the backscatter cross sections of dihedral corner reflectors which have right, obtuse or acute included angles. These theories allow individual backscattering mechanisms of the dihedral corner reflectors to be identified and provide good agreement with experimental results in the azimuthal plane. The advantages and disadvantages of the geometrical and physical theories are discussed in terms of their accuracy, usefulness and complexity. Numerous comparisons of analytical results with experimental data are presented. While physical optics alone is more accurate and more useful than geometrical optics alone, the combination of geometrical optics and geometrical diffraction seems to outperform physical optics and physical diffraction when compared with experimental data, especially for acute angle dihedral corner reflectors.

Some topics which deserve special attention include the continuity of geometrical diffraction fields from flat surfaces bounded by parallel edges, the need to avoid far field approximations in GTD analyses, and two alternative methods for determining double reflected physical optics fields for which tradeoffs in accuracy and complexity are encountered.

TABLE OF CONTENTS

LIST OF FIGURES

CHAPTER 1

INTRODUCTION

In the interest of promoting the advancement of radar technology, engineers in the past years have endeavored to establish methods to determine the backscatter characteristics of representative radar targets. Evaluating the radar echo strength of a particular target, as a function of the orientation of the target relative to the radar, has become a topic of major concern because the relative strength of the echo returned from a target can be related to the maximum distance at which that target can be detected or observed by a given radar system.

The radar cross section of a target, alternatively referred to as the backscatter cross section whenever the directions of incidence and observation are the same, is a quantitative measure of the target's scattering properties, and relates the given target to a measure of an equivalent area which would reflect the same power density in a specific direction given the same incident power density. The radar cross section is a useful quantity because it identifies scattering properties of an object independent of the radar system which is to observe that object and independent of the distance of observation provided the distance is large in comparison to the target or the radar antenna.

When considering the scattering properties of a conducting object, the two dominant mechanisms which come into account are reflections from surfaces and diffraction from edges. Other mechanisms which may arise in certain target configurations include corner diffractions and creeping waves. Understanding these mechanisms has become of great importance in recent years for the development of

methods to reduce radar backscatter from ships, planes, missiles and spacecraft. The design of these "low-observable" vehicles, which are fabricated so as to reduce the possibility of radar detection, is often a complex task. However, in the future, the construction of nearly every major new military vehicle is expected to incorporate some form of radar cross section shaping.

Two of the most popular methods for determining approximate scattered fields due to surface reflection and edge diffraction are the combination of Geometrical Optics (GO) and the Geometrical Theory of Diffraction (GTD) [1]-[10], and the combination of Physical Optics (PO) and the Physical Theory of Diffraction (PTD) [11]-[16]. These theories have been used extensively, with much success, in many electromagnetic scattering problems [17]-[24]. The theories are especially useful because they provide good agreement with experimental results, they provide insight into specific scattering mechanisms, they involve simple functions available on most computer systems, and their solutions are relatively simple to construct in comparison to exact methods. Numerous comparisons of the GTD and PTD methods have been written by various authors. Some of the foremost of these comparisons are found in [24]-[29].

Geometrical optics is a simple approximate method for determining fields reflected from a surface, given the incident fields. The theory relies on straight ray travel of electromagnetic waves and simply requires that each ray satisfy Snell's Law of Reflection at each reflection point; that is, each ray must be geometrically constructed such that the angle of incidence equals the angle of reflection. As

such the geometrical optics field becomes a function of the curvature of the incident wavefront and the curvature of the reflecting surface [6], [7]. The Geometrical Theory of Diffraction (GTD), originated by Keller [1], and refined by Kouyoumjian and Pathak [2], [3] supplements geometrical optics by adding contributions due to edge diffraction at perfectly conducting edges. The Geometrical Theory of Diffraction introduces diffraction coefficients which are functions of the angles of incidence and observation, the edge geometry, and the incident wavefront curvature. The purpose of these diffracted fields is to remove discontinuities in the reflected fields which are inherent in a geometrical ray approach. In regions where the geometrical optics field is zero, the diffraction theory often predicts nonzero fields.

Physical optics is an alternate technique for determining fields reflected from an illuminated surface. The theory begins by approximating the current density on any perfectly conducting surface in terms of the incident field, and from this current density the reflected fields can be found using conventional radiation integrals of electromagnetics. Unlike geometrical optics, the theory does not require the angle of incidence to equal the angle of reflection; hence, fields are predicted in many directions in which no geometrical optics field exists. The Physical Theory of Diffraction, originated by Ufimtsev [11], supplements physical optics to provide corrections to the scattered field due to diffraction at edges of conducting surfaces. Ufimtsev suggested the existence of nonuniform ("fringe") edge currents in addition to the uniform physical optics surface currents. The Physical Theory of Diffraction bears some resemblance to the Geometrical

Theory of Diffraction in the method of application. The theory differs in that the physical diffracted fields are continuous everywhere since the physical optics field is generally continuous everywhere. In contrast, the geometrical diffracted fields are discontinuous to compensate for discontinuities in the geometrical optics field.

When exact solutions are required, field configurations can be found through electromagnetic boundary value methods. These solutions, while considered exact, are often difficult to obtain for all but the simplest geometries. They are often in the form of infinite summations of complex functions which do not shed insight into specific scattering mechanisms, and they may require multiple solutions of simultaneous higher order transcendental equations. Another analytical technique, known as the Moment Method [25], has found usefulness in a variety of problems [8] and arises from a numerical solution of electromagnetic boundary value problems. As a numerical technique, it can be as accurate as desired by taking smaller increments in numerical integration algorithms. However, the results do not lend themselves well to interpretation of the scattering mechanisms. Computationally, the Moment Method is efficient for objects which are not too large in comparison to the field wavelength.

In this report, the methods of the geometrical and physical theories of reflection and diffraction are reviewed, and each is applied to the dihedral corner reflector. The discussion of the theories distinguishes the differences in their application and usefulness, and through the dihedral corner reflector analysis, for which limited experimental results are available, the accuracy of the theories can be

evaluated. The dihedral corner reflector was chosen because it exhibits many of the scattering mechanisms of more complex bodies; namely strong specular reflections from both singly and doubly reflected fields, and significant second and third order diffracted fields. The dihedral corner is analyzed when the interior angle is right, acute, and obtuse to exemplify the versatility of the theories. All the techniques mastered in the study of a dihedral corner reflector are applicable to many other more complex structures.

Basic design equations for the dihedral corner reflector, as well as other corner reflectors, are presented in [30]-[32] along with experimental radar cross section patterns. Knott [18] studied the backscattered fields of the dihedral corner reflector using the physical optics theory over the first 70° on each side of the forward direction. Michaeli [24] added physical diffraction in a study of the 90° dihedral corner reflector near grazing incidence. Yu and Huang [20] analyzed the dihedral corner reflector using geometrical optics and geometrical diffraction in the forward region over 180°.

In this report, the geometrical and physical theories are compared when applied to the dihedral corner reflector over the full 360° of the azimuthal plane. The geometrically and physically scattered fields are decomposed into individual diffraction components so that insight into the formulation of the total field may be obtained. The results of the analytical methods, using the combination of geometrical optics and geometrical diffraction and the combination of physical optics and physical diffraction, are compared with limited experimental data for the right, obtuse, and acute dihedral corners. The cross

sections using only the reflected fields are illustrated first to depict the accuracy which can be expected from using geometrical optics or physical optics alone. The refinements of the corresponding diffraction theories are then included to improve the comparison with the experimental results. The accuracy and utility of the two theories can then be compared.

CHAPTER 2

RADAR CROSS SECTION

2.1 Introduction

All objects reflect and diffract electromagnetic waves which impinge upon them. The radar cross section (RCS) is a figure-of-merit which is used to characterize the scattering properties of the object. Objects which scatter a large proportion of the incident power density in a specified direction are said to have a large radar cross section, while objects which direct only a small proportion of the incident power density in a specified direction are said to have a small radar cross section. The radar cross section of an object has dimensions of area. It can be said to be an area which encloses an amount of power from the incident electromagnetic wave, such that if this power were scattered isotropically it would produce the same power density in the scattered direction as the actual object.

As such, the radar cross section is not indicative of the physical size of an object, and it can vary over many orders of magnitude for objects of approximately the same size or even for the same object viewed from different directions. The spherical conductor is the only object whose backscatter radar cross section is independent of aspect. The sphere's cross section is nearly equal to its physical cross section, πb^2 (where b is the sphere radius) provided that the radius is much larger than the field wavelength, and the incidence direction and scattering direction are identical [32].

The term "radar target" is a conventional name for any object

which the radar system is to observe. The term originated from the important military applications of radar systems, and it is now routinely used in many nonmilitary applications including tracking commercial aircraft and spacecraft, enforcement of speeding laws, mapping ground terrain, or even monitoring insect migration [33].

2.2 Definition

For three-dimensional targets intercepting spherical waves, the formal definition of radar cross section is given by

$$\sigma = \lim_{R\to\infty} \left[4\pi R^2 \frac{W^s}{W^i} \right]$$

$$= \lim_{R\to\infty} \left[4\pi R^2 \left| \frac{\vec{E}^s}{\vec{E}^i} \right|^2 \right] = \lim_{R\to\infty} \left[4\pi R^2 \left| \frac{\vec{H}^s}{\vec{H}^i} \right|^2 \right] \qquad (2\text{-}1)$$

where

σ = the radar cross section

R = the distance of observation from the target

W^i, W^s = the incident and scattered power densities, respectively.

$\vec{E}^i$, $\vec{E}^s$ = the incident and scattered electric fields, respectively.

$\vec{H}^i$, $\vec{H}^s$ = the incident and scattered magnetic fields, respectively.

The incident and the scattered fields are measured, respectively, at the target and observation locations.

The radar cross section, σ, defined in this manner is proportional to a ratio of power densities and is independent of phase. The radar cross section is defined for specific incidence and scattering

directions. If the directions of incidence and scattering are identical, σ is designated as a monostatic cross section; otherwise it is referred to as a bistatic cross section. The monostatic radar cross section is also commonly called the backscatter cross section.

The cross section definition does not explicitly consider polarization losses. To remedy this situation, any of the field quantities $\bar{E}^i$, $\bar{E}^s$, $\bar{H}^i$, and $\bar{H}^s$ can be taken as the total field or as just a component of the total field. If the incident and scattered components are mutually parallel or mutually perpendicular, σ is referred to as the primary or cross-polarized radar cross section respectively.

The topic of two-dimensional cross section is important in some analytical approaches. Also known as the radar cross section per unit length, the two-dimensional cross section is defined for two-dimensional objects as [17]

$$\sigma_l = \lim_{\rho\to\infty} \left[2\pi\rho \left| \frac{\bar{E}^s}{\bar{E}^i} \right|^2 \right] = \lim_{\rho\to\infty} \left[2\pi\rho \left| \frac{\bar{H}^s}{\bar{H}^i} \right|^2 \right] \qquad (2\text{-}2)$$

where

σ_l = the radar cross section per unit length

ρ = the radial distance in cylindrical coordinates

$\bar{E}^i$, $\bar{E}^s$, $\bar{H}^i$, $\bar{H}^s$ = the incident and scattered fields

For this definition, it is assumed that the object is z-independent (i.e. the longitudinal axis lies parallel to the z-axis). If an object is of finite length but is z-independent along this length, then the

three-dimensional radar cross section of the truncated object can be related to the two-dimensional radar cross section per unit length of the corresponding z-independent object by [17], [19], [34]

$$\sigma = \frac{8\ L^2}{\lambda}\ \sigma_1 \qquad (2\text{-}3)$$

where

σ = the three-dimensional radar cross section of the truncated two-dimensional object

σ_1 = the radar cross section per unit length of the two-dimensional object

L = the finite length of the truncated object

λ = the free space wavelength

This transformation equation is useful for simplifying certain analyses [17], [19]. The truncation of a two-dimensional shape is illustrated in Fig. 2-1.

Although the three-dimensional radar cross section has dimensions of area, it is commonly measured and reported using a decibel scale relative to an area of one square meter, with units "decibels above one square meter" or dBsm. Since the cross section is directly proportional to a power ratio, the equation of conversion is

$$\sigma\ (\text{dBsm}) = 10\ \log_{10}\left[\ \sigma(\text{m}^2)\ \right] \qquad (2\text{-}4)$$

where

σ (dBsm) = the radar cross section in decibels above one square meter

σ (m^2) = the radar cross section in square meters

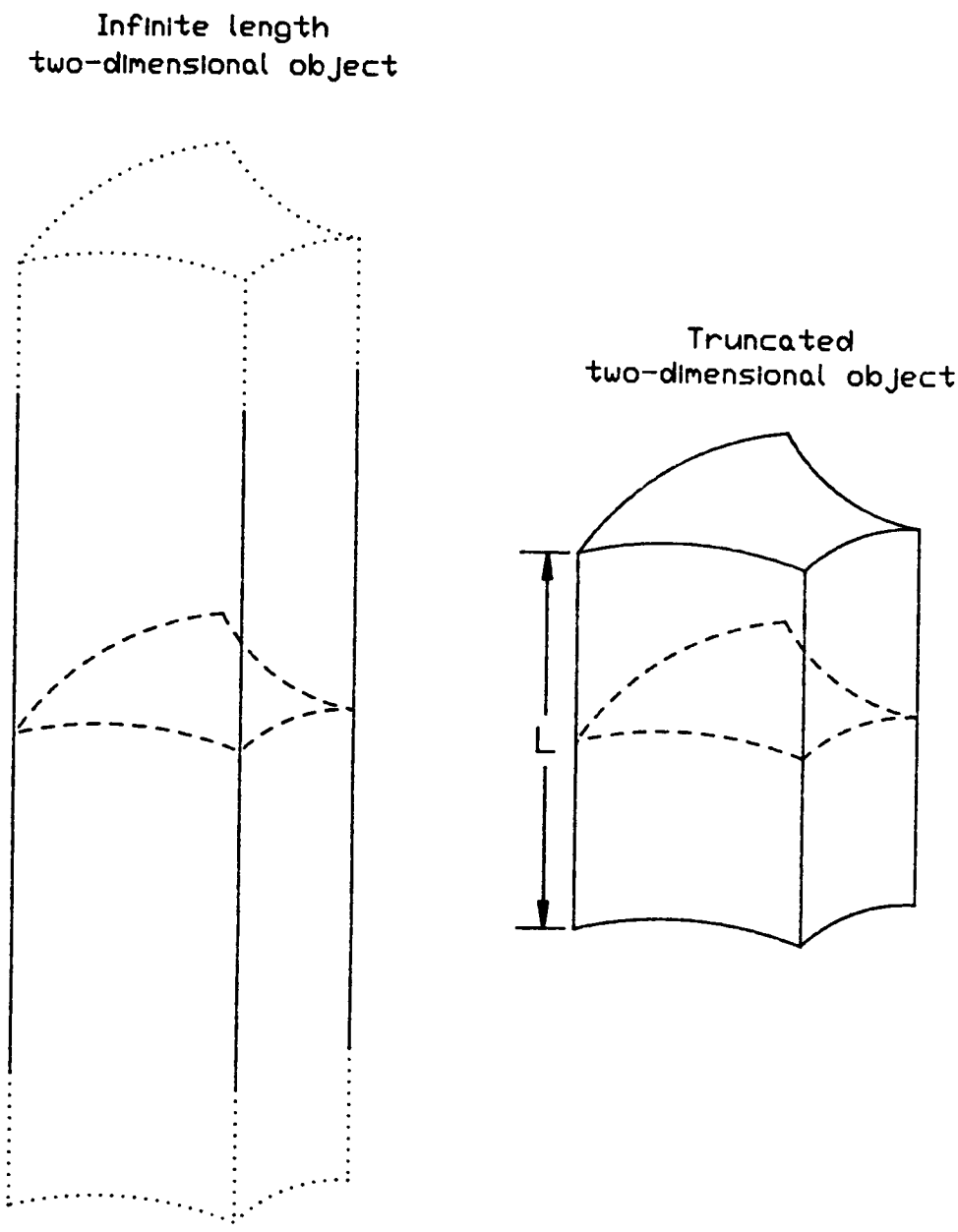

Fig. 2-1. Truncated two-dimensional object geometry.

On a complex target, the backscattered fields from different scattering centers can constructively or destructively interfere producing large fluctuations in the radar cross section if the object rotates. It is not uncommon for the radar cross section of a complex target to vary over several orders of magnitude, or tens of dB, for just a few degrees of rotation.

2.3 Applications

The most important application in which the quantity, σ, arises is in the radar range equation [8]

$$\frac{P_r}{P_t} = \frac{\sigma G_{01} G_{02}}{4\pi} \left[\frac{\lambda}{4\pi R_1 R_2} \right]^2 \qquad (2\text{-}5)$$

for the bistatic case of Fig. 2-2 where

σ = the radar cross section

P_t, P_r = the power of the transmitted and received signals, respectively

G_{01}, G_{02} = the gain of the transmitting and receiving antennas

R_1 = the distance from the object to the transmitter

R_2 = the distance from the object to the receiver

The equation as given here does not consider losses, antenna mismatch, and polarization mismatch. In addition, the distances R_1 and R_2 must be in the radar's far field.

For the monostatic case ($R_1 = R_2 = R$, $G_{01} = G_{02} = G$), (2-5)

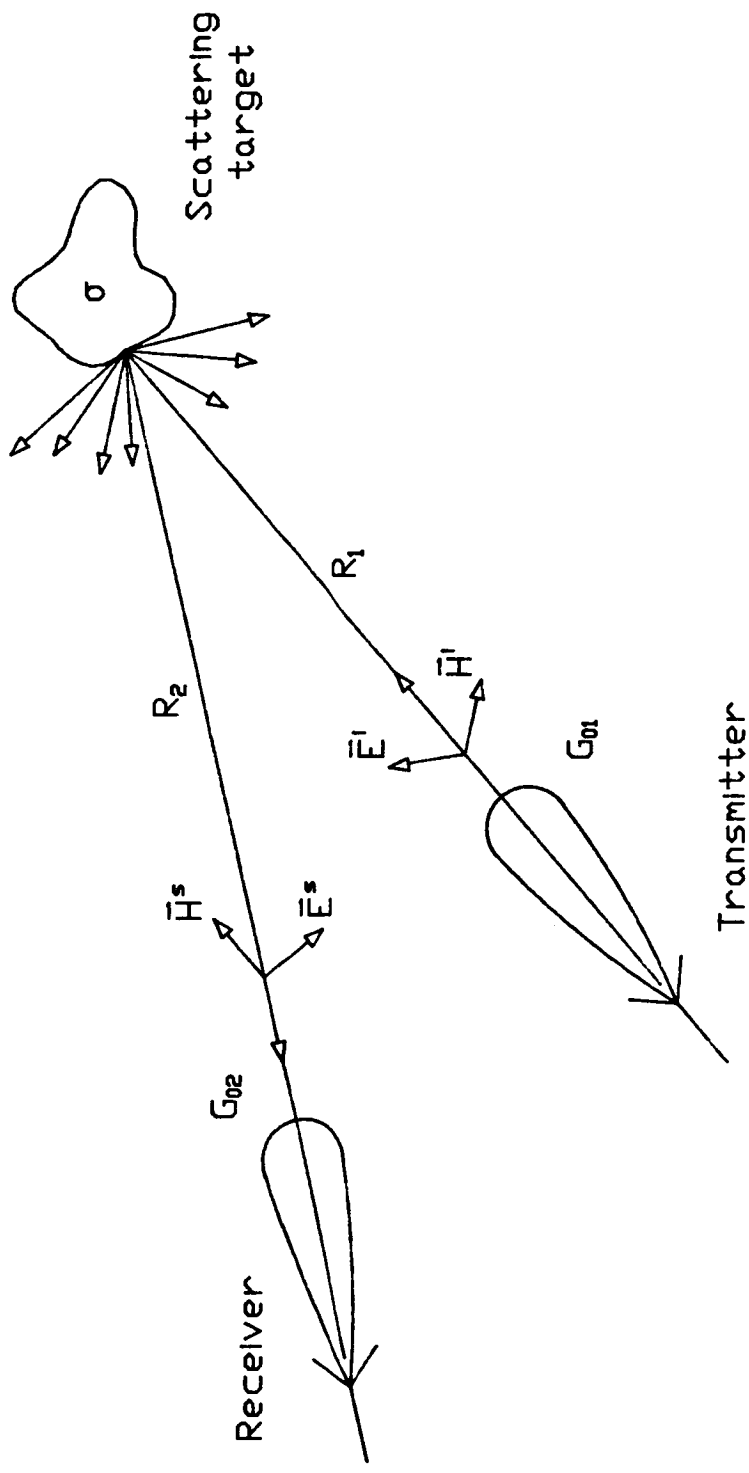

Fig. 2-2. Radar detection configuration.

reduces to

$$R = \left[\frac{P_t G^2 \lambda^2 \sigma}{(4\pi)^3 P_r} \right]^{\frac{1}{4}} \qquad (2\text{-}6)$$

If P_r is taken as the minimum detectable radar signal, then R becomes the maximum distance for radar detection. The equation in this form explicitly illustrates the necessity for determining the radar cross section of a given radar target in order that the maximum distance for detection of that target may be determined. Indeed, the cross section over a wide range of aspect angles should be known, because in many practical situations the orientation of the radar target relative to the radar is unknown. For this reason, developing experimental and analytical methods of determining radar cross section has always been of great importance in radar technology for predicting target detection, recognition, or imaging capabilities.

Under certain circumstances, it may be important to develop techniques whereby radar cross sections of various objects might be reduced or enhanced under some type of optimizing criteria. Analytic studies of scattering mechanisms are invaluable toward discovering these techniques. Furthermore, the advancement of radar technologies, such as target imaging and recognition, benefits from a clear understanding of the scattering mechanisms involved in reflection and diffracting from complex targets. For these reasons the analytical methods of the Geometrical Theory of Diffraction and the Physical Theory of Diffraction are deemed to be important, because they provide insight to the

mechanisms and components which produce certain characteristics of the radar cross section for a particular target. For the shapes which can be studied analytically using available techniques, experimental measurements of backscattered fields would always be possible. However experimental methods often do not indicate where and through what mechanism the scattering takes place. In an experiment, conclusions can be drawn only after many repetitions of the experiment have been performed and systematic manipulations of the target parameters are recorded alongside the pertinent experimental data. The analytical theories are very desirable because they avoid the need for experimental tests which can be expensive and time-consuming. In this respect, the geometrical and physical theories of diffraction can be useful for parametric and design studies.

CHAPTER 3

GEOMETRICAL THEORY OF REFLECTION AND DIFFRACTION

3.1 Introduction

The combination of Geometrical Optics (GO) and the Geometrical Theory of Diffraction (GTD) provides a powerful analytic tool for determining high-frequency solutions to electromagnetic field problems which in many cases would be too difficult to solve, or would be impossible to solve by exact boundary-value methods. The geometrical theories allow more simple approximate expressions for field distributions to be obtained, and in addition, the expressions are in such a form that a more clear understanding of the inner mechanisms of reflection and diffraction can be grasped. The exact boundary—value solutions, if they can be found at all, often are in the form of infinite summations of complex functions and, for many problems, provide insufficient understanding of the origins of the field configurations. In contrast, geometrical optics and the geometrical theory of diffraction identify specific radiating points on each component of a complex structure which are said to contribute to the total field distribution. As such the geometrical theories can provide intuition from which both inductive and deductive conclusions can be drawn.

3.2 Geometrical Optics

The theory of geometrical optics, as the name implies, was employed first for optical rays, and it was later employed at lower electromagnetic frequencies when interacting objects were much larger then the electromagnetic wavelength. In geometrical optics,

electromagnetic fields are assumed to propagate in narrow tubes of rays along straight line paths in homogeneous media. The phase of the electromagnetic wavefront is directly proportional to the distance traveled, and the constant of proportionality is the phase constant k. In lossless media, the field strength of the electromagnetic wave can be determined by requiring that power must be conserved along any narrow tube of rays and therefore the power density associated with a wave is inversely proportional to the tube's cross section.

The interaction of tubes of rays with discontinuities in media are found from extensions of Snell's Law of Reflection and Snell's Law of Refraction. A geometrical reflection, with its associated image, is illustrated in Fig. 3-1. Snell's laws are obtained from an examination of the interaction of a plane wave with a plane boundary between two media, and they stipulate requirements on the angles of reflection and refraction given the angle of incidence of a plane wave. The geometrical theory extends these results by considering an interacting object to be locally plane if its radii of curvature in two orthogonal planes are large. In this manner, Snell's law's can be applied, granting a certain amount of approximation, in many diverse situations.

Geometrical optics, by itself, however, has certain disadvantages when applied to some problems. First the theory predicts that the field will be nonzero only if a ray path can be constructed from the source to the observation point such that this path satisfies Snell's laws at each reflection and refraction. A point at which the field is identically zero, because no such paths exist, is said to be in a shadow region. Similarly the theory predicts that the field at a point will be infinite

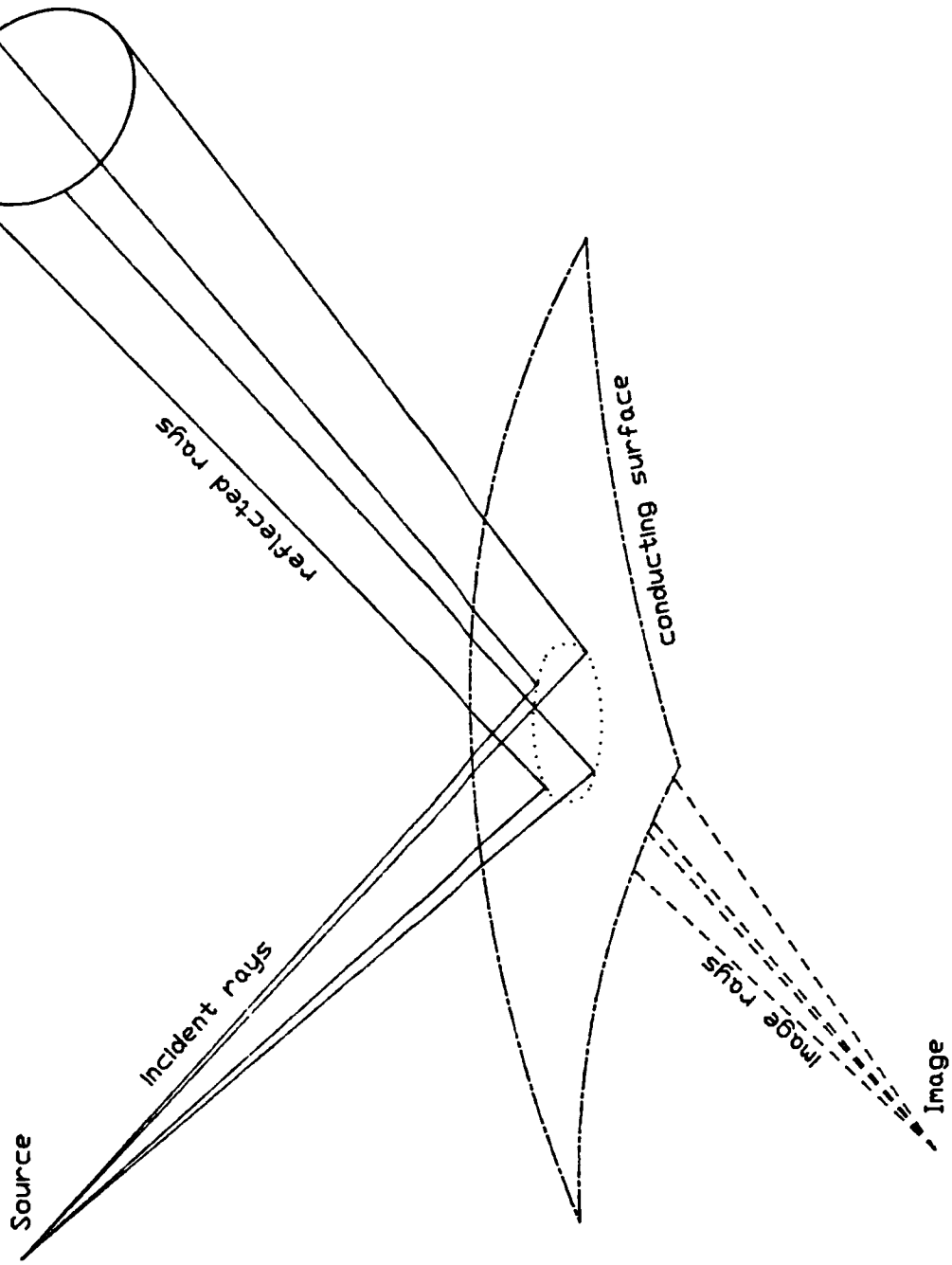

Fig. 3-1. Geometrical optics reflection from conducting surfaces.

if an infinite number of ray paths can be extended from the source to the point; such a point is said to be at a caustic of the geometrical optics field. These characteristics are disadvantages of geometrical optics because, through experimental techniques and through other analytical methods, it has been verified that fields do exist in shadow regions of the geometrical optics field, discontinuities in the field do not exist as an observation point passes from an illuminated region to a shadow region, and infinite fields do not exist at caustics of the geometrical optics field.

A comprehensive overview of the techniques of geometrical optics has been prepared by Deschamps [6] and describes the origins of the theory as well as its validity in comparison to more complex methods based on rigorous interpretation of Maxwell's equations. The details of geometrical optics reflection from conducting plates have been worked out by Lee [7]. The theory is very well defined and has been refined over many years to include most of the dominant features of electromagnetic waves; namely, intensity and phase variations, polarizations, wavefront curvatures, reflections, refractions, caustics, and interference phenomena in homogeneous or inhomogeneous media. Deschamps [6] offers an interesting analogy between the relationship of ray optics and wave optics to the relationship of classical mechanics and quantum mechanics because of the nature of the problems which can be solved by each.

3.3 Geometrical Theory of Diffraction

The Geometrical Theory of Diffraction, originated by Keller [1], is an extension to geometrical optics to remove shadow regions of the

geometrical optics field by introducing diffraction mechanisms by which a ray can be scattered when incident on an edge of a conducting object. By the addition of these diffracted fields, rays are allowed into regions which might otherwise have been in shadow. In addition, the diffracted fields also modify the total field strength in regions which are illuminated by the reflected and refracted fields. The disadvantages of Keller's diffraction theory is that the diffracted fields become infinite at the boundaries of shadow regions, and are inaccurately large near the shadow boundary.

Kouyoumjian and Pathak [2], [3] brought significant improvement to Keller's diffraction theory by a more exact evaluation of the diffraction coefficients which simultaneously removed the singularities in Keller's coefficients near the shadow boundaries and guaranteed continuity of the field when crossing a shadow boundary. By the methods of [2] and [3], the Geometrical Theory of Diffraction can be applied to edges or curved surfaces on conducting bodies. The improvement of the diffraction coefficients established the geometrical theory of diffraction as a powerful tool in electromagnetic analysis. Commonly, Kouyoumjian and Pathak's diffraction theory is called the Uniform Theory of Diffraction (UTD). In this document, when reference is made to the Geometrical Theory of Diffraction (GTD), it is understood that the improved diffraction coefficients are utilized. In addition, only the term GTD (or UTD) may be used to identify the combination of geometrical optics and geometrical diffraction since the geometrical optics field can be shown to be the leading term of a Luneberg-Kline series from which the diffraction terms are extracted.

3.3.1 Normal and Oblique Incidence

A general edge geometry is illustrated in Fig. 3-2. The edge is the vertex of the angle formed by two perfectly conducting flat surfaces. The included angle between the two surfaces is referred to as the wedge angle WA. Using the ray techniques of geometrical optics the surface would be expected to cast a shadow in the region not directly visible to the source, and in this region the geometrical optics field would be identically zero. The incident shadow boundary line in Fig. 3-2 marks the extent of this shadow region. An abrupt discontinuity in the geometrical optics field exists across this boundary.

Since the surfaces are perfectly conducting, they also cause a reflected geometrical optics field to exist in regions where Snell's Law of Reflection can be satisfied. In regions where no point of reflection can be located, no reflected field will exist. The reflected shadow boundary line in Fig. 3-2 defines the extent of the region in which a reflected field may exist. Another abrupt discontinuity in the geometrical optics field is created along this boundary.

To remove the discontinuities in the geometrical optics field, the edge is said to diffract an incident field into all space surrounding the wedge. The diffracted field is added to the geometrical optics field to assure continuity across the incident and reflected shadow boundaries. In this way, the diffracted field refines the geometrical optics field to bring the approximate analytical solution closer to the exact boundary value solution in all space.

The diffraction phenomenon is not limited to two-dimensional geometries, and it can be illustrated for a general three-dimensional wedge shown in Fig. 3-3. Figure 3-2 can be considered to be the

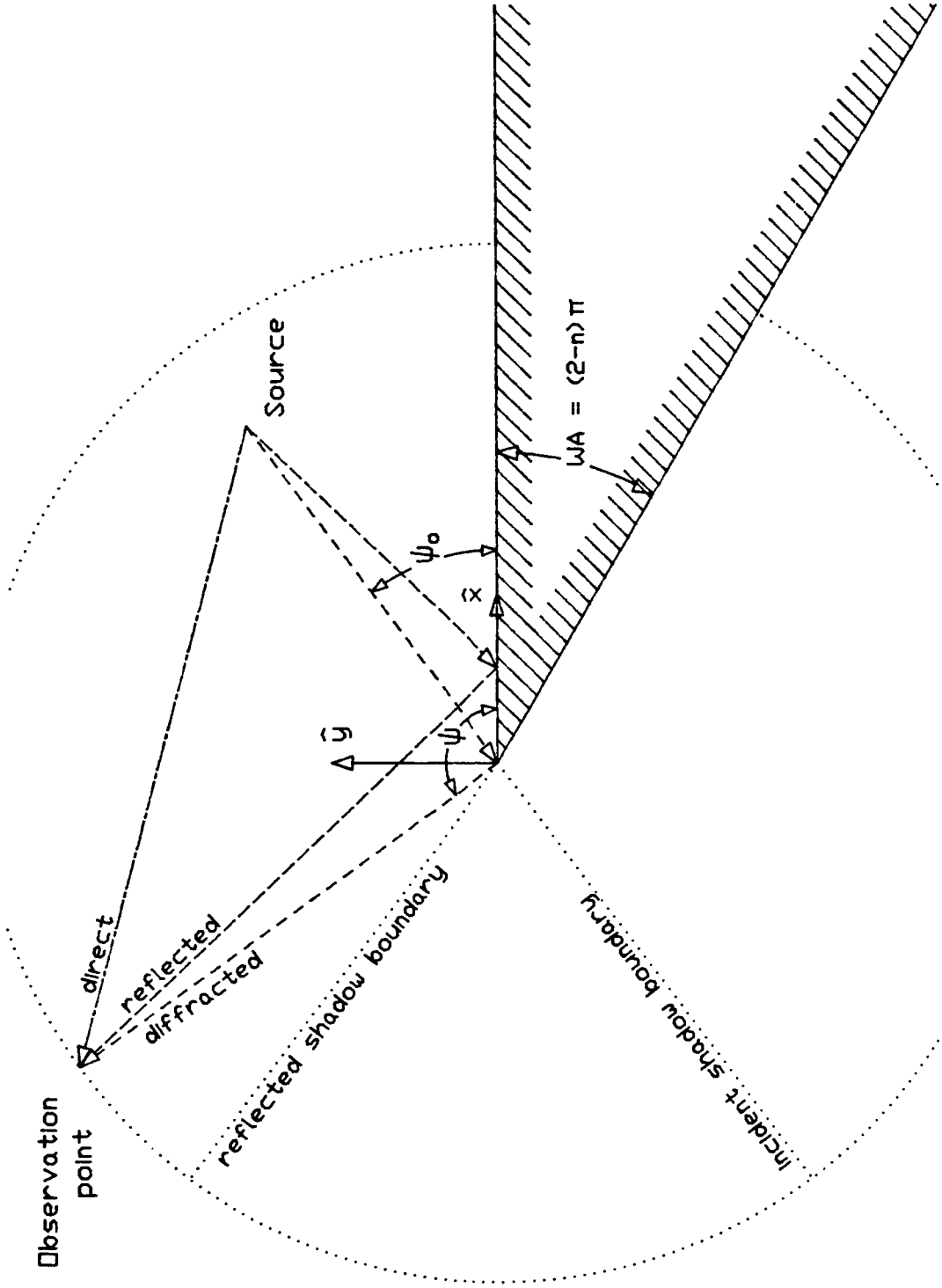

Fig. 3-2. Geometrical diffraction from a conducting edge.

projection of Fig. 3-3 into the plane perpendicular to the edge at the diffraction point Q. In the theory, the diffracted ray is said to lie on a cone generated as the locus of all directions from the diffraction point such that the angle subtended by the incident ray and the edge is equal to the angle subtended by the diffracted ray and the edge. This cone has conventionally been termed the Keller cone, and it is not merely a theoretical contrivance but has been shown to exist experimentally [35]. For any given source and observation point, the diffraction is normally limited to one point (or at most a finite number of points) on the edge, unless the observation point happens to be at a caustic of the diffracted field. If no point can be located at which the Keller cone criterion can be satisfied, no diffracted ray can exist unless the method of equivalent currents, as described in Section 3.3.2, is utilized.

To determine the field diffracted from an arbitrarily oriented edge, an edge fixed coordinate system is constructed, as shown in Fig. 3-3 such that $\hat{e}_z$ is a unit vector along the edge, $\hat{e}_x$ is a unit vector perpendicular to $\hat{e}_z$ and lying in one face of the edge, and $\hat{e}_y=\hat{e}_z\times\hat{e}_x$. A diffraction point Q is then located on the edge such that if $\hat{s}'$ is a unit vector from the source to the diffraction point and $\hat{s}$ is a unit vector from the diffraction point to the observation point, then the condition

$$\hat{s}' \cdot \hat{e}_z = \hat{s} \cdot \hat{e}_z = \cos \beta_0 \qquad (3\text{-}1)$$

holds so as to guarantee that the diffracted ray subtends an angle from the edge identical to the angle subtended by the incident ray and the edge. This ensures that the diffracted ray lies on the Keller cone.

Relative to the diffraction point, coordinate vectors associated with the incident and diffracted rays are defined by

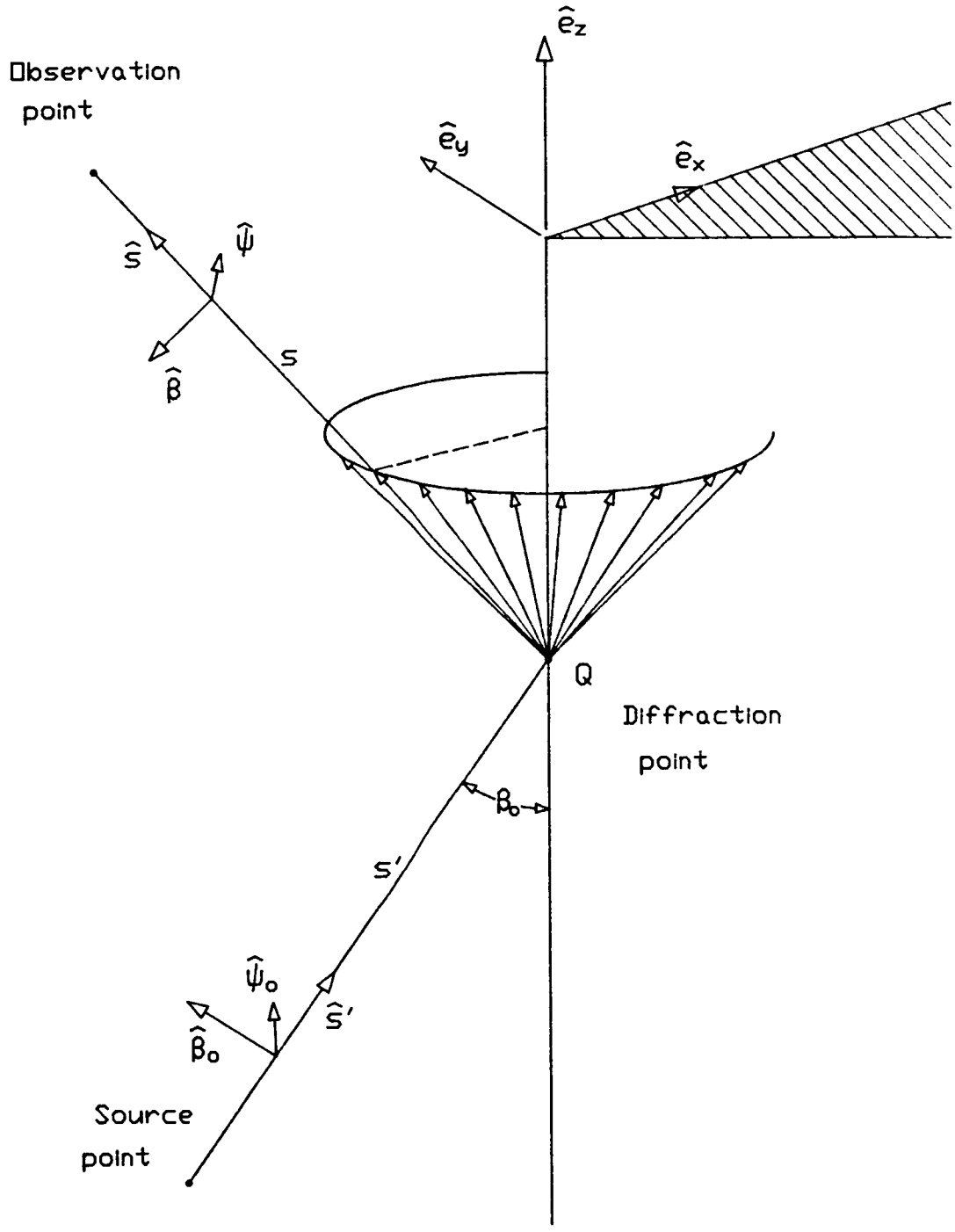

Fig. 3-3. Geometrical diffraction at oblique incidence.

$$\hat{\psi} = \frac{\hat{s} \times \hat{e}_z}{|\hat{s} \times \hat{e}_z|} \qquad \hat{\psi}_0 = \frac{\hat{e}_z \times \hat{s}'}{|\hat{e}_z \times \hat{s}'|} \tag{3-2}$$

$$\hat{\beta} = \hat{s} \times \hat{\psi} \qquad \hat{\beta}_0 = \hat{s}' \times \hat{\psi}_0$$

These coordinate vectors compose a ray-fixed coordinate system which reduces the complexity of the diffraction formulation. The incident field at the point of diffraction, $\bar{E}^i(Q)$, is decomposed into two components which are parallel to the $\hat{\psi}_0$ and $\hat{\beta}_0$ directions, respectively,

$$E_{\beta_0}^i(Q) = \hat{\beta}_0 \cdot \bar{E}_i(Q) \tag{3-3}$$

$$E_{\psi_0}^i(Q) = \hat{\psi}_0 \cdot \bar{E}_i(Q) \tag{3-4}$$

The diffracted field due to the diffraction from the edge, as a function of distance from the diffraction point, is given by [8]

$$\begin{bmatrix} E_\beta^d(s) \\ E_\psi^d(s) \end{bmatrix} = \frac{-1}{\sin\beta_0} \begin{bmatrix} D_s & 0 \\ 0 & D_h \end{bmatrix} \begin{bmatrix} E_{\beta_0}^i(Q) \\ E_{\psi_0}^i(Q) \end{bmatrix} A(s,s')\, e^{-jks} \tag{3-5}$$

and the total diffracted field, as a function of the distance s from the diffraction point Q is

$$\bar{E}^d(s) = \bar{E}_\beta^d(s)\, \hat{\beta} + \bar{E}_\psi^d(s)\, \hat{\psi} \tag{3-6}$$

The factor A(s,s') is known as the spatial attenuation factor and is given by

$$A(s,s') = \begin{cases} \dfrac{1}{\sqrt{s}} & \text{for plane and cylindrical wave incidence} \\ \sqrt{\dfrac{s'}{s(s+s')}} & \text{for spherical wave incidence} \end{cases} \tag{3-7}$$

The factor L, known as the distance parameter, is defined as

$$L = \begin{cases} s \sin^2\beta_0 & \text{for plane and cylindrical wave indidence} \\ \dfrac{s\, s'\, \sin^2\beta_0}{s + s'} & \text{for spherical wave incidence} \end{cases} \qquad (3\text{-}8)$$

According to the geometry of Fig. 3-3, s' is the distance from the source to the diffraction point, and s is the distance from the diffraction to the observation point.

The diagonal matrix elements, D_s and D_h, are referred to, respectively, as the soft and hard polarization diffraction coefficients. In general, D_s and D_h are function of the distance parameter L, the incident and diffracted angle Ψ and Ψ_0, and the edge wedge parameter n

$$n = 2 - \frac{WA}{\pi} \qquad (3\text{-}9)$$

where WA is the interior wedge angle as shown in Fig. 3-2.

The diffraction coefficients D_s and D_h are given as

$$D_s = D_s(L,\Psi,\Psi_0,n) = D^i(L,\Psi-\Psi_0,n) - D^r(L,\Psi+\Psi_0,n) \qquad (3\text{-}10)$$

$$D_h = D_h(L,\Psi,\Psi_0,n) = D^i(L,\Psi-\Psi_0,n) + D^r(L,\Psi+\Psi_0,n) \qquad (3\text{-}11)$$

D^i and D^r are referred to as the incident and reflected diffraction coefficients and are given by [8]

$$D^i(L,\Psi-\Psi_0,n) = \frac{-e^{-j\frac{\pi}{4}}}{2n\sqrt{2\pi k}} \times \qquad (3\text{-}12)$$

$$\left\{ C^+(\Psi-\Psi_0,n)\, F\left[kLg^+(\Psi-\Psi_0)\right] + C^-(\Psi-\Psi_0,n)\, F\left[kLg^-(\Psi-\Psi_0)\right] \right\}$$

$$D^r(L,\Psi+\Psi_0,n) = \frac{-e^{-j\frac{\pi}{4}}}{2n\sqrt{2\pi k}} \times \qquad (3\text{-}13)$$

$$\left\{ C^+(\Psi+\Psi_0,n)\, F\left[kLg^+(\Psi+\Psi_0)\right] + C^-(\Psi+\Psi_0,n)\, F\left[kLg^-(\Psi+\Psi_0)\right] \right\}$$

The C and F functions are defined as

$$C^+(\Psi\pm\Psi_0,n) = \cot\left[\frac{\pi+(\Psi\pm\Psi_0)}{2n}\right] \tag{3-14}$$

$$C^-(\Psi\pm\Psi_0,n) = \cot\left[\frac{\pi-(\Psi\pm\Psi_0)}{2n}\right] \tag{3-15}$$

$$F\left[kLg^+(\Psi\pm\Psi_0)\right] = 2j\sqrt{kLg^+(\Psi\pm\Psi_0)}\; e^{jkLg^+(\Psi\pm\Psi_0)} \times \int_{\sqrt{kLg^+(\Psi\pm\Psi_0)}}^{\infty} e^{-j\tau^2}\, d\tau \tag{3-16}$$

$$F\left[kLg^-(\Psi\pm\Psi_0)\right] = 2j\sqrt{kLg^-(\Psi\pm\Psi_0)}\; e^{jkLg^-(\Psi\pm\Psi_0)} \times \int_{\sqrt{kLg^-(\Psi\pm\Psi_0)}}^{\infty} e^{-j\tau^2}\, d\tau \tag{3-17}$$

where

$$g^+(\Psi\pm\Psi_0) = 1 + \cos\left[\,(\Psi\pm\Psi_0)-2n\pi N^+\,\right] \tag{3-18}$$

$$g^-(\Psi\pm\Psi_0) = 1 + \cos\left[\,(\Psi\pm\Psi_0)-2n\pi N^-\,\right] \tag{3-19}$$

N^+ and N^- are the integers which most nearly satisfy

$$2n\pi N^+ - (\Psi\pm\Psi_0) = +\pi \qquad \text{for } g^-(\Psi\pm\Psi_0) \tag{3-20}$$

$$2n\pi N^- - (\Psi\pm\Psi_0) = -\pi \qquad \text{for } g^+(\Psi\pm\Psi_0) \tag{3-21}$$

The F function involves a Fresnel integral and can be computed efficiently using a numerical algorithm given in [36]. A FORTRAN computer subroutine which uses this algorithm to calculate the diffraction coefficients D_s and D_h can be found in [8] or in [37].

In radar cross section analysis, where the source and observation point recede to infinity, the distance parameter L increases to infinity. The argument of the F functions then becomes large

everywhere except at the single points where $g^{-}(\Psi \pm \Psi_0)$ or $g^{+}(\Psi \pm \Psi_0)$ equals zero. With the exception of these points, which happen to be along the incident and reflected shadow boundaries, the F functions can be shown to approach unity, and the diffraction coefficients reduce to those originally proposed by Keller where [8]

$$D_s = \frac{e^{-j\frac{\pi}{4}} \sin\left[\frac{\pi}{n}\right]}{n\sqrt{2\pi k}} \left[\frac{1}{\cos(\frac{\pi}{n}) - \cos(\frac{\Psi-\Psi_0}{n})} - \frac{1}{\cos(\frac{\pi}{n}) - \cos(\frac{\Psi+\Psi_0}{n})} \right] \quad (3\text{-}22)$$

$$D_h = \frac{e^{-j\frac{\pi}{4}} \sin\left[\frac{\pi}{n}\right]}{n\sqrt{2\pi k}} \left[\frac{1}{\cos(\frac{\pi}{n}) - \cos(\frac{\Psi-\Psi_0}{n})} + \frac{1}{\cos(\frac{\pi}{n}) - \cos(\frac{\Psi+\Psi_0}{n})} \right] \quad (3\text{-}23)$$

The terms in these expressions become infinite as a shadow boundary is approached. At the shadow boundaries, $\Psi+\Psi_0$ or $\Psi-\Psi_0$ equals π, and hence one of the denominators in the expressions for D_s and D_h will be zero.

The diffraction coefficients contain certain symmetries due to the cylindrical symmetry of the wedge geometry of Fig. 3-3, and due to reciprocity. To satisfy the wedge symmetry, the diffraction doefficients D_s and D_h satisfy

$$D_{s,h}(L,\Psi,\Psi_0,n) = D_{s,h}(L,n\pi-\Psi,n\pi-\Psi_0,n) \quad (3\text{-}24)$$

and to guarantee reciprocity, the diffraction coefficients satisfy

$$D_{s,h}(L,\Psi,\Psi_0,n) = D_{s,h}(L,\Psi_0,\Psi,n) \quad (3\text{-}25)$$

These identities can be used to advantage in certain configurations.

3.3.2 Equivalent Current Method

The method of equivalent currents is introduced to the theory of geometrical diffraction to predict field distributions when no diffraction points exist, or to predict fields at caustics when an

infinite number of diffraction points exist. It is quite simple to envision object geometries for which there are no diffraction or reflection points but for which the scattered field is experimentally nonzero. For these geometries, the method of equivalent currents can be used to determine the total field. Many of the early papers credit a series of three monographs by Millar as the basis for the equivalent current method [38]-[40].

The equivalent current method has been used by Ryan and Peters [4], by Knott and Senior [5], [27] and by Sikta, et al. [21], [23]. This technique defines an edge current on the diffracting wedge which produces a field on the diffraction cone identical to the field predicted by the diffracted ray. The equivalent current obtained can then be used to find the fields diffracted in directions away from the diffraction cone or in directions of caustics. These currents are nonphysical in the sense that they depend not only on the incident field direction but also on the observation direction.

The equivalent edge currents can be either electric or magnetic in nature, and they are determined in terms of the components of the incident electric and magnetic fields which are parallel to the edge vertex. The equivalent currents are expressed as

$$I_z^e = \frac{\sqrt{8\pi k}}{\eta k} \frac{e^{-j\frac{\pi}{4}}}{\sin\beta_0} E_z^i(Q)\, D_s(L,\Psi,\Psi_0,n) \qquad (3\text{-}26)$$

$$I_z^m = \frac{\eta\sqrt{8\pi k}}{k} \frac{e^{-j\frac{\pi}{4}}}{\sin\beta_0} H_z^i(Q)\, D_h(L,\Psi,\Psi_0,n) \qquad (3\text{-}27)$$

where

E_z^i, H_z^i = the incident electric and magnetic fields parallel to the edge at the point of diffraction

D_s, D_h = the diffraction coefficients of (3-10) and (3-11)

From the equivalent currents, the magnetic vector potential $\bar{A}$ and the electric vector potential $\bar{F}$ can be found by integrating the contributions of infinitesimal current elements. From the vector potentials, the diffracted electric and magnetic fields may then be obtained. The equations which are used in this procedure are presented in Chapter 4 as they form an essential part of the Physical Theory of Diffraction. The diffracted fields from the equivalent current method are found in all space although diminishing accuracy should be expected as the observation point moves away from the Keller cone.

3.4 Application to Backscatter Analysis

The theory of geometrical optics can satisfactorily predict the fields backscattered from conducting objects provided that a specular reflection point exists on the object, the specular point is not near to an abrupt discontinuity such as an edge, and the object is doubly curved at the specular point [25]. The radar cross section under these conditions is

$$\sigma = \pi a_1 a_2 \qquad (3\text{-}28)$$

where

σ = the radar cross section

a_1, a_2 = the principle radii of curvature of the body at the specular point.

From this formula it is evident that if the body is singly curved (i.e.

a cylindrical structure) or the body is planar (i.e. a flat plate) then one or both radii will be infinite. The radar cross section is then infinite for single curved or planar structures provided a specular point exists. However if no specular point exists on the conducting surface, then the cross section is identically zero.

The diffraction coefficients of the geometrical theory can become less convenient to use when applied to radar cross section analysis. The diffraction coefficients of (3-10) and (3-11) revert to the original forms proposed by Keller, as given in (3-22) and (3-23), as the distance parameter for the single diffracted fields becomes unbounded. Unfortunately these diffraction coefficients are plagued by discontinuities near incident and reflection shadow boundaries. For backscattering from a straight edge joining two planar surfaces, the diffraction shadow boundary occurs at an aspect normal to either planar surface.

Considering the reflected and diffracted field from a flat surface bounded by straight edges, it is evident that at normal incidence the backscatter cross section due to geometrical optics and the backscatter cross section due to geometrical diffraction from an edge are both infinite. Fortunately, however, it is possible to use the theory in certain cases if the cross section is found at some finite, yet large, distance from the object (rather than at an infinite distance). As the finite distance increases, the cross section will approach some finite value for all aspects. A rule which can be used for choosing the minimum distance of observation is given by the "far-field" criterion [8]

$$R_{min} = 2\ D^2 / \lambda \qquad (3\text{-}29)$$

where

R_{min} = the minimum distance

D = the maximum dimension of the target

λ = the free space wavelength

Ross [17] showed that for the rectangular flat plate the diffraction coefficients for each edge were infinite near normal incidence but the singularities from each edge cancelled against each other to yield finite cross sections at all aspects for the singly diffracted field. This occured because the edges are mutually parallel and the edge parameters n are identical. Sikta [21], [23] used this property in his analysis of a general polygonal plate by subdividing each polygon into a number of rectangular strips to ensure continuity of the diffracted field near normal incidence. It is shown in Appendix A that the diffracted field singularities will mutually cancel regardless of the edge wedge angles provided the edges are mutually parallel. This is an important result because it allows the subdivision of a general geometry into rectangular strips so that the theory is not limited solely to flat plates.

The geometrical theory works well for the analysis of truncated two-dimensional objects as described in Section 2.2 whenever the objects are formed of flat surfaces bounded by straight edges. If a target is a more general three-dimensional object, three other methods may be considered for the analysis. One method would be to subdivide a general three-dimensional target into rectangular segments following Sikta [21], [23], and incorporating the equivalent current method. A second method

utilizes the corner diffraction coefficients empirically proposed by Burnside and Pathak [21], [22], [23]. The semi-heuristic corner diffraction coefficient was used by Sikta in the analysis of polygonal flat plates, and it is applicable to corners formed by the intersection of a pair of finite straight edges (as on a polygonal flat plate). This is one type of corner which is commonly found on more complex structures such as the dihedral corner reflector. A third method utilizes the generalized equivalent edge current theory presented by Michaeli [9], [10], [25], [29]. The equivalent edge currents presented by Michaeli can be used to determine the diffracted fields from an edge given arbitrary directions of illumination and observation. The expressions, however, are fraught with singularities, much like Keller's diffraction coefficients. Perhaps cancellations in these singularities can be found to allow appropriate solutions to be obtained for certain geometries.

CHAPTER 4

PHYSICAL THEORY OF REFLECTION AND DIFFRACTION

4.1 Introduction

The combination of Physical Optics (PO) and the Physical Theory of Diffraction (PTD) can be used to provide approximate expressions for the fields scattered by a conducting object. The theory evolves from an approximation of the current densities on reflecting surfaces and the edge currents on diffracting edges, from which the scattered fields can be computed.

The methods of physical optics and physical diffraction provide an alternative to the more difficult solution of the boundary value problem associated with a given scattering geometry. These methods share many of the advantages of the geometrical theory in that the solutions can be solved in terms of elementary functions, and the results provide a clear understanding of which reflection and diffraction mechanisms are most important for a given angle of observation. Unlike the geometrical theory, however, the physical theory includes an intermediate step when finding the scattered fields; namely, the currents on surfaces and edges must be determined in terms of the incident fields. From these induced currents, the scattered fields can be computed through conventional methods utilizing the radiation integrals of electromagnetics. The geometrical theory, in contrast, determines the scattered fields directly in terms of the incident fields and circumvents the need to perform tedious or costly integrations (an exception being the method of equivalent currents of

Section 3.3.2).

The physical optics theory, unlike geometrical optics, can predict fields in directions which do not satisfy Snell's Law of Reflection and thereby avoids the discontinuities in fields associated with geometrical reflection and shadow boundaries. Knott [25] discusses the usefulness of the physical optics theory and asserts that the theory is acceptably accurate for flat and singly curved surfaces. Harrington [15] provides an explanation of the method of physical optics in the context of electromagnetic integral equations.

4.2 Physical Optics

The theory of physical optics stems from a study of the reflection of a plane wave from a perfectly conducting plane which is infinite in extent. The current density on a flat conducting surface which is infinite in extent is given by

$$\bar{J}_s = \hat{n} \times \bar{H}_t \qquad (4\text{-}1)$$

where

$\bar{J}_s$ = the surface current density

$\bar{H}_t$ = the total magnetic field on the surface of the plate

$\hat{n}$ = a unit normal to the plate

For an incident plane wave, the total tangential magnetic field is twice the incident tangential magnetic field so that [15]

$$\bar{J}_s = 2\hat{n} \times \bar{H}_i \qquad (4\text{-}2)$$

where

$\bar{H}_i$ = the incident magnetic field of the surface of the plate

Equation (4-2) is used as an approximate solution for the current density on any perfectly conducting locally smooth surface which has finite dimensions. It is commonly referred to as the "physical optics approximation". For a general conducting object the incident field is taken to be the ray optic incident field from the source, and the current is said to exist only in the illuminated portions of the conducting object where the direct source rays or reflected source rays impinge upon the object. In this manner the theory of physical optics uses the idea of straight line ray paths from geometrical optics for determining illuminated regions of an arbitrary surface. If the geometrical optics incident field in a region of the object is identically zero because no incident rays exist from the source to the region, then the physical optics current in this region is identically zero.

Once the surface currents over a conducting object are determined via the physical optics approximation, the reflected field due to the surface current density can be determined by first finding the magnetic vector potential $\bar{A}_s$ by [8]

$$\bar{A}_s = \frac{\mu}{4\pi} \int\int_{S'} \bar{J}_s \frac{e^{-jkR}}{R} \, ds' \qquad (4\text{-}3)$$

where

$\bar{A}_s$ = the magnetic vector potential

μ = the permeability of free space

R = the distance from an infinitesimal surface

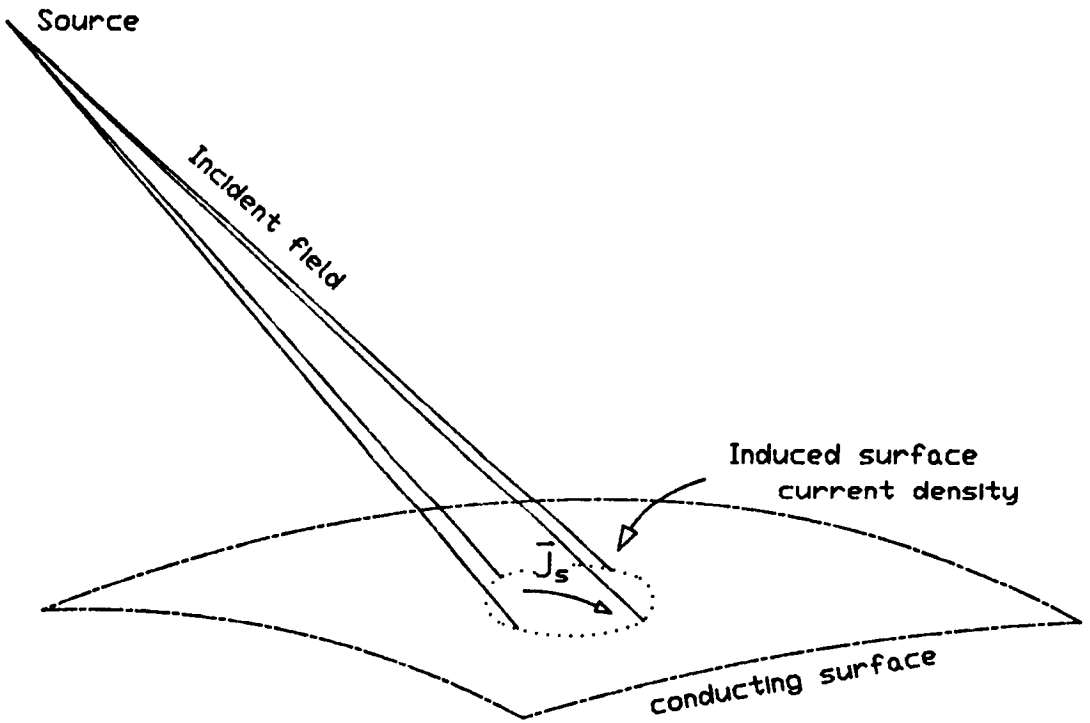

Fig. 4-1. Physical optics reflection from conducting surfaces.

current element to the point of observation

The surface integration is performed only over the illuminated portion of the conducting surface. The field due to the potential can be found by [8]

$$\vec{E}_s = -j\omega\vec{A}_s - j\frac{1}{\omega\mu\varepsilon}\nabla(\nabla\cdot\vec{A}_s) \qquad (4\text{-}4)$$

which reduces, in the far field to

$$\vec{E}_s \cong -j\omega\vec{A}_s \qquad (4\text{-}5)$$

where

$\vec{E}_s$ = the reflected electric fields

ω = the source radial frequency

μ = the permeability of the medium

ε = the permittivity of the medium.

Although the radial component of the field is typically nonzero, it is taken to be zero in the far field because its value is much smaller than the θ or ϕ components.

An issue of concern in physical optics analysis is the method of determining the fields due to double reflection; that is, fields which reflect from one conducting surface, are incident upon and reflect from a second conducting surface, and are subsequently received at the point of observation. The method of determining these double reflected fields can take the following two forms:

a. The first and second reflection can be performed using physical optics integrations over the illuminated portion of the reflecting surfaces.

b. The first reflection can be performed using simple geometrical optics ideas and the second reflection can be performed using a physical optics integration over the illuminated portion of the second surface.

The first of these methods is generally the more complex, involving multiple integrations and differentiations over what may be complex geometries; however, it often gives superior results. The second method, used previously by Knott [18], can greatly reduce the complexity of the field calculations for certain configurations. This second method is justified by the argument that the physical optics currents are conventionally found in terms of the incident geometrical optics fields, and the incident field could come from a source or from the image of a source.

4.3 Physical Theory of Diffraction

The Physical Theory of Diffraction, formulated by Ufimtsev [11]-[13], supplements the physical optics theory by adding contributions due to diffractions at the edges of conducting surfaces. These diffracted fields serve to refine the physical optics fields to account for edge effects which are not considered in the physical optics approximation. The diffraction coefficients are incorporated to include the nonuniform fringe currents which exist near the edges of a conducting object, in addition to the uniform physical optics currents.

The diffracted field can be determined in one of two ways in a manner very much analogous to the method of geometrical diffraction. In one method, the diffracted fields are found directly in proportion to the incident field and a diffraction coefficient. In the second method,

an intermediate step of finding equivalent edge currents is introduced, from which the edge diffracted fields can be found using a line integration of differential current elements. This second method is extremely useful for complex three-dimensional objects and is chosen as the focus of the physical diffraction formulation here because it allows fields to be calculated off the specular scattering direction. It is worth noting that a third method by Mitzner [14], [25], [29] develops an incremental length diffraction coefficient (ILDC) which allows fields off the specular direction to be determined. Knott [25] maintains that the ILDC formulation is essentially a description of equivalent currents.

For the general case, the equivalent currents considered in the physical theory of diffraction must be both equivalent magnetic currents, I_e, and equivalent electric currents, I_m. The diffracted electric field can then be determined from the magnetic vector potential $\vec{A}$ and the electric vector potential $\vec{F}$. The potentials are [8]

$$\vec{A} = \frac{\mu}{4\pi} \int_l I_e \frac{e^{-jkR}}{R} \, dl \qquad (4\text{-}6)$$

$$\vec{F} = \frac{\epsilon}{4\pi} \int_l I_m \frac{e^{-jkR}}{R} \, dl \qquad (4\text{-}7)$$

and the scattered electric field is

$$\vec{E} = -j\omega\vec{A} - j \frac{1}{\omega\mu\epsilon} \nabla (\nabla \cdot \vec{A}) - \frac{1}{\epsilon} \nabla \times \vec{F} \qquad (4\text{-}8)$$

In the far field, the θ and ϕ components are given by

$$\vec{E} \cong -j\omega\vec{A} + j\omega\eta \, \hat{a}_r \times \vec{F} \qquad (4\text{-}9)$$

Although the radial component is nonzero, it is taken to be zero since it is much smaller than the θ or ϕ components. The line integrations of (4-6) and (4-7) are performed only over the illuminated portion of the diffracting edge.

If the edge is taken to be parallel to the z axis, as shown in Fig. 4-2, the equivalent currents are given in [16] as

$$I_z^e = j\frac{2}{\omega\mu} f_1 E_z^i \tag{4-10}$$

$$I_z^m = j\frac{2}{\omega\varepsilon} g_1 H_z^i \tag{4-11}$$

where

I_z^e, I_z^m = z-components of the equivalent electric and magnetic currents

E_z^i, H_z^i = z-components of the incident electric and magnetic fields at the diffraction point

ω = the source radial frequency

μ,ε = the permeability and permittivity of the medium

The functions f_1 and g_1 are similar to Keller's diffraction coefficients D_s and D_h in (3-22) and (3-23) and are given by [16]

$$f_1 = f - f_0 \tag{4-12}$$

$$g_1 = g - g_0 \tag{4-13}$$

where

$$f = \frac{1}{n}\sin\frac{\pi}{n}\left[\frac{1}{\cos(\frac{\pi}{n}) - \cos(\frac{\Psi-\Psi_0}{n})} - \frac{1}{\cos(\frac{\pi}{n}) - \cos(\frac{\Psi+\Psi_0}{n})}\right] \tag{4-14}$$

$$g = \frac{1}{n}\sin\frac{\pi}{n}\left[\frac{1}{\cos(\frac{\pi}{n}) - \cos(\frac{\Psi-\Psi_0}{n})} + \frac{1}{\cos(\frac{\pi}{n}) - \cos(\frac{\Psi+\Psi_0}{n})}\right] \tag{4-15}$$

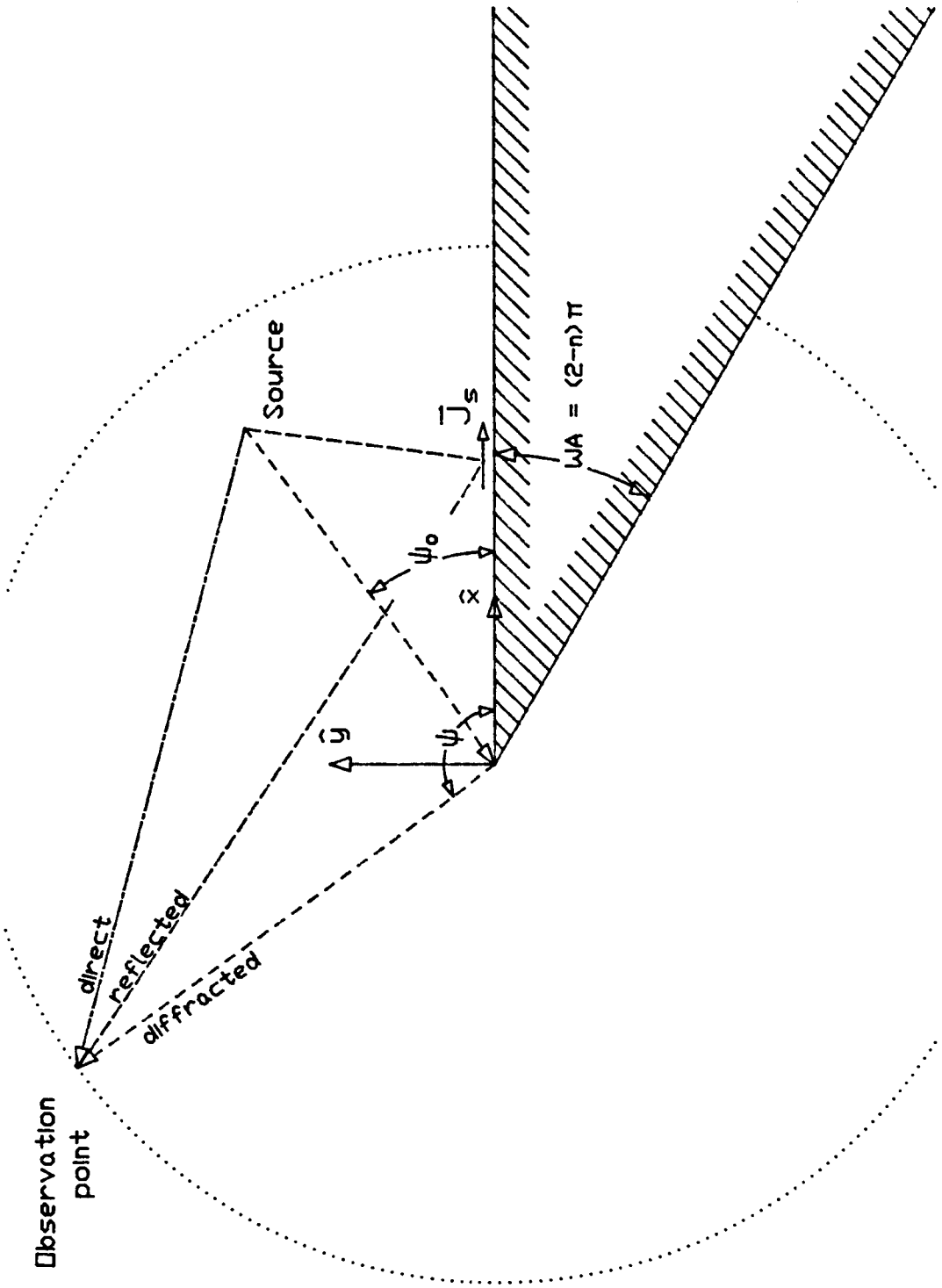

Fig. 4-2. Physical diffraction edge configuration.

Since the diffraction coefficients are functions as the direction of observation, the equivalent currents are said to be non-physical because any real physical currents should be independent of the observation direction.

Although f and g become infinite at the shadow boundaries, the singularities are cancelled by singularities in the f_0 and g_0 functions. Expressions for the f_0 and g_0 functions at these shadow boundaries are available in [11] and in [16]. However, as described in [41], computers are notoriously inaccurate when subtracting two large numbers whenever the difference is small, and, therefore, precautions should be observed.

The f_0 and g_0 functions are given by [16]

$$f_0 = \begin{cases} f_a & 0 < \psi_0 \leq (n-1)\pi \\ f_a+f_b & (n-1)\pi < \psi_0 \leq \pi \\ f_b & \pi < \psi_0 < n\pi \end{cases} \tag{4-16}$$

$$g_0 = \begin{cases} g_a & 0 < \psi_0 \leq (n-1)\pi \\ g_a+g_b & (n-1)\pi < \psi_0 \leq \pi \\ g_b & \pi < \psi_0 < n\pi \end{cases} \tag{4-17}$$

where n is the edge parameter given by (3-9). Here

$$f_a = \frac{\sin\psi_0}{\cos\psi + \cos\psi_0} \tag{4-18}$$

$$g_a = \frac{-\sin\psi}{\cos\psi + \cos\psi_0} \tag{4-19}$$

$$f_b = \frac{\sin(n\pi-\psi_0)}{\cos(n\pi-\psi) + \cos(n\pi-\psi_0)} \tag{4-20}$$

$$g_b = \frac{-\sin(n\pi-\psi)}{\cos(n\pi-\psi) + \cos(n\pi-\psi_0)} \tag{4-21}$$

Expressions (4-16) through (4-21) are valid for n>1; that is for the exterior edge diffraction case. Expressions are given in [16] for the

f_i and g_i diffraction coefficients when n<1, and these expression are derived to consider the existence of multiply reflected fields. In addition, expressions for f_i and g_i are given near the incident and reflected shadow boundaries for both the interior and exterior diffraction coefficients.

4.4 Application to Backscatter Analysis

The theory of physical optics and physical diffraction, as presented here, provide a convenient method for determining the scattered field from a given conducting object. The approximate surface currents and equivalent edge currents are uniquely defined in terms of the incident fields, where the incident fields are normally taken to be the ray-traced geometrical optics fields, except in the case of multiple reflections. For multiple reflections either geometrical or physical optics could be used for the initial reflections, with the physical optics integration being performed over the final reflection.

A formulation for determining the reflected field from conducting flat surfaces bound by straight edges, assuming an incident plane wave, has been presented in [16]. For a flat surface bounded by straight edges which is illuminated by a plane wave, the surface integrals of physical optics can be resolved, in general, in closed form expressions involving elementary functions. Similarly the line integrations of physical diffraction can be resolved into closed form expressions. Then for the class of objects formed of such surfaces and edges, analysis of the backscatter fields, and hence the backscattered cross section can be methodically formulated.

The theory of physical optics and physical diffraction provides a powerful tool for analyzing backscatter from objects whenever the objects are composed of a conglomerate of flat surfaces bound by straight edges or surfaces which can be sufficiently approximated by subdivision into flat surfaces. The theory is sufficiently general for three dimensional objects to allow automated solutions to electromagnetic scattering problems, and this is one of its most appealing traits. The problem normally becomes most dependent on the mastering of the geometrical orientations of a target. The intent is to discern, for arbitrary aspect angles, the illuminated portions of each surface and the illuminated portions of each edge, so as to identify the contributions to the total field by mechanisms of first and higher order reflections or diffractions. The decomposition of an object geometry can be a complex and formidable task if a general method applicable to any arbitrary configuration is desired. In the analysis, the second and higher order reflections would, realistically, have to be performed using the combination of physical and geometrical optics described previously. This method retains the plane wave structure of the reflected wave so that the physical optics integrations can be performed in closed form. In later chapters and in Appendix B, an example is given of the method of determining a double reflected field using solely physical optics. The resulting expression is a complicated quadruple integral which must be integrated numerically. This method is not considered feasible for a manageable automated method of solution, but it can be used in less complex geometries to provide an improvement in accuracy.

CHAPTER 5

GEOMETRICAL THEORY ANALYSIS OF A CORNER REFLECTOR

5.1 Dihedral Geometry

The usefulness and accuracy of geometrical optics and the geometrical theory of diffraction can best be evaluated through a study of the radar cross section of a complex object. The object which has been chosen for this study is the dihedral corner reflector shown in Fig. 5-1. This corner reflector is comprised of two rectangular flat conducting plates which are joined along an edge, forming an interior angle of 2α. The dihedral corner reflector is oriented such that its vertex is along the z-axis and the bottom edges lie in the x-y plane. The monostatic radar cross section is computed analytically in the azimuthal plane where $\theta = 90^\circ$ and $0^\circ < \phi < 360^\circ$. The two cases of vertical and horizontal polarization are considered, where the vertically polarized radar cross section is determined using the components of the incident and scattered electric fields which are parallel to the z-axis, and the horizontally polarized radar cross section is determined using the components of the incident and scattered electric fields which are perpendicular to the z-axis.

5.2 Method of Analysis

The best technique to find the backscattered fields from the dihedral corner reflector begins by considering the dihedral to be a truncated two-dimensional object, as described in Chapter 2, which is illuminated by an incident cylindrical wave. If the radar cross section per unit length of the corresponding two-dimensional dihedral can be

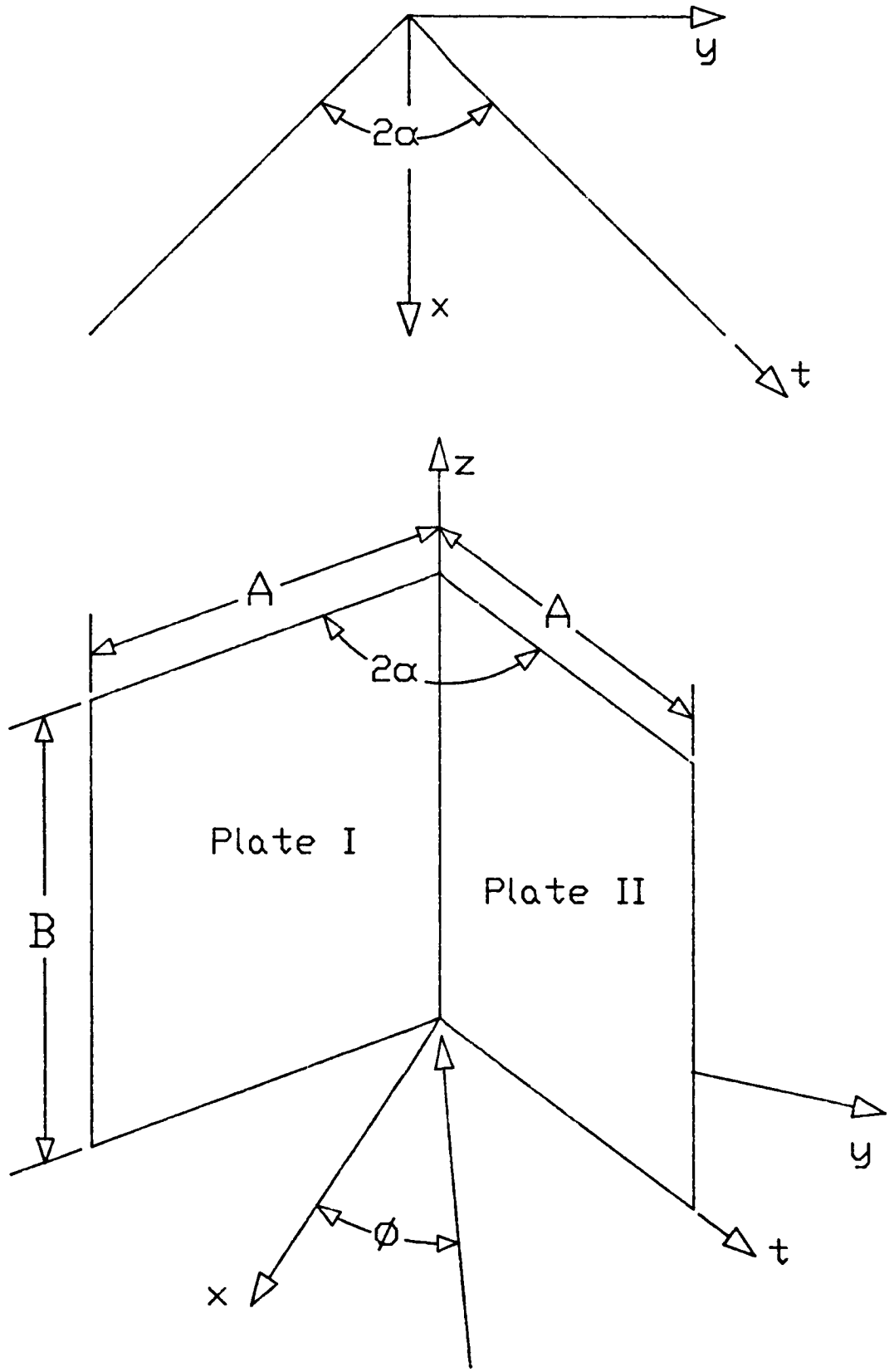

Fig. 5-1. Dihedral corner reflector geometry.

found, the radar cross section of the truncated dihedral can be found using (2-3). The cross section of the two-dimensional dihedral is shown in Fig. 5-2.

It is necessary to develop some strategy for naming scattering mechanisms from both geometrical optics and geometrical diffraction. Toward meeting this requirement, a naming convention has been developed in which each edge diffraction and each surface reflection is assigned a unique number as follows:

- The diffraction from the exterior edge of plate I is assigned the number 1.
- The reflection from the surface of plate I is assigned the number 2.
- The diffraction from the edge where plate I joins plate II is assigned the number 3.
- The reflection from the surface of plate II is assigned the number 4.
- The diffraction from the exterior edge of plate II is assigned the number 5.

With this notation, every possible component of the backscattered field can be assigned a unique number describing the sequence of reflections and diffractions. The component is specified by a coalescence of the digits of the individual scattering mechanisms. The notation adopted here is to precede each component by a capital letter C to identify the digits as the description of a component of the backscattered field. The order of the digits defines the order of occurence of the individual reflections and diffractions. As an example, the notation C251 uniquely

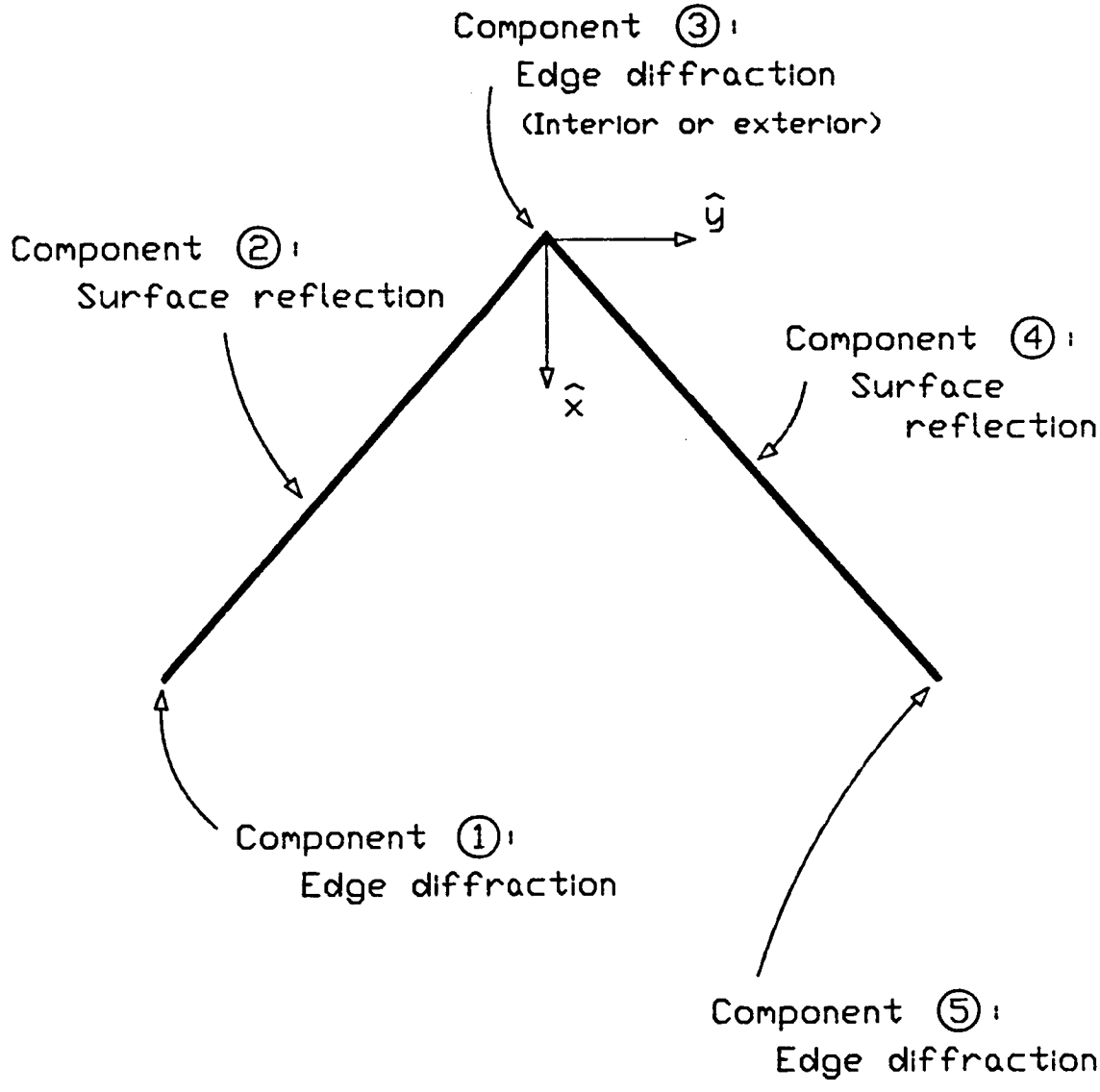

Fig. 5-2. Dihedral corner backscatter nomenclature.

defines the component of the total backscattered field which is due to reflection from plate I (reflection 2) followed by diffraction from the outside edge of plate II (diffraction 5) and diffraction from the outside edge of plate I (diffraction 1). The final diffraction direction should be toward the original direction of incidence for the monostatic case. Some typical scattering mechanisms are shown in Fig. 5-3.

Using the described notation, the total backscattered field can be found as a summation of the following terms:

- Components due to single reflections.
  * C2 C4
- Components due to single diffractions.
  * C1 C3 C5
- Components due to double reflections.
  * C24 C42
- Components due to one reflection and one diffraction.
  * C14 C41 C25 C25
- Components due to two diffractions.
  * C13 C31 C53 C35 C15 C51
- Components due to three reflections.
  * C242 C424
- Components due to two reflections and one diffraction.
  * C252 C414 C142 C241 C524 C425
- Components due to one reflection and two diffractions.
  * C141 C525 C125 C251 C514 C415
    C253 C352 C413 C314
- Components due to three diffractions.

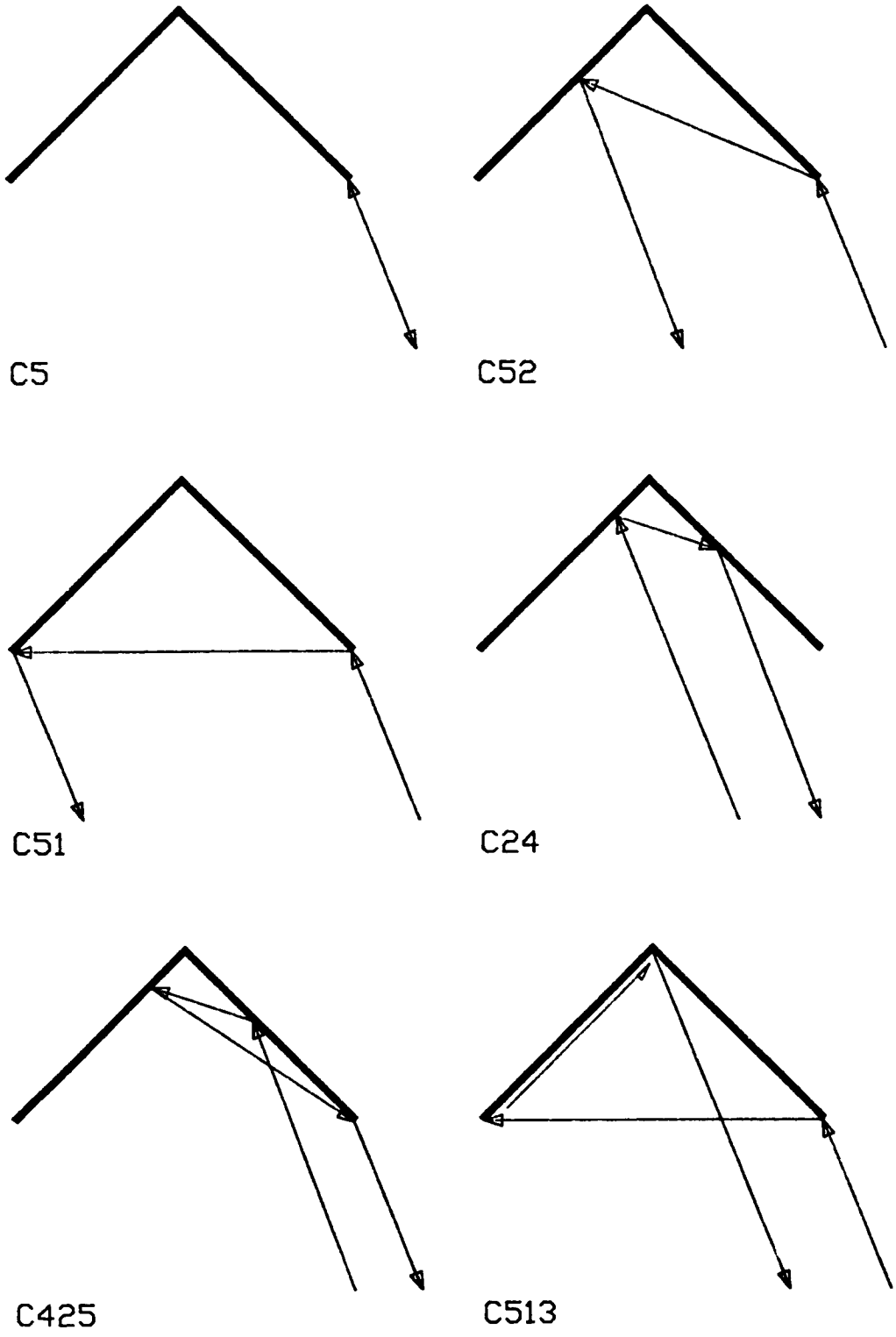

Fig. 5-3. Examples of components of the geometrical optics and geometrical diffraction backscattered field.

* C131 C535 C135 C531 C153 C351

C513 C315 C151 C515 C313 C353

All these components, and one other to be discussed later, are included in the analysis of backscatter of the dihedral corner for the horizontally polarized case. For the vertically polarized case, however, the components which include multiple diffraction between two edges of the same plate will vanish due to the nature of the diffraction coefficients, which impose the electromagnetic boundary condition that tangential electric fields to a perfect conductor are identically zero. These components,however, would be nonzero if the slope diffraction coefficients [37] of GTD were utilized.

For a target composed solely of flat plates, the method of images becomes especially convenient for cross section analysis. In a cylindrical coordinate system, as shown in Fig. 5-1, the source and all subsequent images for the dihedral corner lie in the x-y plane, so that the coordinates of the location of all images can be tabulated using only the ρ and ϕ coordinates while the z coordinate will always be identically zero. The location of the source, diffraction points, and all images of the source can be tabulated using the geometry of Fig. 5.1. Here R represents the distance from the source to the vertex of the dihedral corner, and A is the length of one edge of the dihedral corner. The locations of the source, images, and diffraction points are given in a cylindrical coordinate system (ρ, ϕ, z), as

- the source location:

  $P = (R, \phi, 0)$

- the location of the point of diffraction on edge 1:

$P_1 = (A,\ 2\pi-\alpha,\ 0)$

- the location of the point of diffraction on edge 5:

  $P_5 = (A,\ \alpha,\ 0)$

- the location of the point of diffraction on edge 3:

  $P_3 = (0,\ 0,\ 0)$

- the image of the source through surface 2:

  $P_2 = (R,\ 2\pi-2\alpha-\phi,\ 0)$

- the image of the source through surface 4:

  $P_4 = (R,\ 2\alpha-\phi,\ 0)$

- the image of P_2 through surface 4:

  $P_{24} = (R,\ 4\alpha+\phi-4\pi,\ 0)$

- the image of P_4 through surface 2:

  $P_{42} = (R,\ 2\pi-4\alpha+\phi,\ 0)$

- the image of P_1 through surface 4:

  $P_{14} = (A,\ 3\alpha,\ 0)$

- the image of P_5 through surface 2:

  $P_{52} = (A,\ 2\pi-3\alpha,\ 0)$

Next it is necessary to find the distance between any two points for the geometrical theory. If any two points P_a and P_b are given in terms of their cylindrical coordinates, then the distance D, between P_a and P_b, can be found by

$$D = \left[\rho_a^2 + \rho_b^2 - 2\rho_a\rho_b\cos(\phi_a-\phi_b) + (z_a-z_b)^2 \right]^{\frac{1}{2}} \qquad (5\text{-}1)$$

The diffraction coefficients D_s and D_h include a parameter, n, which is defined in terms of the edge wedge angle, WA, as given in (3-9). For the dihedral corner reflector, four edge parameters can be

defined as

- diffractions from edge 1:

  $WA = 0$, $n_1 = 2$

- diffractions from edge 5:

  $WA = 0$, $n_5 = 2$

- diffractions from the interior of edge 3:

  $WA = 2\pi - 2\alpha$, $n_{3i} = 2\alpha/\pi$

- diffractions from the exterior of edge 3:

  $WA = 2\alpha$, $n_{3e} = 2(1-\alpha/\pi)$

It is necessary to determine if a given component exists for a given direction of aspect. In geometrical optics, a reflected field can only exist if a specular point exists on the conducting surface so as to satisfy Snell's law of reflection. Similarly in geometrical diffraction, a diffracted field can only exist if a specular point exists such that the diffracted rays lie on the Keller diffraction cone (this condition can be removed if the method of equivalent currents is utilized). Associated with each reflection or diffraction are two locations: the originating location from which the incident ray is radiated and the terminating location at which the ray is observed. In a sequence of reflections and diffractions of a single ray, there is one originating location and one terminating location associated with each individual reflection and diffraction. The originating locations are the locations of the preceding source or edge diffraction while the terminating locations are the subsequent observation or edge diffraction locations.

For a given reflection to exist, the ray from the originating

location to the associated terminating location must pass through the reflecting plate. In this case, either the originating or terminating location is actually an image of a preceding or subsequent source or diffraction point. If the originating point is given in terms of its rectangular coordinates in the x-y plane as (x_a,y_a), and if the terminating point is given in terms of its rectangular coordinates in the x-y plane as (x_b,y_b), then the line through the two points is given as

$$y = \left[\frac{y_b - y_a}{x_b - x_a}\right] x + \left[\frac{y_a x_b - y_b x_a}{x_b - x_a}\right] \qquad (5\text{-}2)$$

A point on the plates of the dihedral, in the x-y plane can be given in terms of its cylindrical coordinates where $\phi = 2\pi-\alpha$ on plate I and $\phi = \alpha$ on plate II. The radial distance of the intersection of the ray and the plate is then

$$\rho = \frac{y_a x_b - y_b x_a}{(y_b - y_a)\cos\phi - (x_b - x_a)\sin\phi} \qquad (5\text{-}3)$$

The reflection exists if ρ lies in the range $0 < \rho < A$ where A is the width of the dihedral plates. Equation (5-3) has no solution if $\tan\phi = (y_b-y_a)/(x_b-x_a)$, and hence no reflection can exist.

For any reflection-diffraction sequence which begins or ends with a reflection, the reflection surface must also be visible to the source and observation points. For the monostatic cross section of the dihedral corner, the plates are visible or partially visible at certain aspects.

For reflection 2, the surface is

- entirely visible if $0<\phi<\alpha$ or $\pi-\alpha<\phi<2\pi$ (5-4a)
- not visible if $\cos^{-1}\left[\frac{A\cos\alpha}{R}\right] <\phi<\pi-\alpha$ (5-4b)
- partially visible elsewhere.

The visible portion of the plate is given by

$$A\frac{\sin(\phi-\alpha)}{\sin(\phi+\alpha)} \leq \rho \leq A \quad (5\text{-}4c)$$

For reflection 4, the surface is

- entirely visible if $0<\phi<\pi+\alpha$ or $2\pi-\alpha<\phi<2\pi$ (5-5a)
- not visible if $\pi+\alpha<\phi<2\pi-\cos^{-1}\left[\frac{A\cos\alpha}{R}\right]$ (5-5b)
- partially visible elsewhere.

The visible portion of the plate is given by

$$A\frac{\sin(\phi+\alpha)}{\sin(\phi-\alpha)} \leq \rho \leq A \quad (5\text{-}5c)$$

In terms of the diffractions mechanisms, all diffractions, if they exist, lie on the Keller cone for a truncated two dimensional geometry. A particular diffraction will exist if the diffracting edge is visible from the source and observation point. For the dihedral corner reflector

- Edge 1 is visible if

$$0<\alpha<\cos^{-1}\left[\frac{A\cos\alpha}{R}\right] \quad \text{or} \quad \pi-\alpha<\phi<2\pi \quad (5\text{-}6a)$$

- Edge 3 is visible if

$$0<\phi<\alpha \quad \text{or} \quad 2\pi-\alpha<\phi<2\pi \quad \text{(interior diffraction)} \quad (5\text{-}7a)$$

$$\alpha<\phi<2\pi-\alpha \quad \text{(exterior diffraction)} \quad (5\text{-}7b)$$

- Edge 5 is visible if

$$0<\phi<\pi+\alpha \quad \text{or} \quad 2\pi-\cos^{-1}\left[\frac{A\cos\alpha}{R}\right]<\phi<2\pi \quad (5\text{-}8a)$$

The angles Ψ and Ψ_0 of the diffraction coefficients of Section 3.3 are found from geometrical considerations. The angle Ψ_0 is the angle between the wedge face and the ray from the originating point to the diffraction point. The angle Ψ is the angle between the wedge face and the ray from the diffraction point to the terminating point. Locating the originating or terminating point by its rectangular coordinates in the x-y plane (x_a, y_a), the corresponding angle, Ψ_0 or Ψ, can be found

- on edge 1 as

$$\Psi_1 = \pi + \alpha + \tan^{-1}\left[\frac{y_a - y_1}{x_a - x_1}\right] \qquad (5\text{-}9)$$

- on edge 3, for interior diffraction as

$$\Psi_{3i} = \alpha + \tan^{-1}\left[\frac{y_a - y_3}{x_a - x_3}\right] \qquad (5\text{-}10)$$

- on edge 3, for exterior diffraction as

$$\Psi_{3e} = -\alpha + \tan^{-1}\left[\frac{y_a - y_3}{x_a - x_3}\right] \qquad (5\text{-}11)$$

- on edge 5 as

$$\Psi_5 = -\alpha + \tan^{-1}\left[\frac{y_a - y_5}{x_a - x_5}\right] \qquad (5\text{-}12)$$

where Ψ_1, Ψ_{3i}, Ψ_{3e}, or Ψ_5 can represent either Ψ or Ψ_0 for a given diffraction, and where (x_j, y_j) are the coordinates of edge j for $j = 1,3,5$. In the application of these equations, particular attention must be paid to the angle of the inverse tangent function. The angle of $\tan^{-1}(y/x)$ lies in

- quadrant I if $y > 0$ and $x > 0$
- quadrant II if $y > 0$ and $x < 0$

- quadrant III if $y < 0$ and $x < 0$
- quadrant IV if $y < 0$ and $x > 0$

and the angle is chosen such that the diffraction angles, Ψ and Ψ_0 will lie in the range $0 \leq \Psi \leq 2\pi$ and $0 \leq \Psi_0 \leq 2\pi$.

Although the diffracted field from a pair of parallel edges is continuous, as is discussed in Section 3.4, cases may exist where both edges of a plate may not be visible near normal incidence. This normally occurs because another unrelated object passes in the line of sight from the target to the radar. Such is the case, for example, in the 90° dihedral corner for ϕ slightly greater than 45° when Plate II obstructs the view of one of the edges of Plate I. Clearly in cases such as this, there is only one edge diffraction existing and the field is no longer continuous near normal incidence.

Geometrically, under these circumstances, one portion of the plate is illuminated while another portion is not illuminated. An abrupt discontinuity in the field incident upon the plate is created because of the shadow cast by the obstructing object. Since abrupt discontinuities must not exist, some diffraction mechanism should be introduced to assure continuity in the radar cross section pattern. In the analysis of the dihedral corner reflector, an edge diffraction was imposed exactly at the shadow edge to account for the field discontinuity. This edge position is a function of the dihedral orientation since the shadow edge moves as the dihedral corner reflector is rotated. This imposed edge diffraction was included if the aspect was such that the incident field was nearly normal to one of the two flat plates, and if, at the same orientation, the second plate cast a

shadow across the first. The appropriate choice of edge parameter, n, is not apparent for this imposed edge so some discretion is allowed. Since only a half plane is illuminated, it seems appropriate to select an equivalent edge which has only one face illuminated; that is an edge with included angle in the range $0^\circ < WA < 90^\circ$. Since the resulting cross section is relatively insensitive to the choice of n, a wedge angle of 0° was chosen; that is, n = 2 for the imposed edge.

In the backscatter analysis using the Geometrical Theory of Diffraction, many terms in the total field are reciprocal. From the notation of Section 5.1 it is evident that to satisfy reciprocity, the terms C241 and C142 are equivalent, the terms C35 and C53 are equivalent, and so on. Other terms, such as C141 and C353 have no reciprocal pair because the sequence of reflections and diffractions is symmetric. Intuitively it is not clear whether these symmetric terms should be included once or twice in the total field, but it can be shown, using the geometry of Fig. 5-4 that these terms should be included twice to insure field continuity. Single reflections and single diffractions, however, are not to be included twice.

In Fig. 5-4, the source/receiver and a diffracting edge (in this case, edge 5) are illustrated along with their images through Reflection 2. A ray from the source image will diffract on the edge image and can follow one of three paths to the receiver; either a direct path, a reflected path (from surface 4) or a diffracted (from edge 5), as illustrated. These three paths correspond to the three backscatter components C52, C524, and C525, respectively, and all three terms are required to assure continuity near the reflected shadow boundary. In

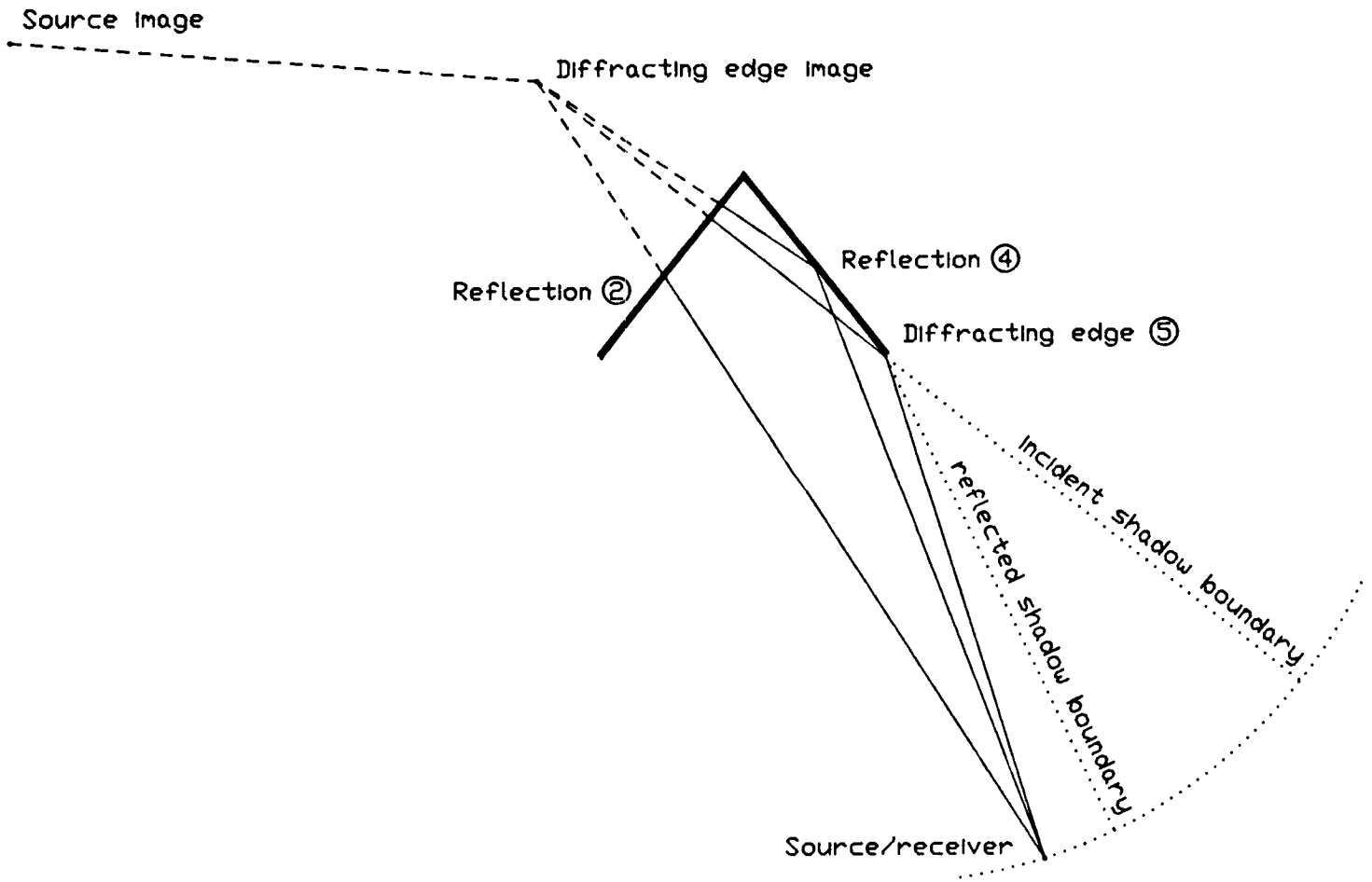

Fig. 5-4. Examples of components of the geometrical theory backscattered fields due to dihedral edge images.

addition, each path also has a reciprocal pair which corresponds to the ray which leaves the source, follows one of three paths to edge 5, after which it diffracts from the source. The three paths in this case correspond to the backscatter components C25, C425 and C525. Again, all the paths must exist to ensure continuity in the vicinity of the reflected shadow boundary. In this geometry, the terms C52 and C25 are reciprocal pairs, the terms C524 and C425 are reciprocal pairs, but C525 has no reciprocal pair. Therefore C525 must be included twice in the analysis. This concept of including symmetrical terms twice (except for the single reflection or single diffraction terms) may not be intuitively obvious but seems to be analytically necessary. Any third order mechanism which is symmetric in its sequence of reflections and diffractions will have no reciprocal pair.

5.3 Backscatter Components

One of the advantages of analyzing target backscatter using the geometrical optics and geometrical diffraction theories is that the effects of different mechanisms can be separated so that the effect of each structural element in the target can be identified. A nomenclature for enumerating the different reflection-diffraction mechanisms was formulated in Section 5.2, and it is utilized in this section to identify each backscatter component.

The dihedral corner reflector was studied for a right, an obtuse, and an acute interior angle for which experimental results were available. The radar cross section components were analyzed at a frequency of 9.4 GHz where the dihedral dimensions A and B were both 5.6088 λ. Two polarizations were considered. The vertical polarization

was the case in which the incident electric field was parallel to the longitudinal axis of the dihedral, and the horizontal polarization was the case in which the electric field was perpendicular to the longitudinal axis of the dihedral. The dihedral corner reflector interior angles for which experimental results were available were 90°, 98° and 77°.

In Figs. 5-5, 5-6, and 5-7 the backscatter cross section for vertical polarization is illustrated for different reflection and diffraction mechanisms as a function of observation direction ϕ. The total radar cross section is subdivided into groups of individual components and the radar cross section due to each group is shown separately. Each figure contains eighteen graphs, and each graph shows the radar cross section of a particular group. The subdivision usually combines only the symmetric or reciprocal components of the total radar cross section. For example, graph 1 shows the backscatter cross section when only components C2 and C4 are considered, where C2 and C4 are the single specular reflection components from the dihedral plates. Graph 4 illustrates the component due to the imposed edge described at the end of Section 5.2. Graph 17 shows the cross section due solely to all the third order diffractions which include diffraction from the vertex of the dihedral (edge 3). These terms are all identically zero for the vertically polarized case since slope diffraction coefficients have not been considered. The final graph, numbered 18, shows the total cross section as the sum of all individual components up to third order mechanisms as described in Section 5.1. In Chapter 7 these total cross sections will be compared with experimental results to illustrate the

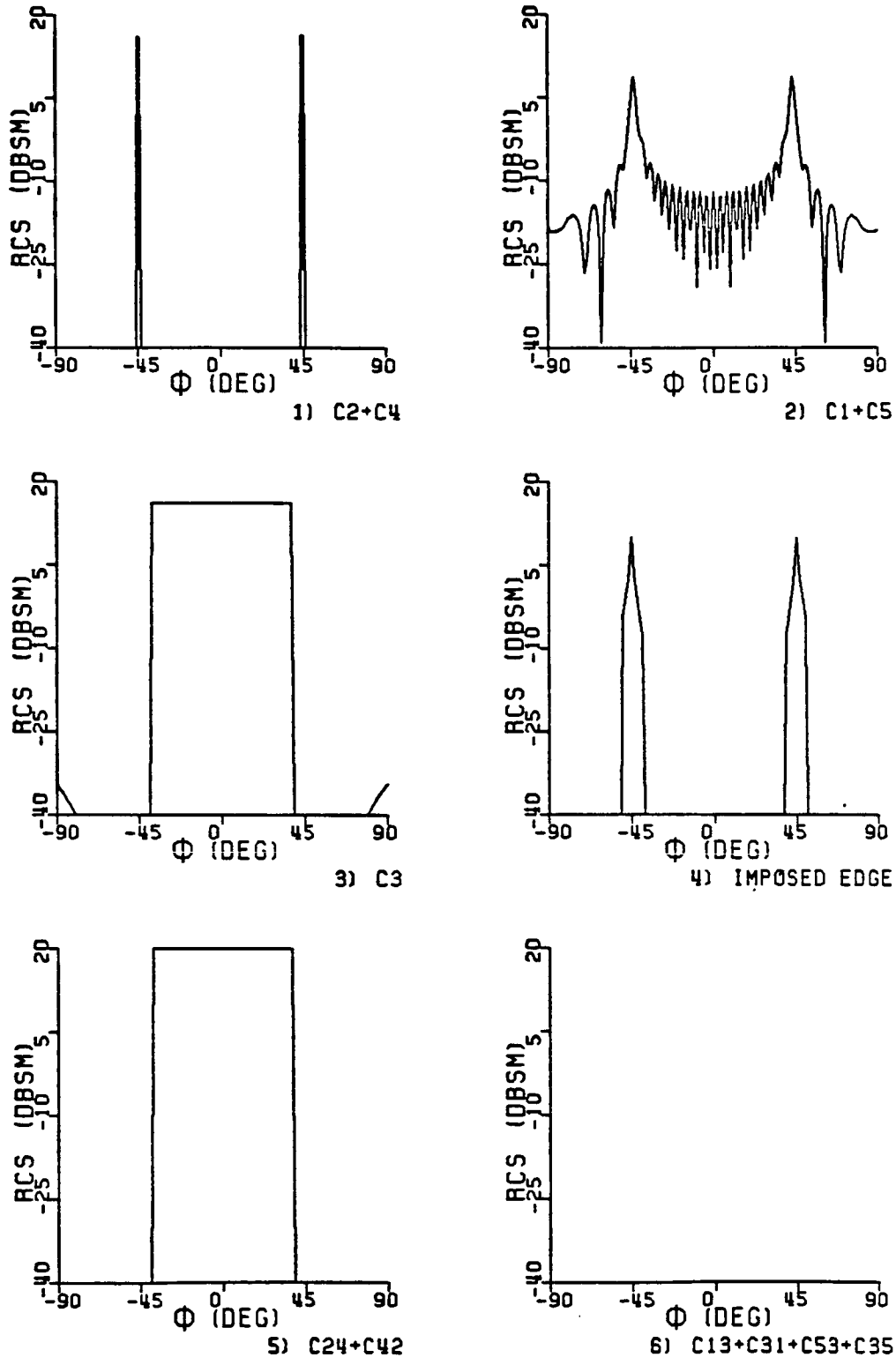

Fig. 5-5. Components of the radar cross section of a 90° dihedral corner reflector using geometrical optics and geometrical diffraction (A = B = 5.6088 λ, vertical polarization, f = 9.4 GHz).

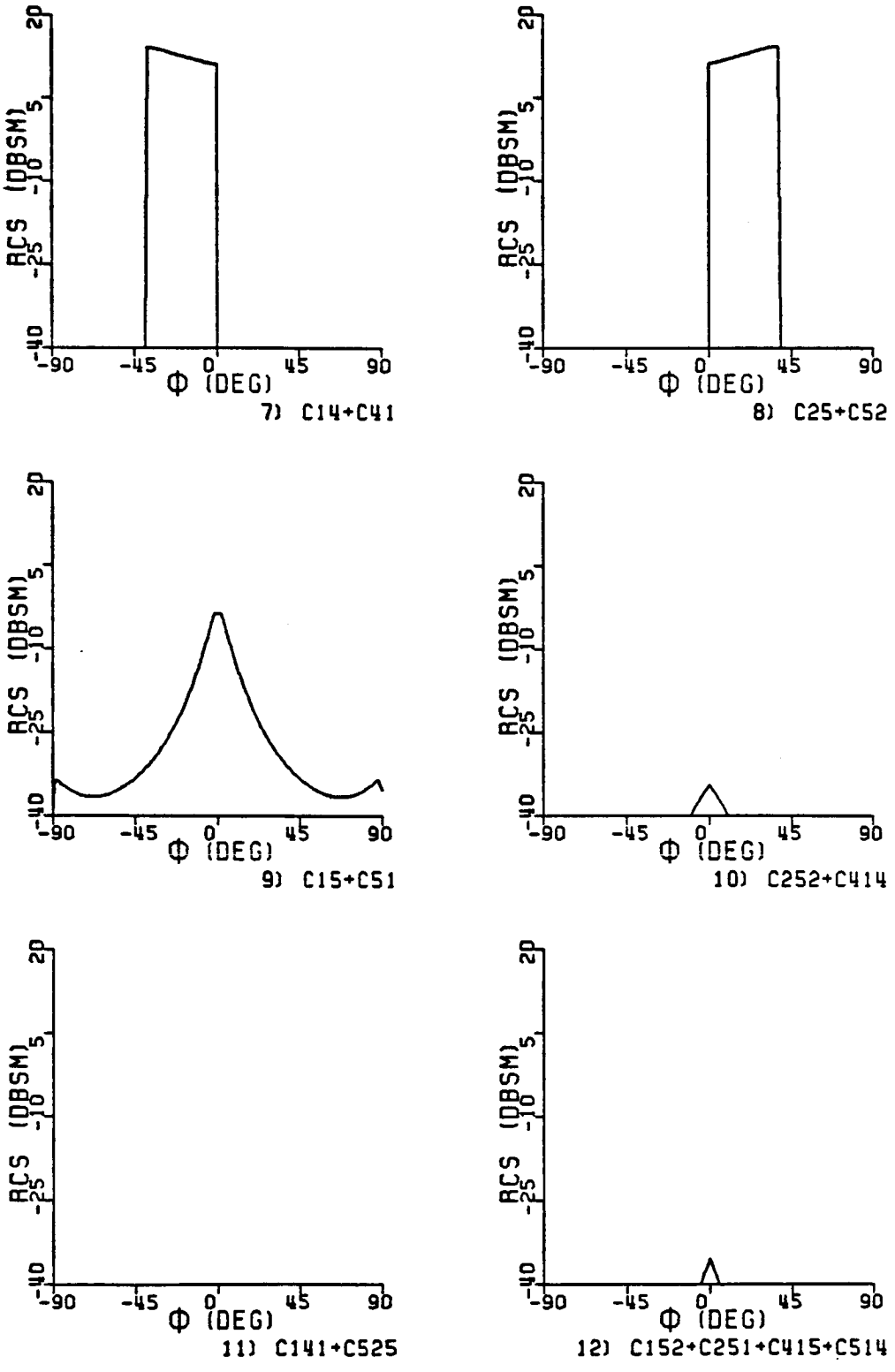

Fig. 5-5. (continued)

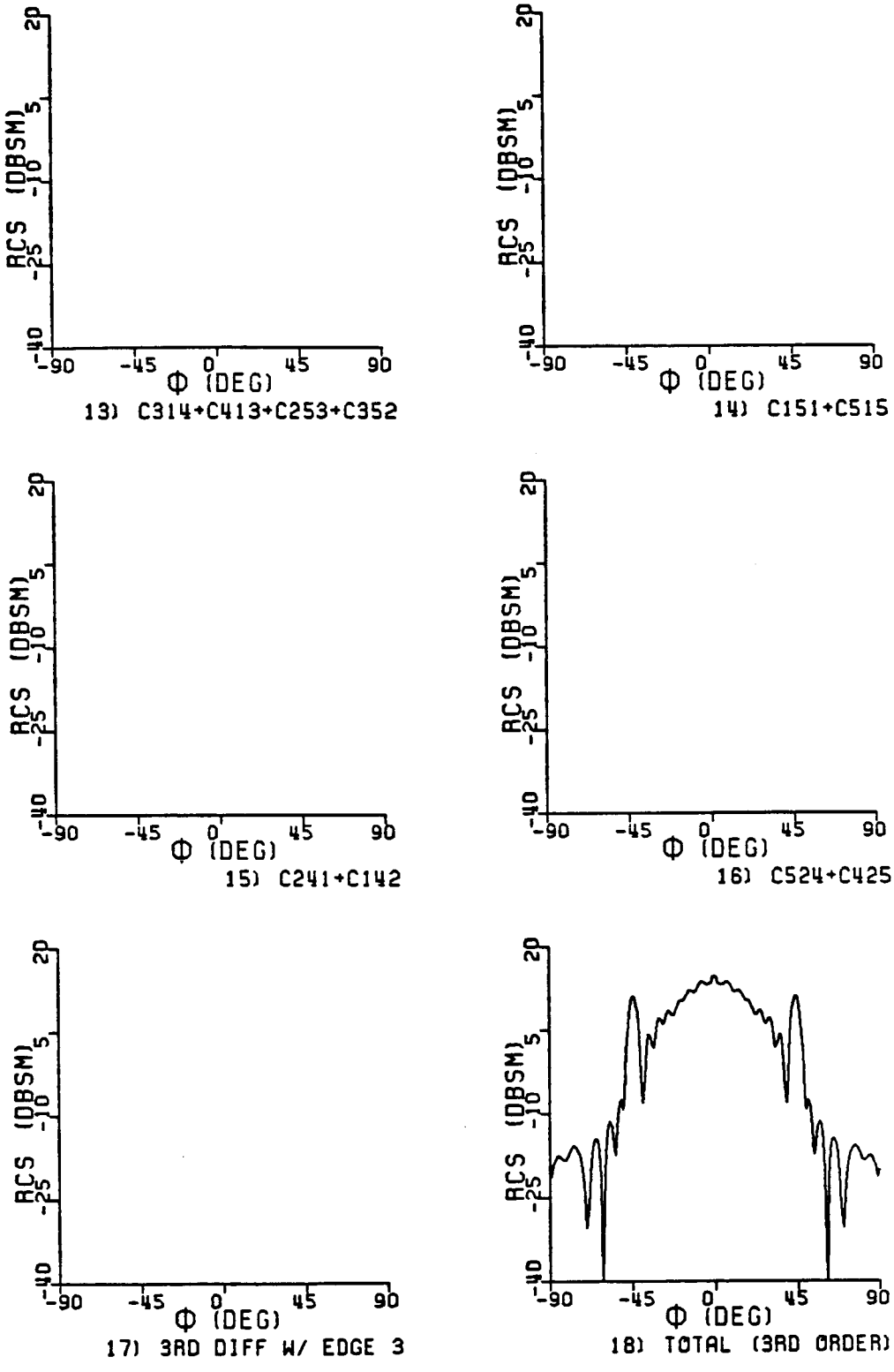

Fig. 5-5. (continued)

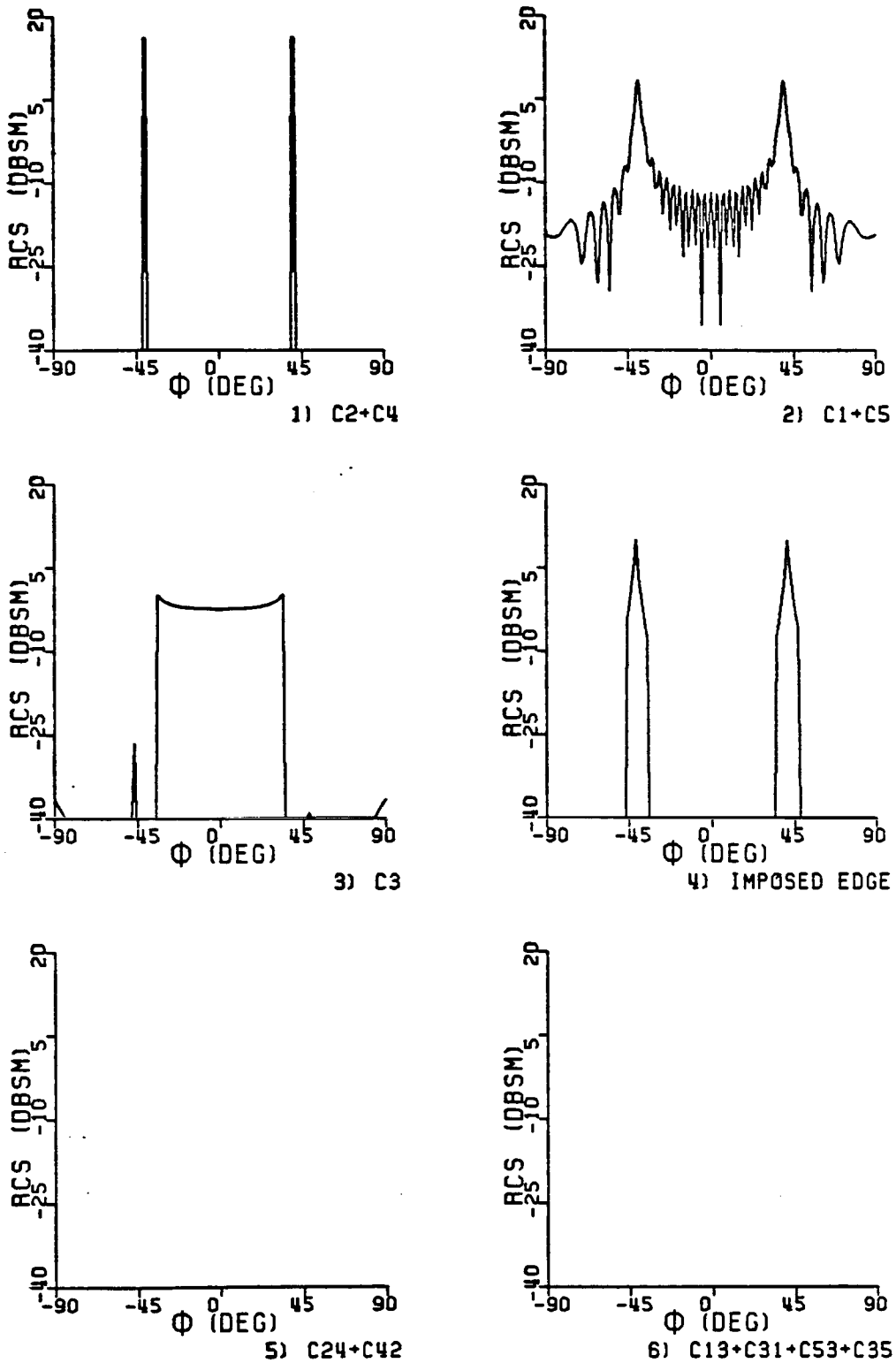

Fig. 5-6. Components of the radar cross section of a 98° dihedral corner reflector using geometrical optics and geometrical diffraction (A = B = 5.6088 λ, vertical polarization, f = 9.4 GHz).

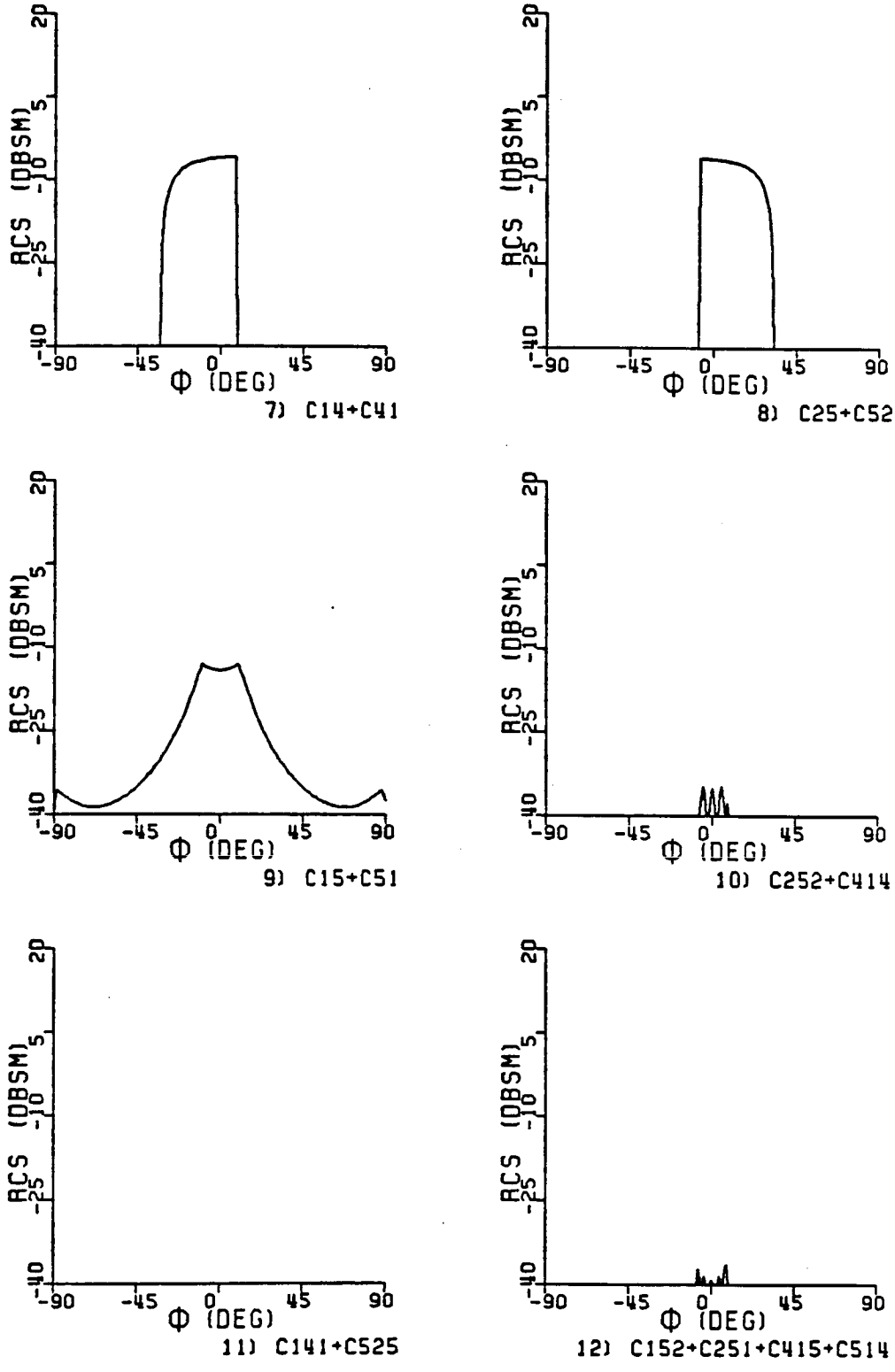

Fig. 5-6. (continued)

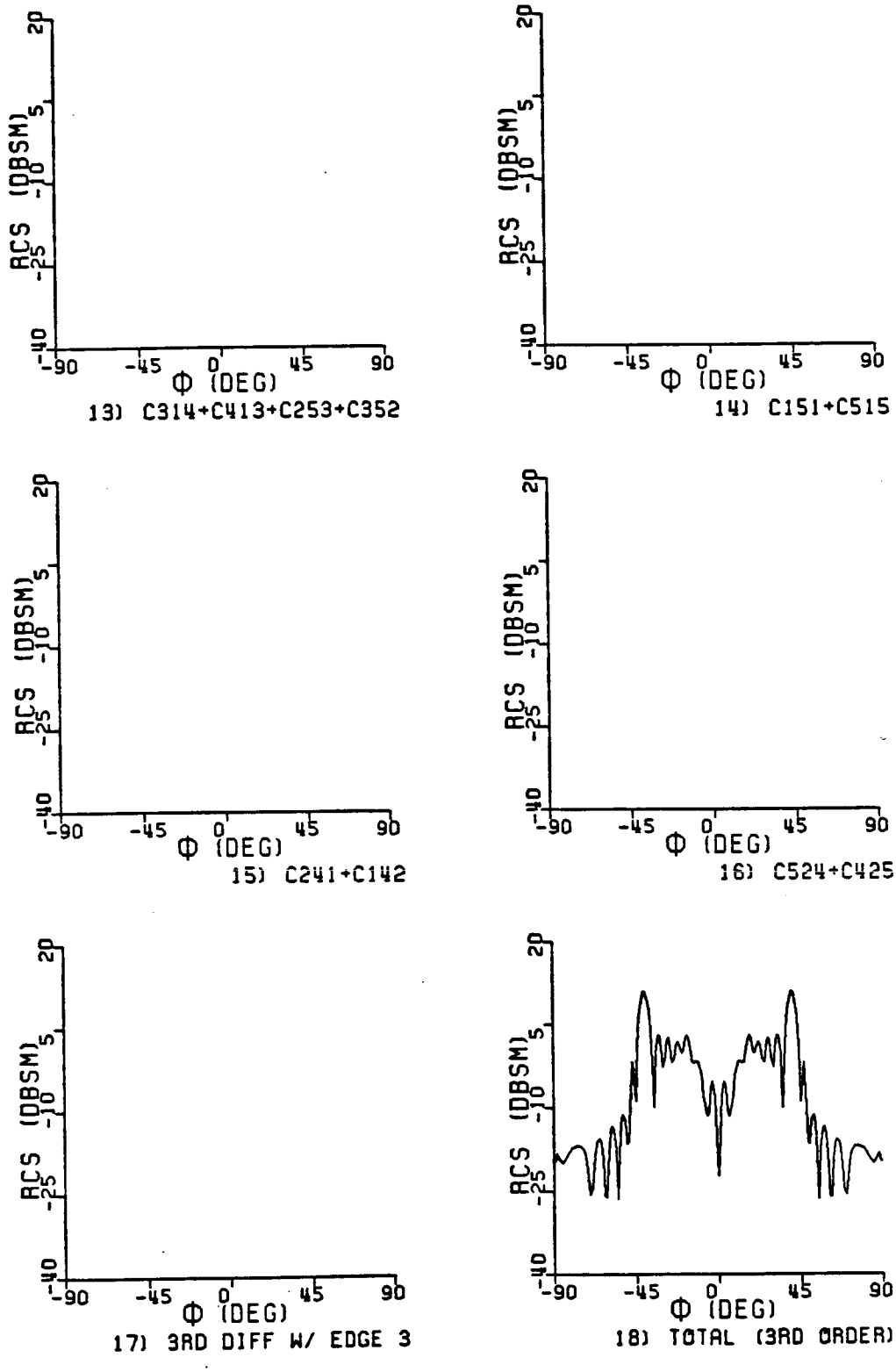

Fig. 5-6. (continued)

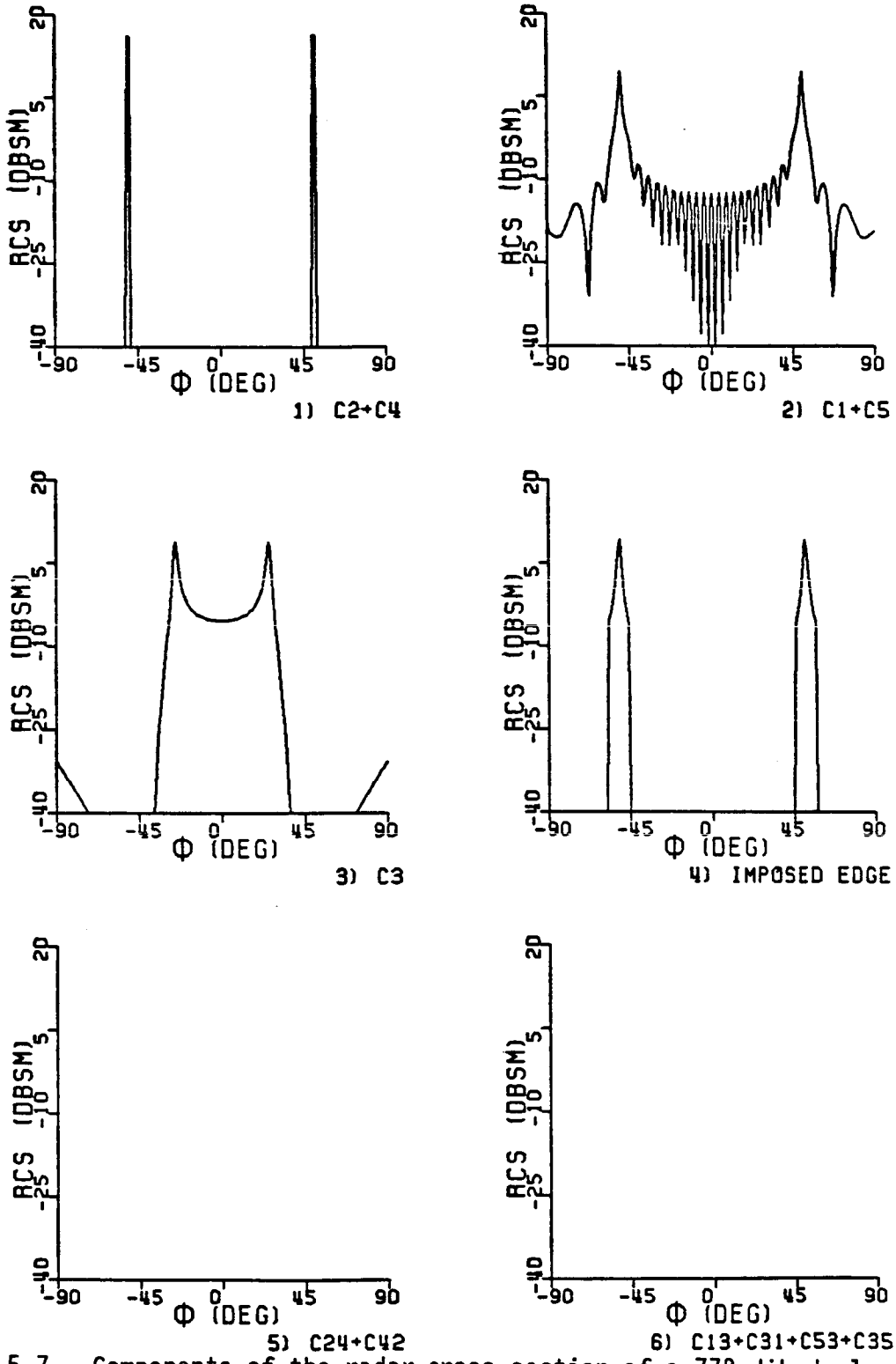

Fig. 5-7. Components of the radar cross section of a 77° dihedral corner reflector using geometrical optics and geometrical diffraction (A = B = 5.6088 λ, vertical polarization, f = 9.4 GHz).

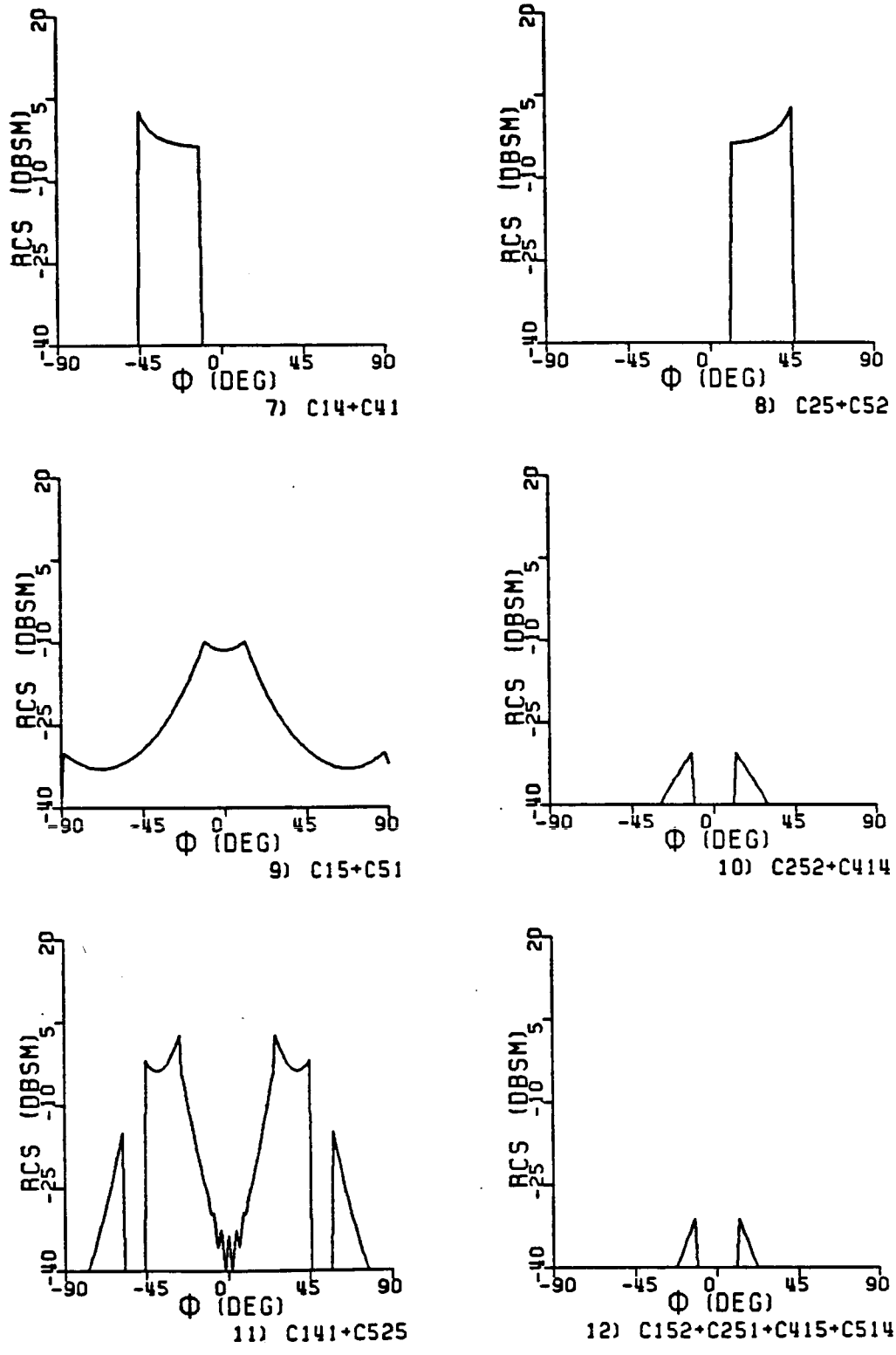

Fig. 5-7. (continued)

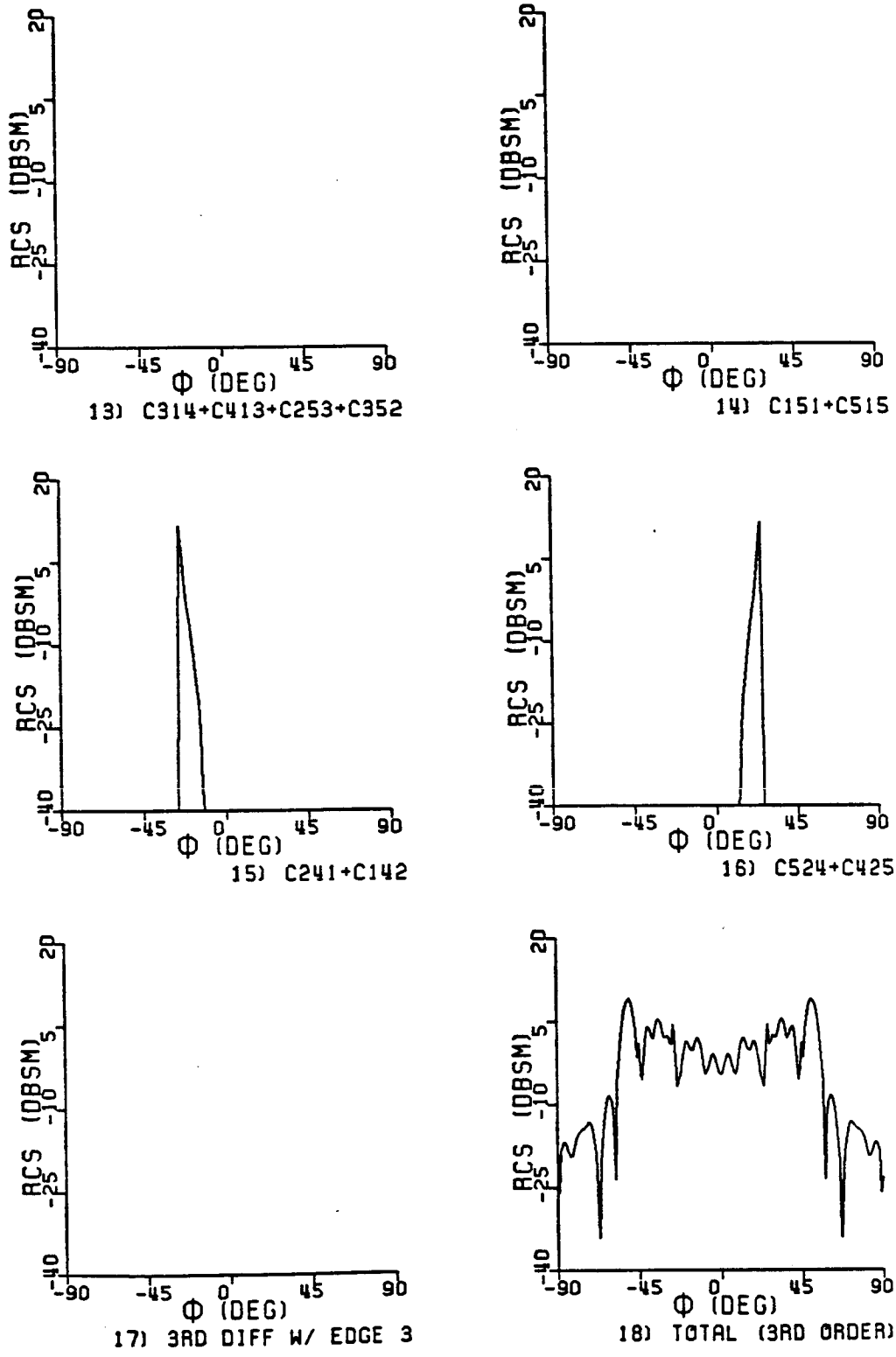

Fig. 5-7. (continued)

accuracy of the geometrical theories.

The third order reflections C242 and C424 were included in the analysis, but they are not shown in the figures because they do not contribute for the right and obtuse dihedrals, and they contribute over less then one half of one degree for the acute dihedral. The graphs of these figures were computer generated using one-degree increments and hence passed over the third order reflection contribution. It has been verified, using a expanded angular scale, that these third-order reflections are necessary to guarantee continuity of the cross section pattern over the half degree range through which they are nonzero.

In Figs. 5-8, 5-9, and 5-10 the backscatter cross section for horizontal polarization of the 90°, 98°, and 77° dihedral corner reflector is decomposed into individual components (in a similar manner as for the vertically polarized cases). Experimental results are not available for this case, but horizontal polarization is important to consider because the multiple diffraction terms are generally stronger for this polarization. In graph 17, all the third-order diffraction terms which included diffraction from the dihedral vertex are nonzero for the horizontal polarization. However, all these terms were zero for the vertical polarization. The total field is again shown in graph 18. Unfortunately, experimental data was not available for the horizontal polarization case so these results could not be compared with measurements.

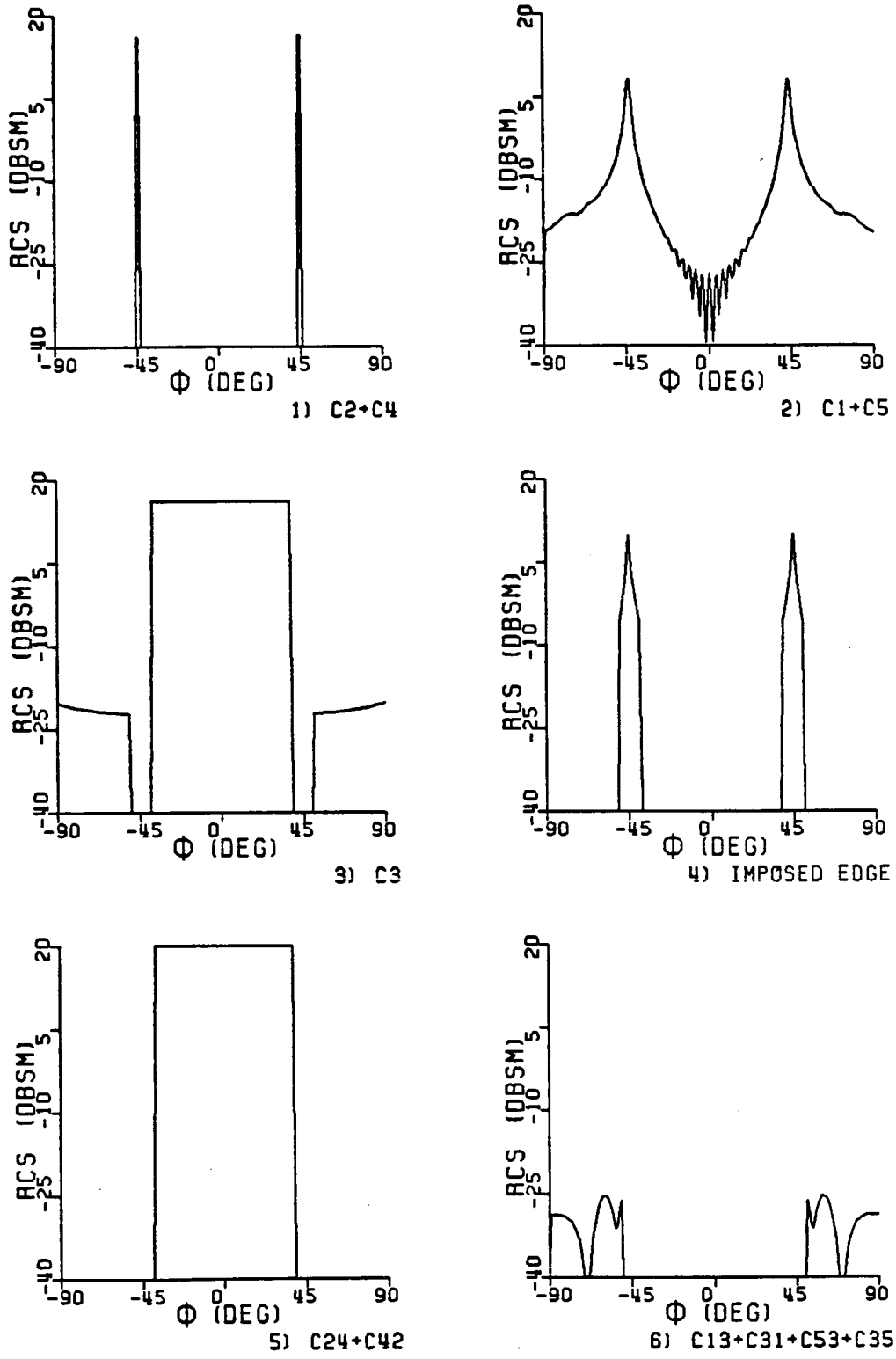

Fig. 5-8. Components of the radar cross section of a 90° dihedral corner reflector using geometrical optics and geometrical diffraction (A = B = 5.6088 λ, horizontal polarization, f = 9.4 GHz).

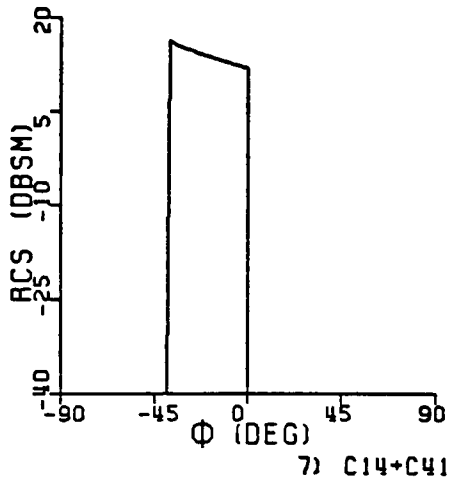

7) C14+C41

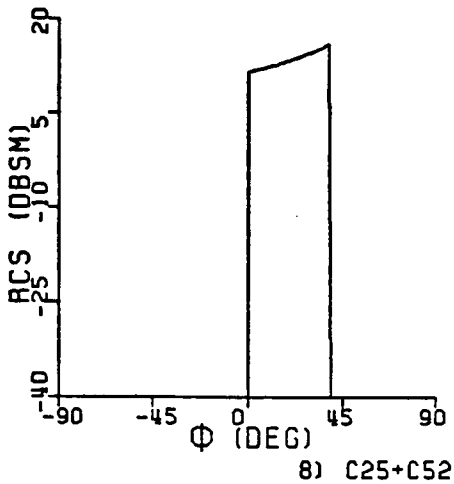

8) C25+C52

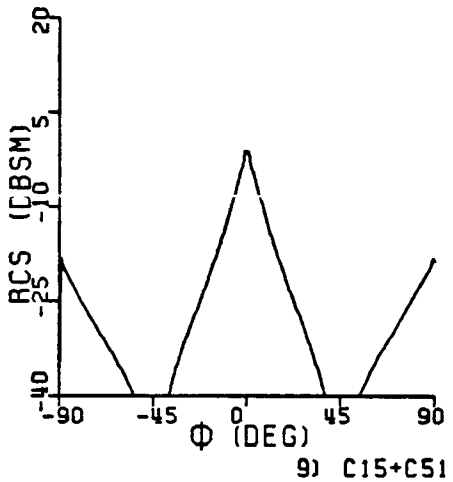

9) C15+C51

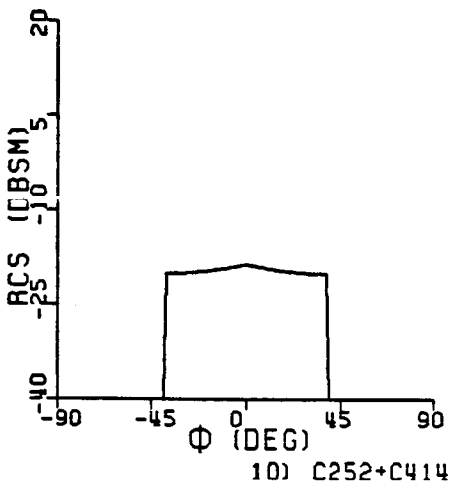

10) C252+C414

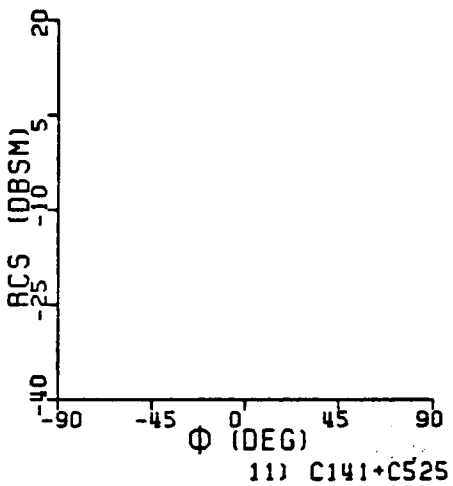

11) C141+C525

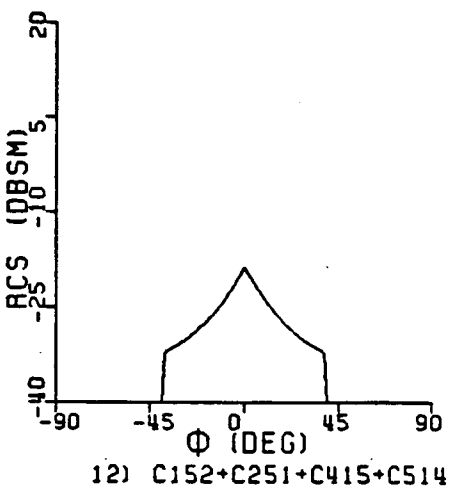

12) C152+C251+C415+C514

Fig. 5-8. (continued)

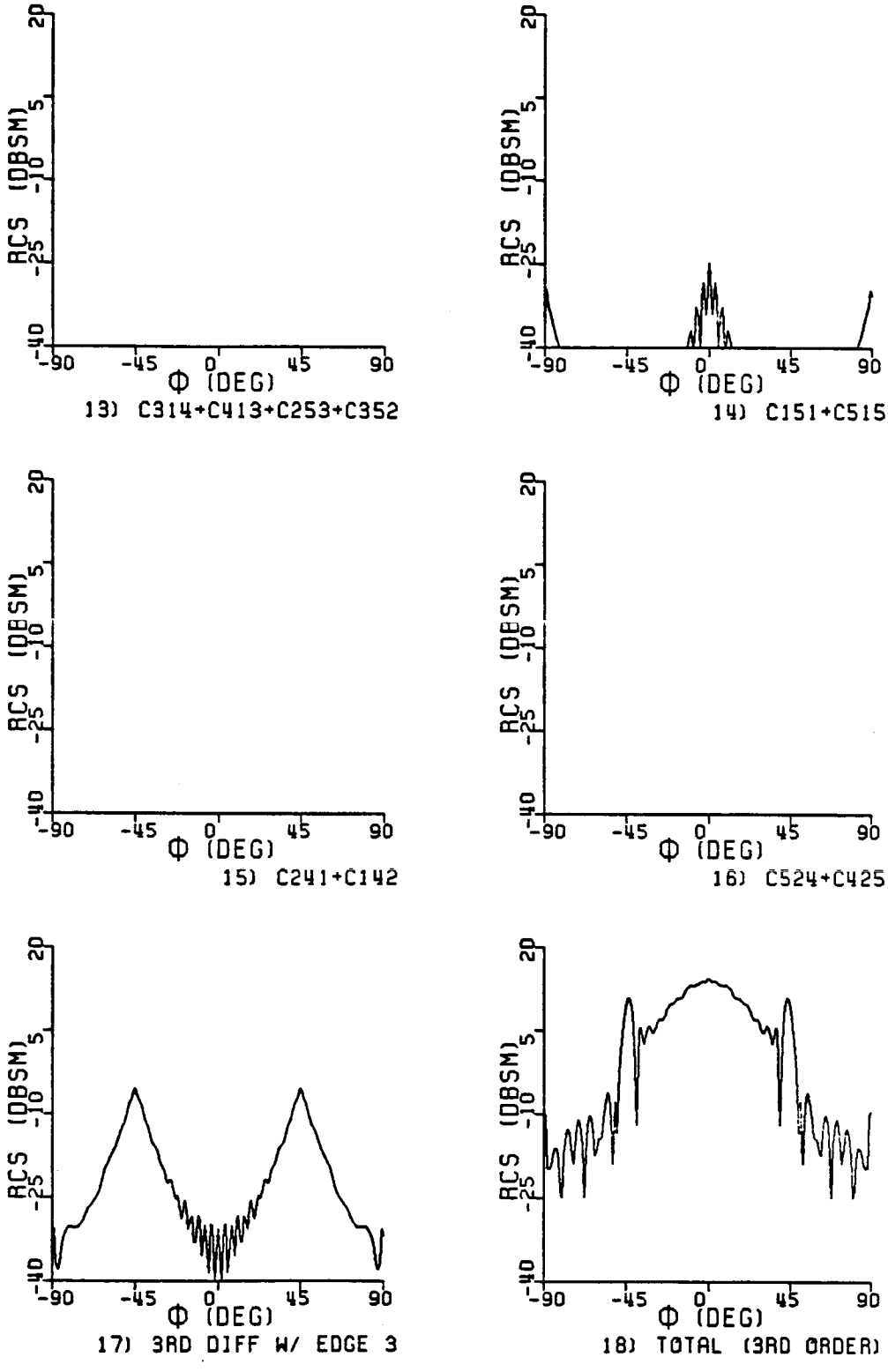

Fig. 5-8. (continued)

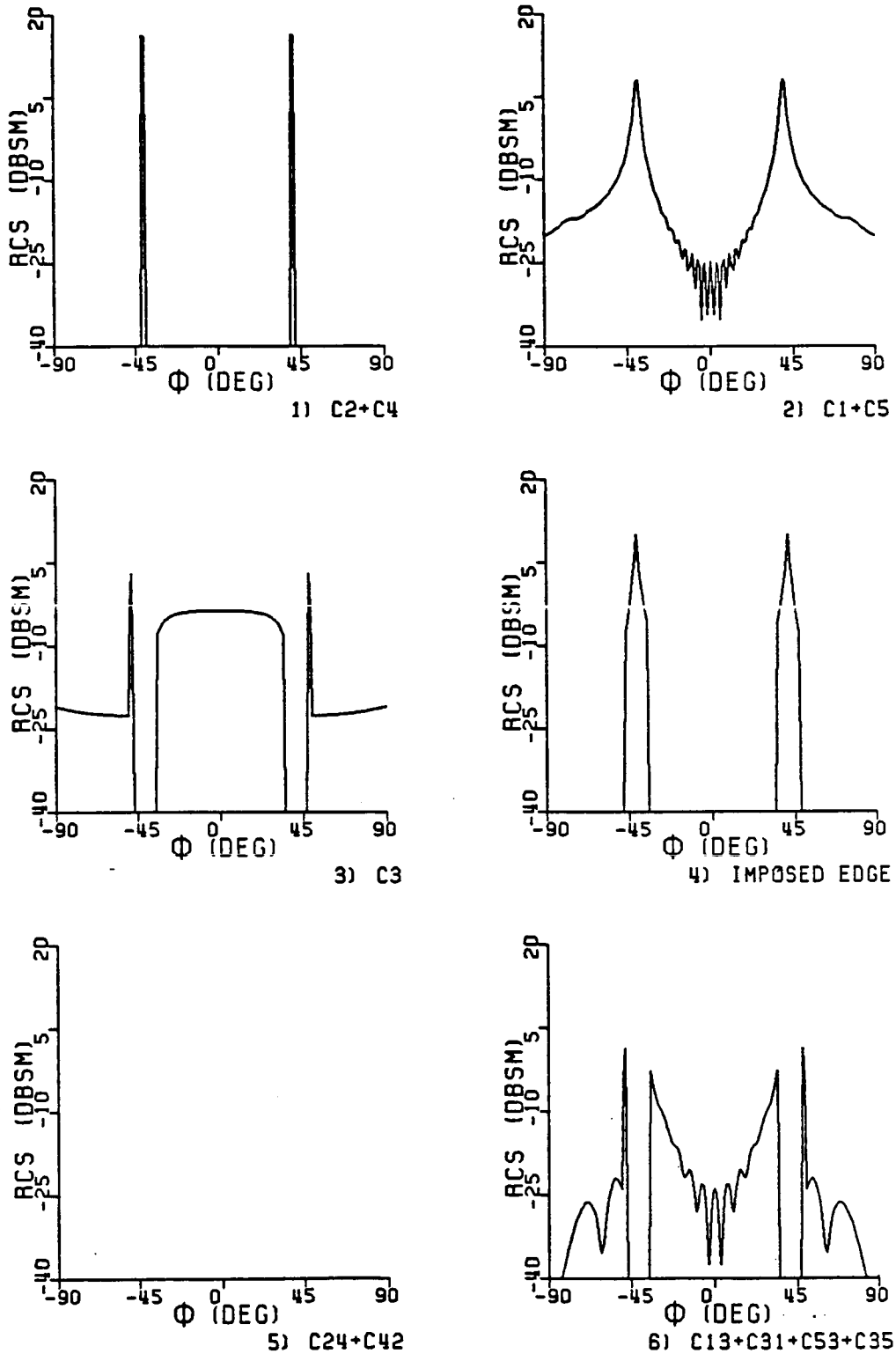

Fig. 5-9. Components of the radar cross section of a 98° dihedral corner reflector using geometrical optics and geometrical diffraction (A = B = 5.6088 λ, horizontal polarization, f = 9.4 GHz).

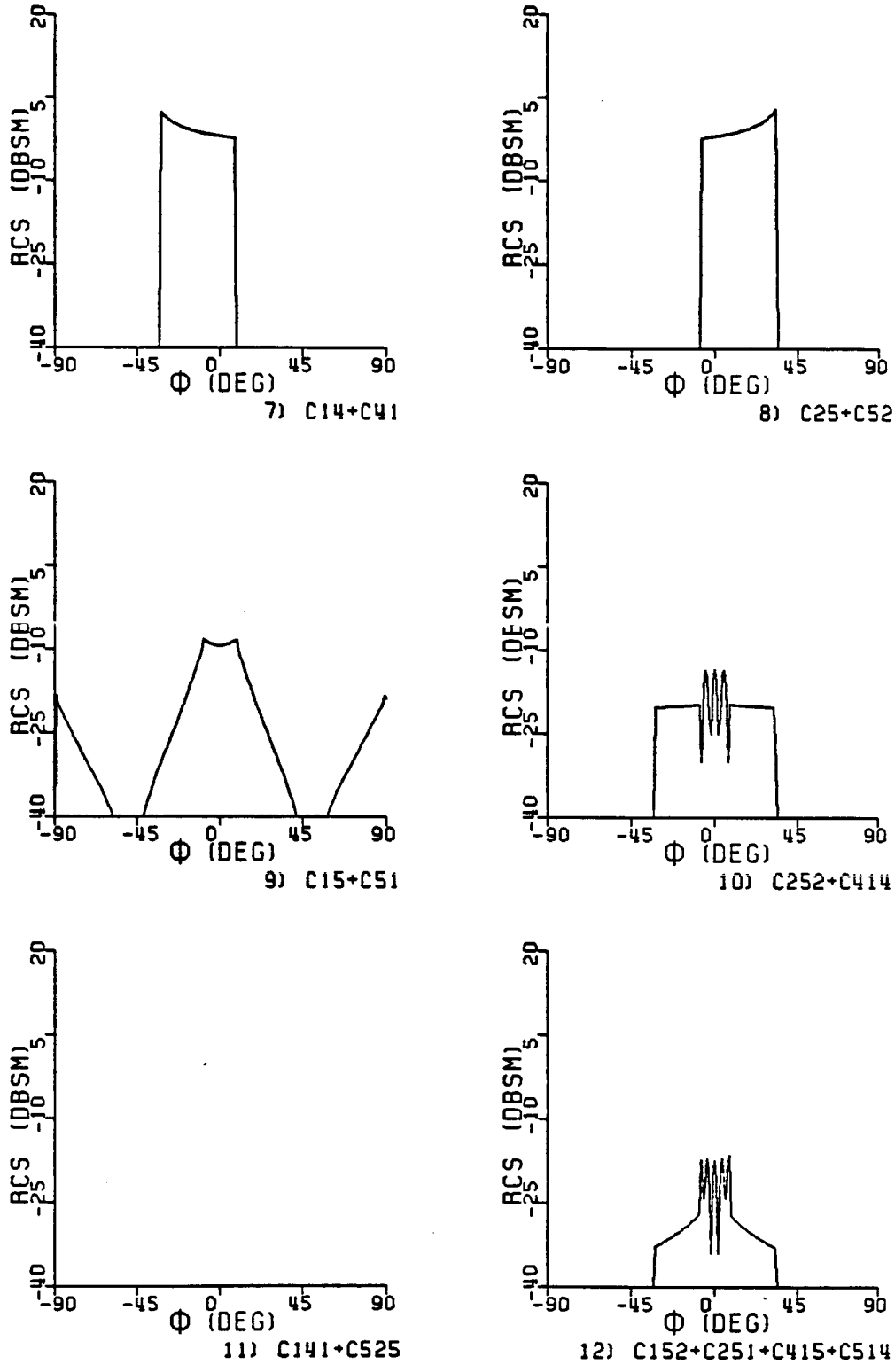

Fig. 5-9. (continued)

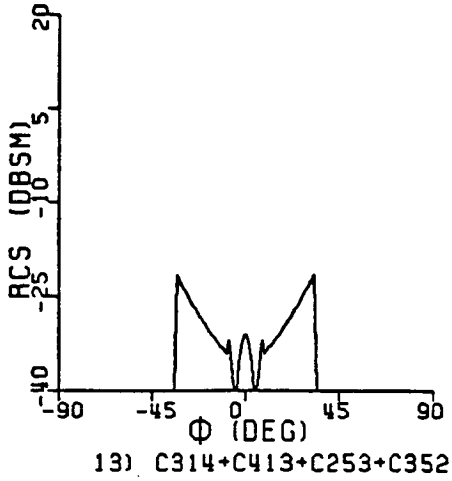

13) C314+C413+C253+C352

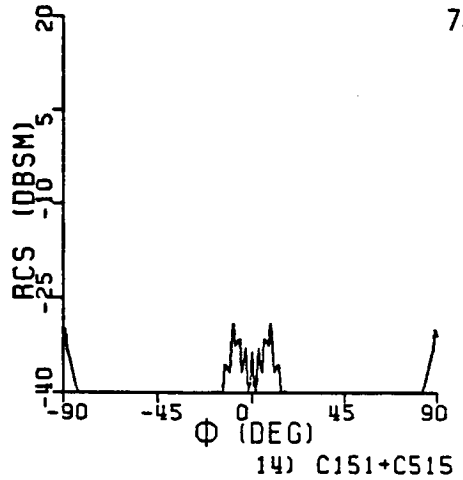

14) C151+C515

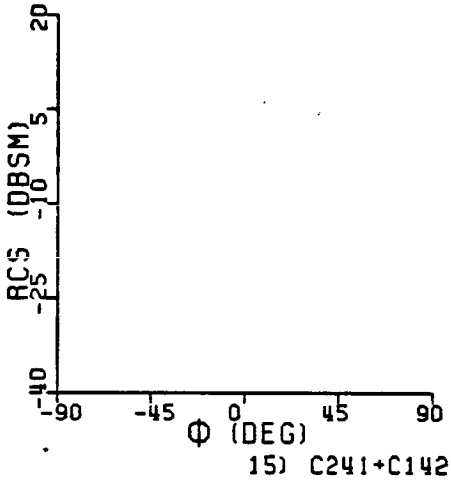

15) C241+C142

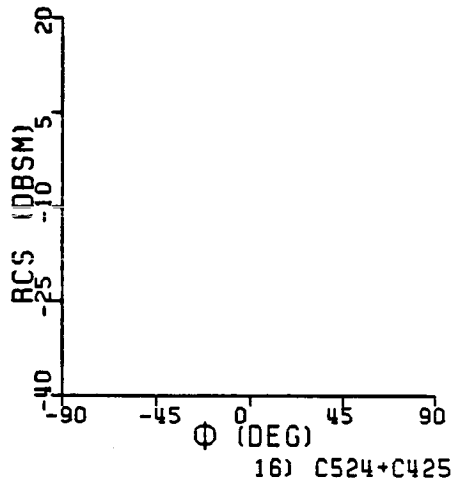

16) C524+C425

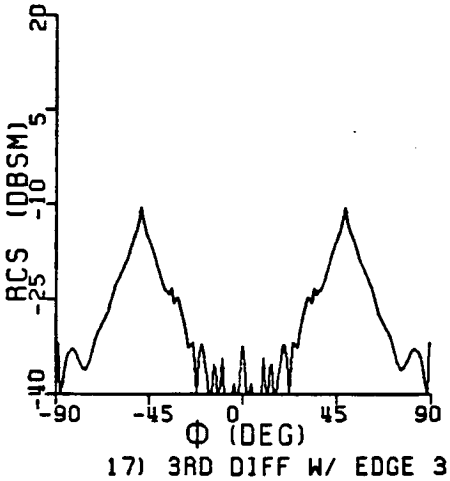

17) 3RD DIFF W/ EDGE 3

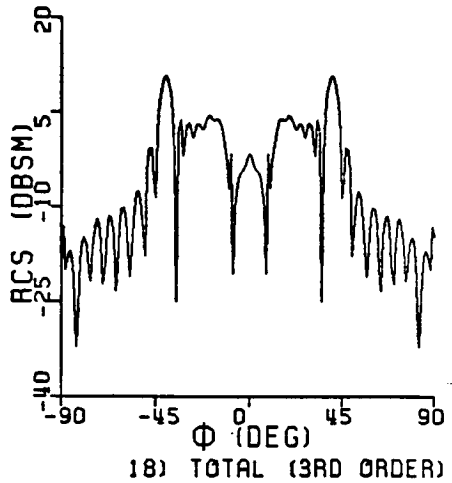

18) TOTAL (3RD ORDER)

Fig. 5-9. (continued)

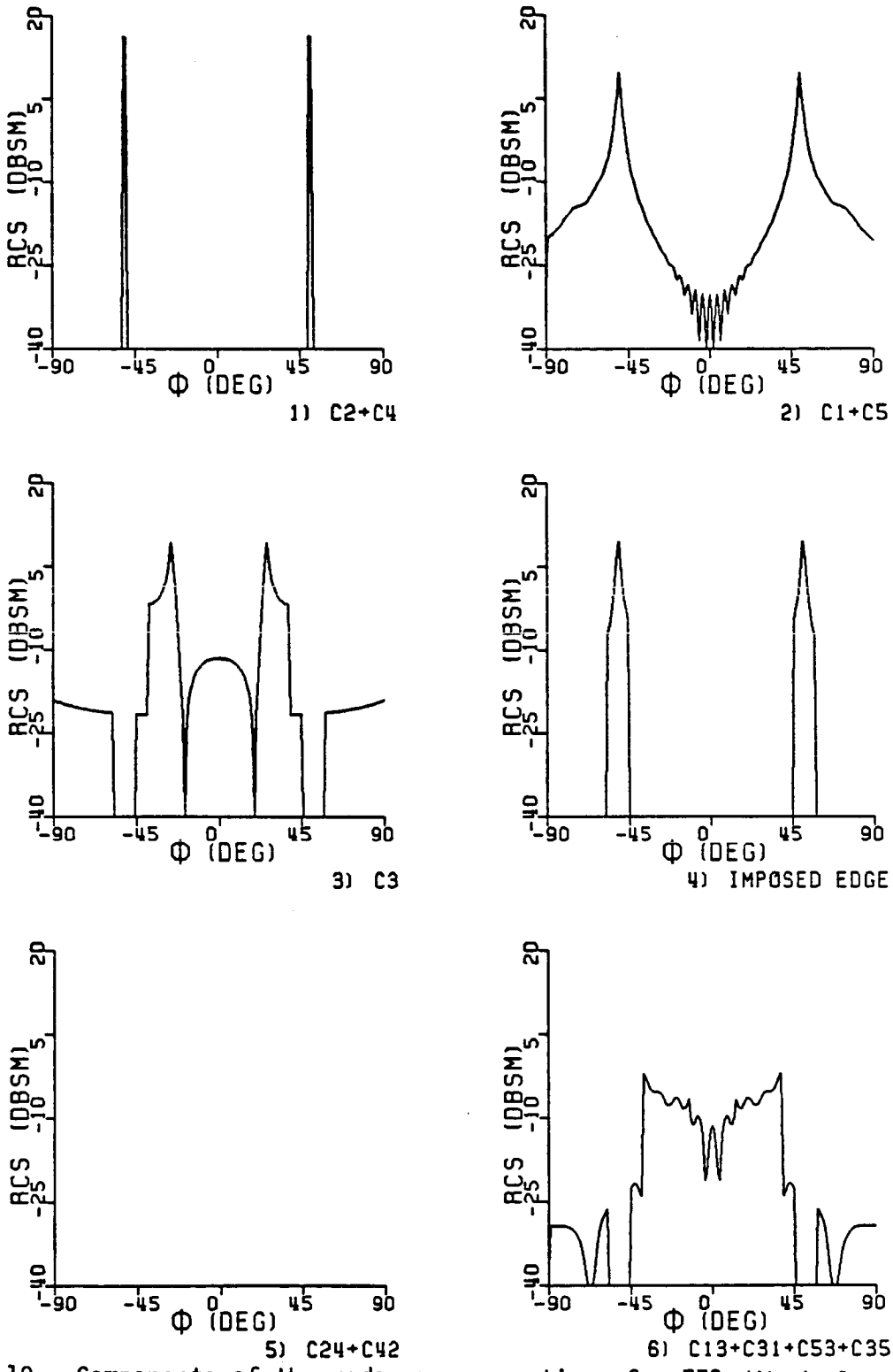

Fig. 5-10. Components of the radar cross section of a 77° dihedral corner reflector using geometrical optics and geometrical diffraction (A = B = 5.6088 λ, horizontal polarization, f = 9.4 GHz).

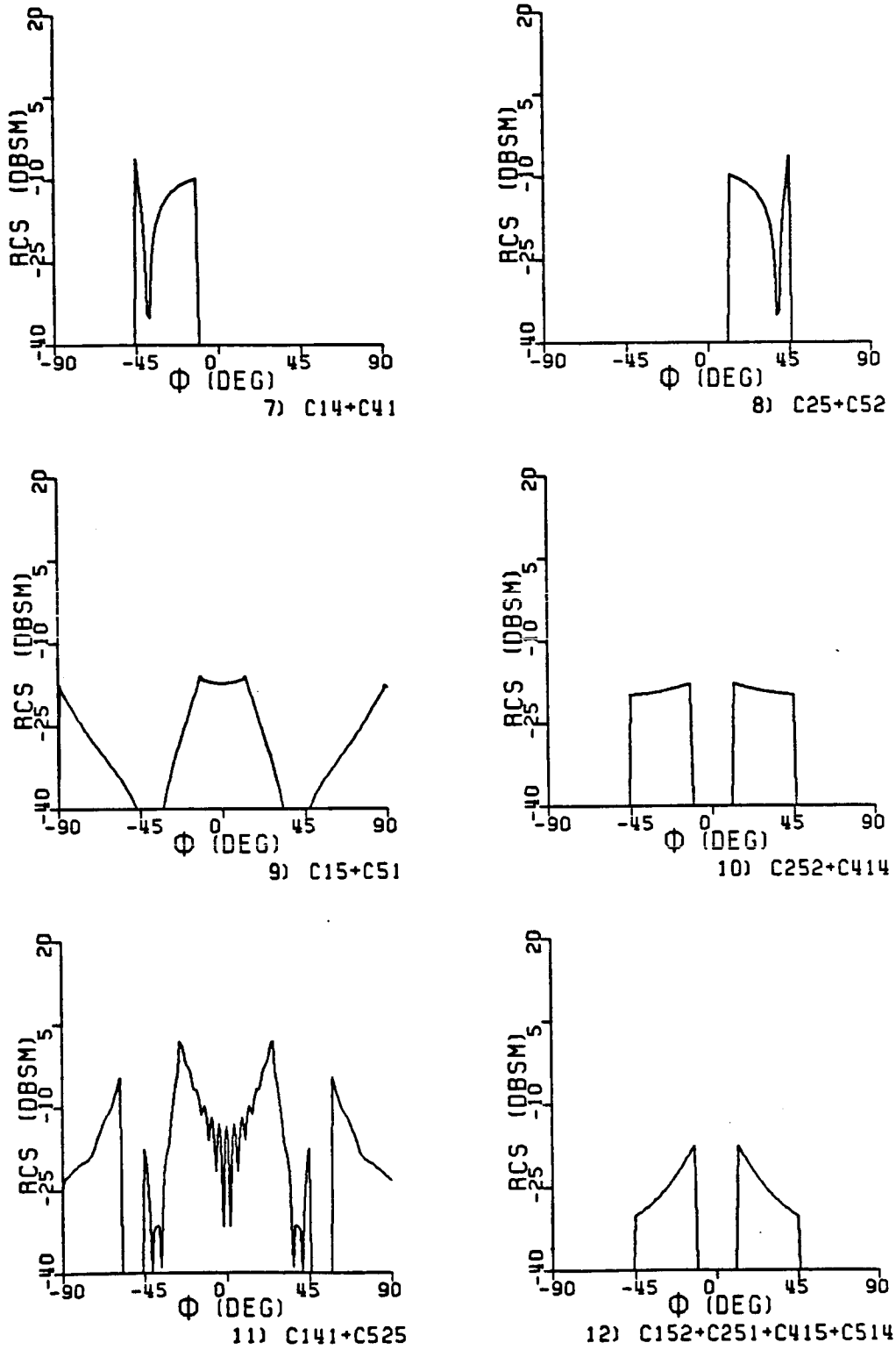

Fig. 5-10. (continued)

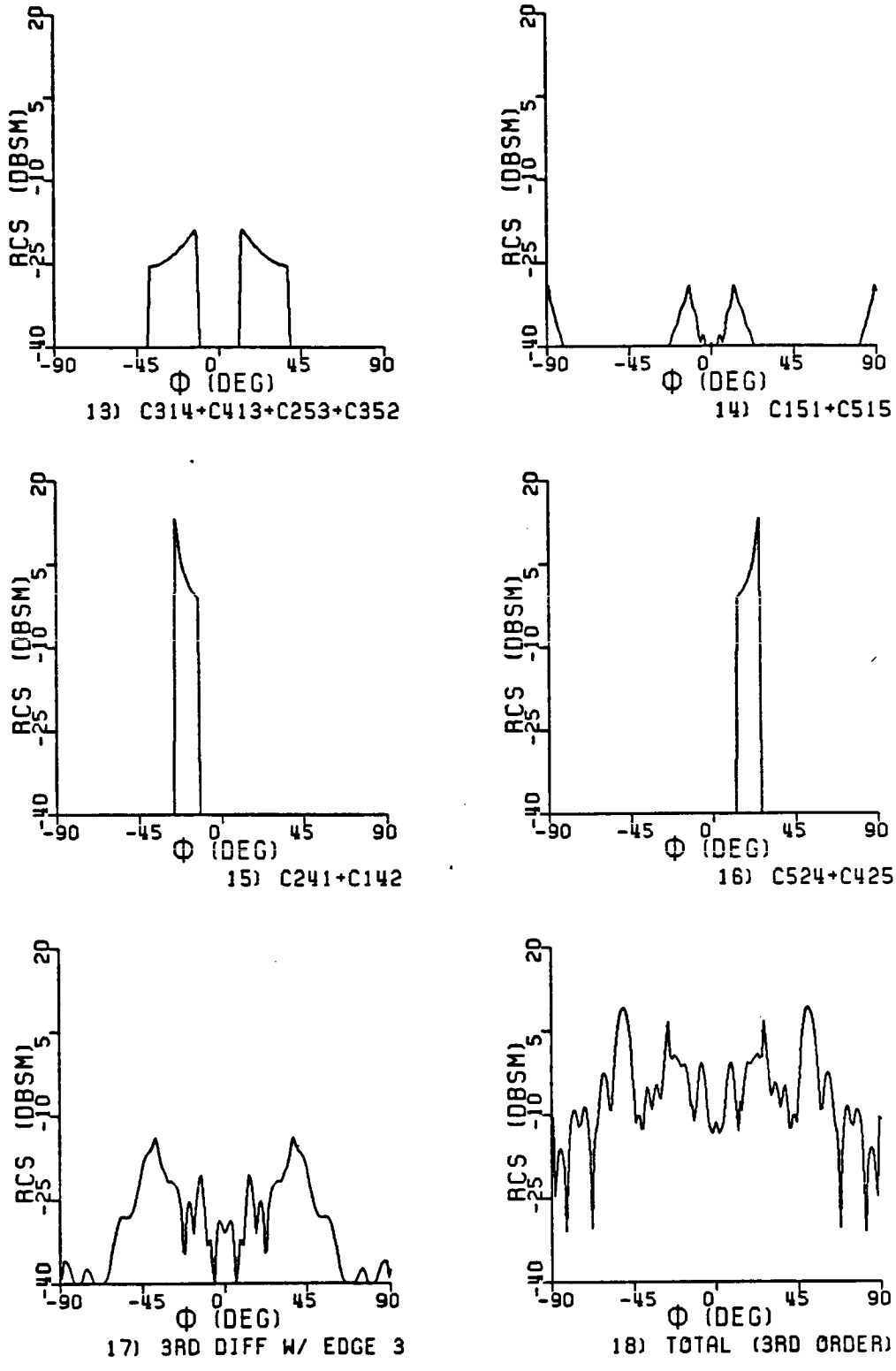

Fig. 5-10. (continued)

CHAPTER 6

PHYSICAL THEORY ANALYSIS OF A CORNER REFLECTOR

6.1 Dihedral Geometry

The physical optics theory and the physical theory of diffraction provide an efficient method for determining the reflected and diffracted fields from an object composed solely of flat plates which is illuminated by an incident plane wave. The accuracy of this theory can be best evaluated by application of the theory to an actual scattering problem for which experimental results are available.

The dihedral corner reflector, described in Section 5.1 and illustrated in Fig. 5-1, is studied using the physical optics theory and the physical diffraction theory in this chapter. Again the backscatter cross section in the azimuthal plane as a function of observation angle is found, just as in Chapter 5, in order that the accuracy of GTD and PTD can be contrasted.

6.2 Method of Analysis

For the analysis of the dihedral corner reflector using the theories of physical optics and physical diffraction, the best technique of analysis was found to be the equivalent current method described in Chapter 4. The PO and PTD fields, being continuous and well behaved, allow approximations in the calculations of diffraction and reflection angles and distances, most notably the so-called far-field approximation. In the "far-field" approximation, distances are commonly approximated by the first term of a Taylor series expansion when used as amplitude variations. When used as the argument of a complex

exponential in phase calculations, they are approximated by the first two terms of the Taylor series expansion. Similarly in the "far-field" analysis, angles (such as ψ and ψ_0 used in the diffraction coefficients) can be found using the approximation that all rays from the target to the distant observation point are parallel. These approximations, permissible in the physical theory, were not allowed in the geometrical theory near shadow and reflection boundaries since small inaccuracies in ψ and ψ_0 can lead to large variations in the diffracted fields and discontinuities in the cross section pattern.

When using the theory of physical optics, the first task in the analysis of the dihedral corner reflector is to identify, for a particular aspect, the illuminated and nonilluminated portions of each plate of the reflector. As illustrated in Fig. 6-1, the illuminated portions are determined using ray tracing methods. In this figure it is convenient to consider the direction of an incident plane wave to be fixed, and allow the corner reflector to be rotated. The results, of course, are identical to those obtained by leaving the dihedral fixed and rotating the incident field direction. The choice of method is purely a matter of convenience.

In Fig. 6-1, only the illuminated portion of Plate II is considered for the single reflected field C4, and Plate I is temporarily ignored except for the shadowing effect it creates at certain aspects. In Fig. 6-2, the illuminated portion of Plate II is identified considering only the double reflected field component C24. In these figures, the lower row illustrates different orientations of the dihedral corner relative to the incident field. In the upper row, the

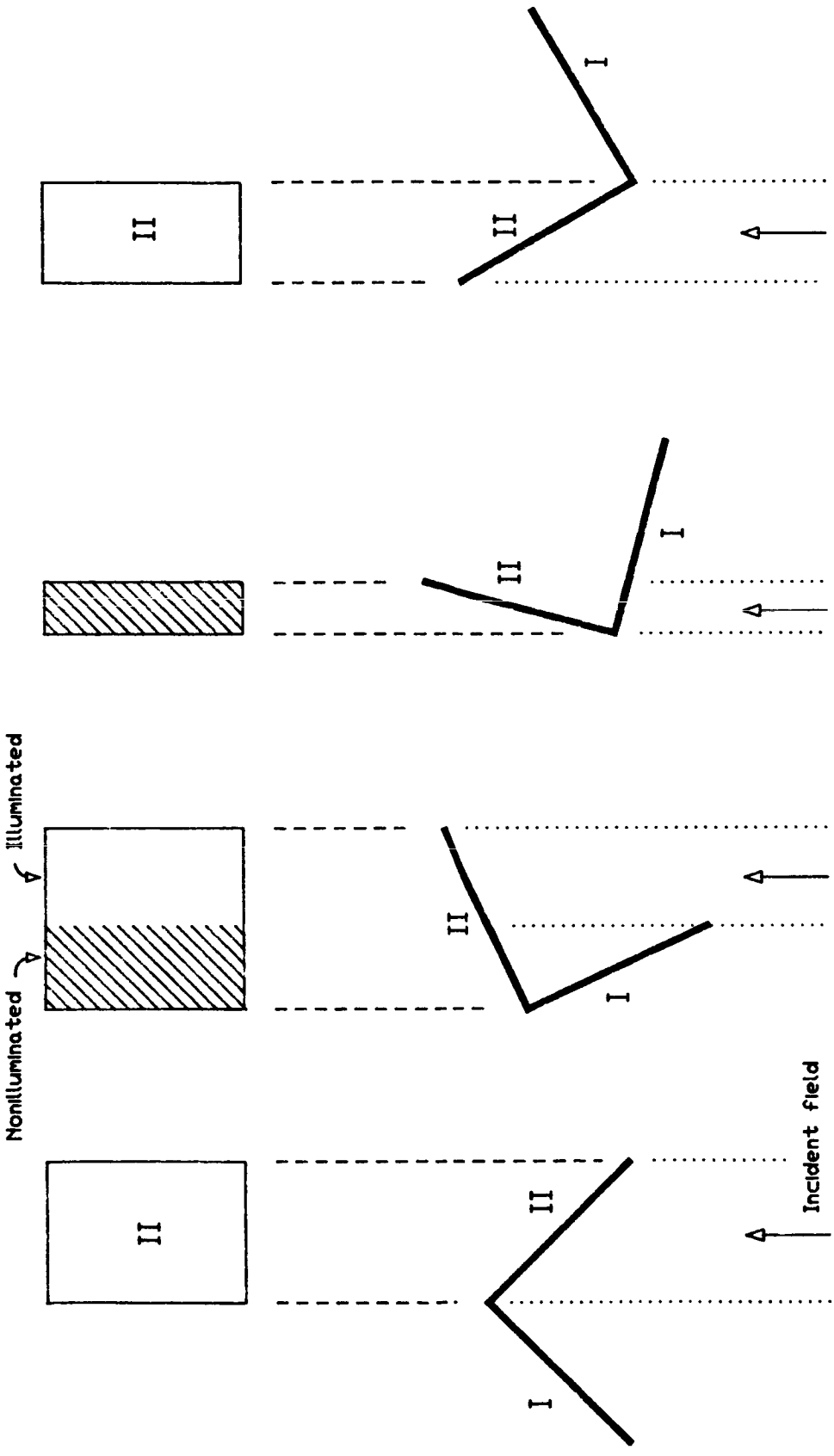

Fig. 6-1. Illuminated portions of one plate of the dihedral corner.

projected view of the illuminated plate (Plate II) is illustrated with the shaded regions indicating nonilluminated regions and the nonshaded regions indicating illuminated regions. Depending upon the orientation of the dihedral corner reflector, Plate II may be entirely, partially or not at all illuminated by the singly and doubly reflected field.

If the methods of analysis presented in [16] are employed, the theories of physical optics and physical diffraction can be conveniently utilized to determine the backscattered fields. The surface integrals associated with physical optics and the line integrals associated with physical diffraction are obtainable in closed form, and they are readily amenable to computer implementations.

Most of the geometry relationships necessary for the physical analysis are identical to those already presented in Chapter 5. The essential method used in finding the reflection terms begins by identifying the corners of the illuminated portion of each plate for different orientations. It happens that in the azimuthal plane cross section analysis, these illuminated portions are always rectangular for the dihedral corner reflector. It is not difficult to then integrate the induced physical optics current density across the plate since the current density is uniform in amplitude and linear in phase across the plate. For the diffracted fields, the directions of incidence and observation can be calculated using exactly the same methods utilized in the geometrical analysis. Even simpler formulations can be obtained using the far-field approximations wherein all rays from the distant source to the dihedral are considered parallel. Once the directions of incidence and diffraction are known, the diffraction parameters ψ, ψ_0 ,

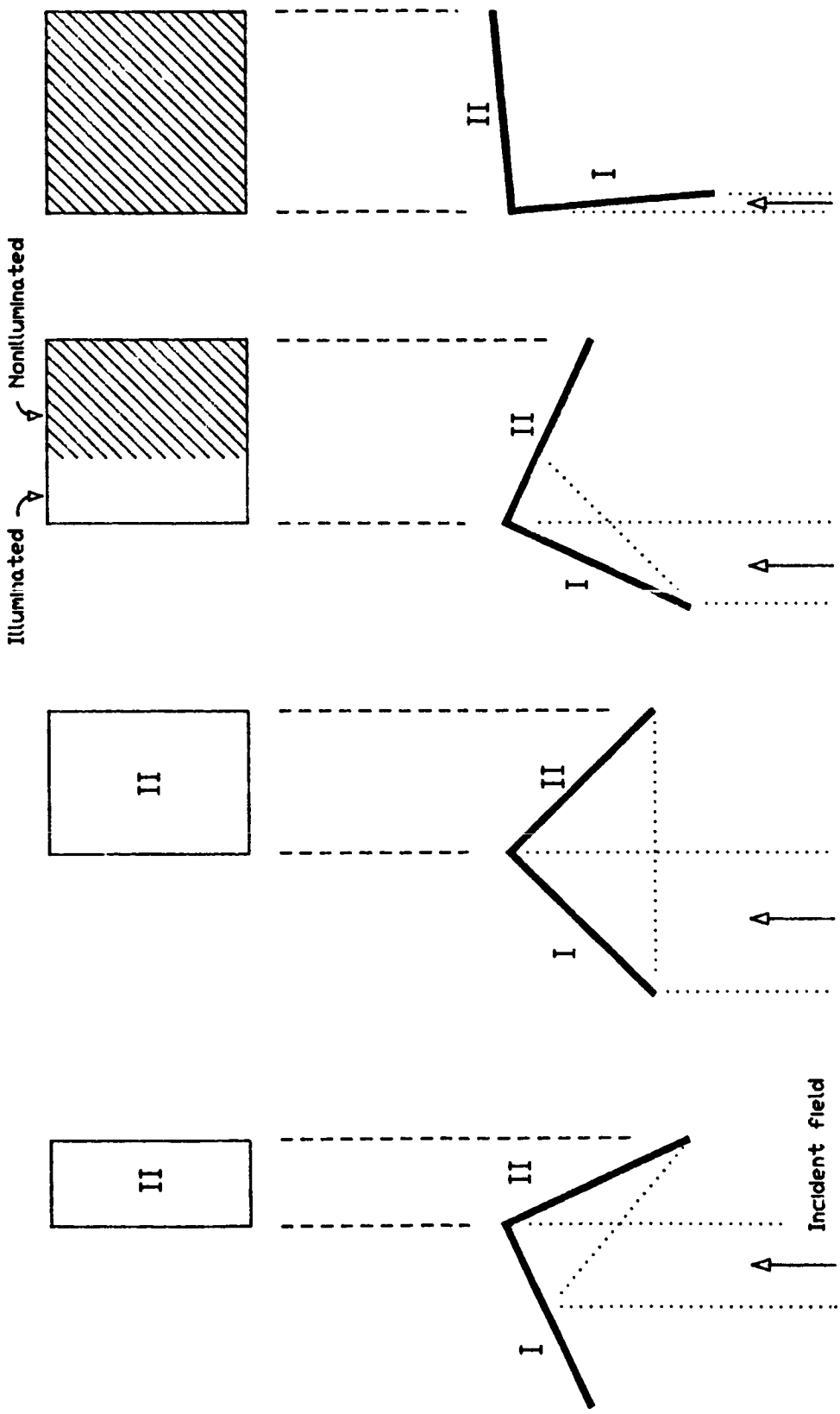

Fig. 6-2. Illuminated portions of one plate of the dihedral corner due to a geometrical reflection from the opposing plate.

and n are used to determine the equivalent edge currents using (4-10) and (4-11). The field due to this current is obtainable from the line integrals of (4-6) and (4-7). These integrals are readily performed along the straight edges since the current is uniform in amplitude and linear in phase along the plate.

6.3 Alternate Methods for Double Reflections

The methods presented thus far for determining the physical optics field are especially convenient for objects composed of flat surfaces illuminated by an incident plane wave. Allowing initial reflections in a reflection/diffraction sequence to be analyzed geometrically using ray techniques maintains the planar nature of the incident field and subsequently renders the theory applicable to computer formulations.

The accuracy of this method when compared with experimental results is reasonably acceptable for the right and obtuse dihedral corner reflector, but it is not as accurate in the acute angle dihedral corner reflector case. To improve the accuracy for this case, a more rigorous analysis technique can be formulated using strictly physical optics theory for all reflections, particularly for the double reflected field. The formulation is presented in Appendix B for the vertical polarization radar cross section of a dihedral corner of arbitrary interior angle. This more rigorous approach does yield more accurate results for the acute angle dihedral in the forward region. However it is much more complex to formulate, and it is probably not tractable for many of the more complex geometries.

It is interesting to compare the current density which exists on

the second plate of the acute dihedral corner reflector due to the double reflection mechanism when either geometrical optics or physical optics is used for the first reflection. If geometrical optics is utilized for the first reflection, the incident field on the second plate (Plate II of Fig. 5-1) is uniform over the illuminated portion of the second plate and is zero over the remaining nonilluminated portion. However, if physical optics is utilized for the first reflection, the incident field on the second plate is found from a complicated integral expression which exists over both the illuminated and nonilluminated regions of the plate. The physical optics approximation may be used to find the current density on the second plate given the incident magnetic field. Hence the physical optics current density on the second plate (Plate II) could take one of two distributions; being proportional to either the incident geometrical optics field or the incident physical optics field.

The normalized amplitude of the current density J_{sz}^{PO} on Plate II, found using geometrical optics theory for the first reflection (on Plate I), is illustrated using contour plotting techniques in Figs. 6-3, 6-5, and 6-7. The corresponding three-dimensional patterns of the normalized current density amplitude are shown in Figs. 6-4, 6-6, and 6-8. The current density J_{sz}^{PO} is normalized to the value of the physical optics current J_{sz}^{GO} where J_{sz}^{GO} represents the physical optics current density which would exist in the illuminated portion of Plate II if geometrical optics theory was used for the first reflection. The current density in these figures has only its magnitude illustrated across the plate. On the contour plots a dashed vertical line has been drawn to indicate the

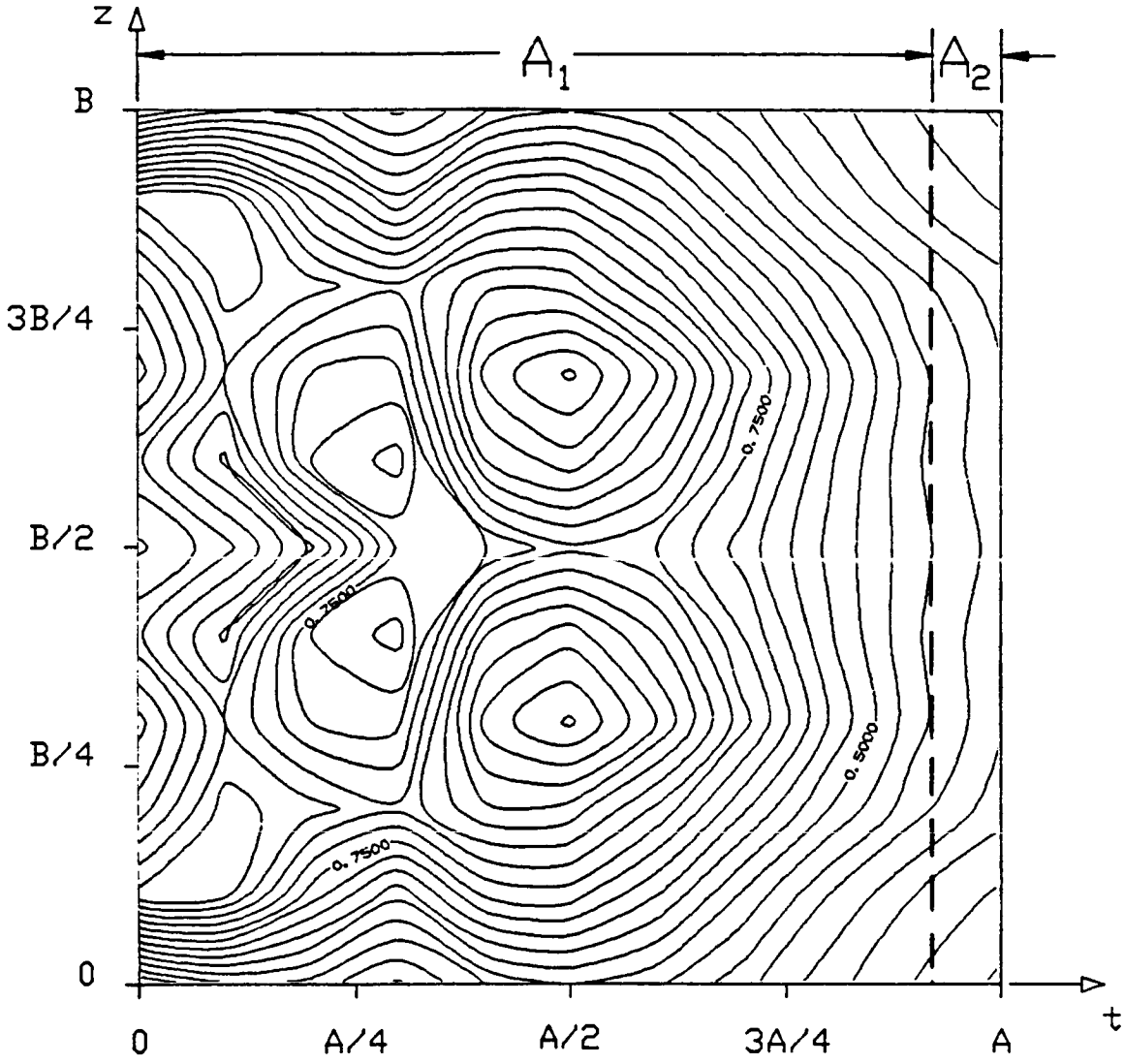

Fig. 6-3. Normalized physical optics surface current density on plate II due to the fields radiated by the physical optics surface current density on plate I. ($2\alpha = 77°$, $\phi = -10°$, $A = B = 5.6088\ \lambda$, vertical polarization).

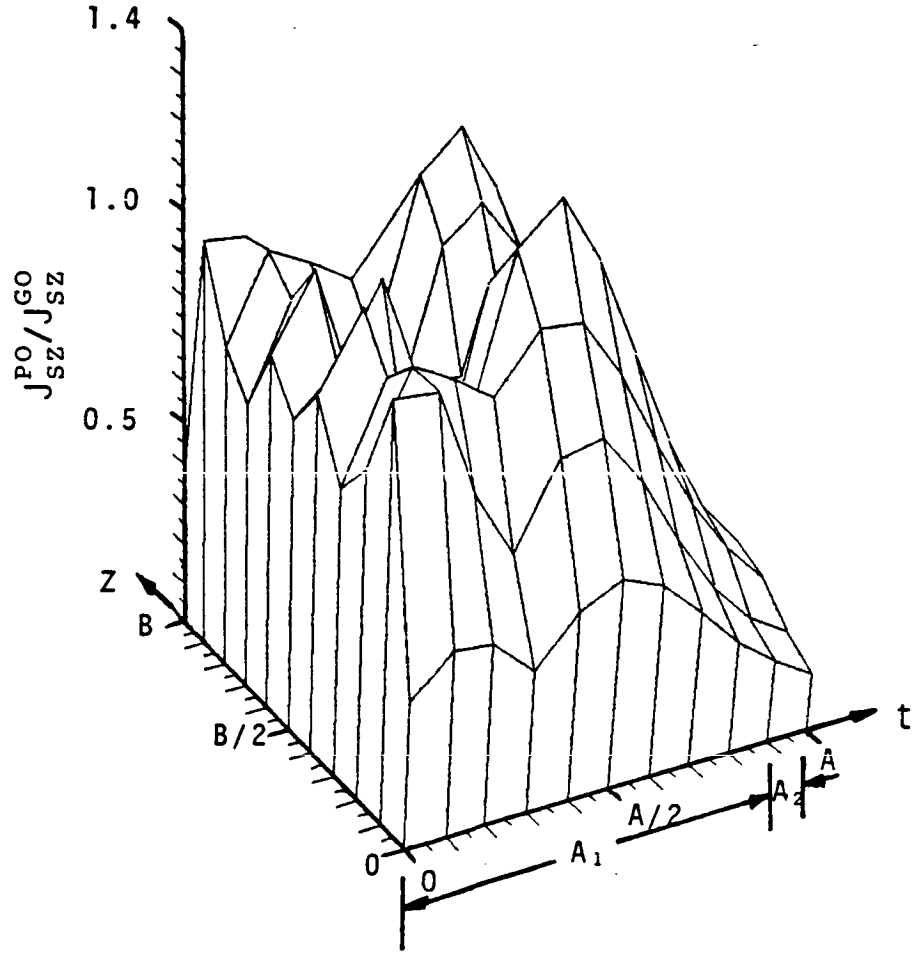

Fig. 6-4. Normalized physical optics surface current density on plate II due to the fields radiated by the physical optics surface current density on plate I. ($2\alpha = 77°$, $\phi = -10°$, $A = B = 5.6088\ \lambda$, vertical polarization).

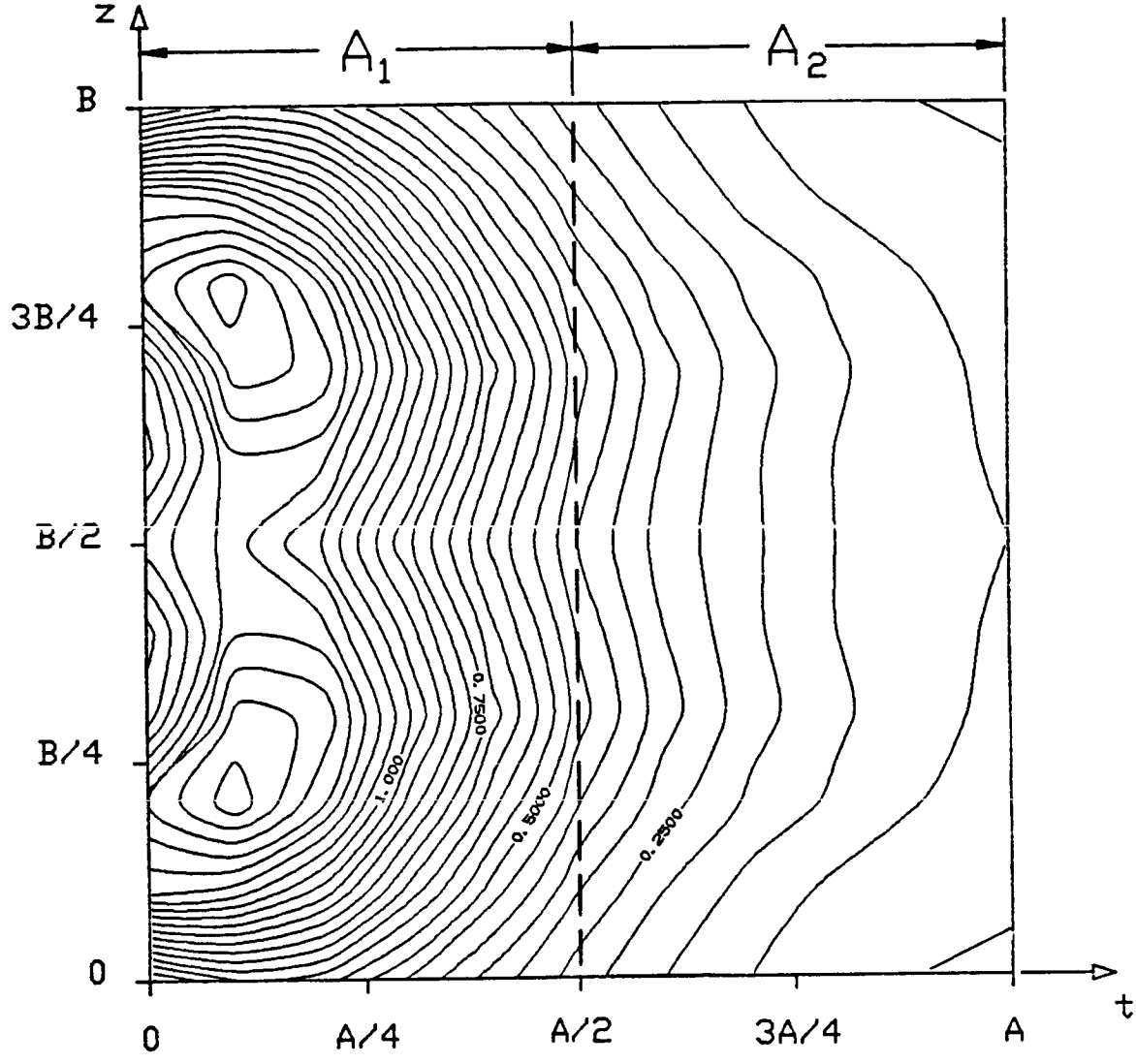

Fig. 6-5. Normalized physical optics surface current density on plate II due to the fields radiated by the physical optics surface current density on plate I. ($2\alpha = 77°$, $\phi = 10°$, A = B = 5.6088 λ, vertical polarization).

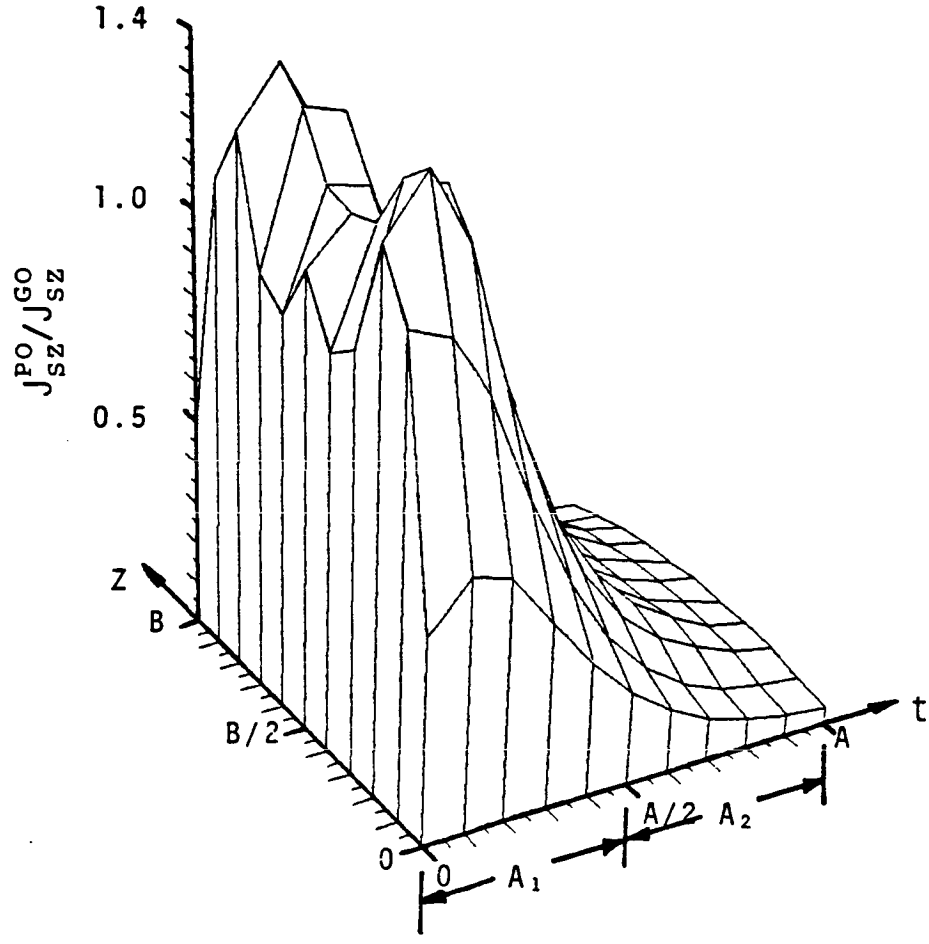

Fig. 6-6. Normalized physical optics surface current density on plate II due to the fields radiated by the physical optics surface current density on plate I. ($2\alpha = 77°$, $\phi = 10°$, $A = B = 5.6088\ \lambda$, vertical polarization).

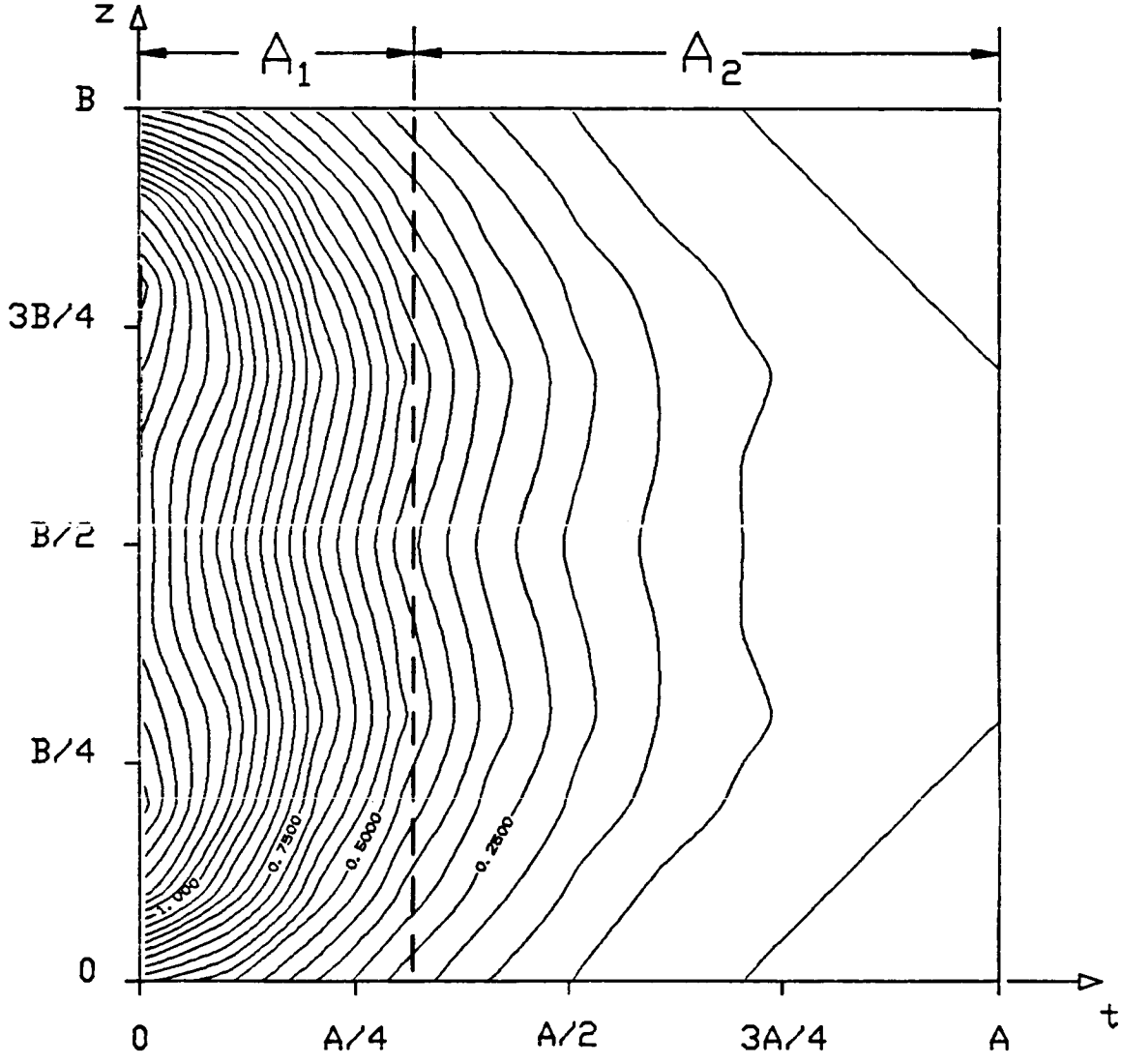

Fig. 6-7. Normalized physical optics surface current density on plate II due to the fields radiated by the physical optics surface current density on plate I. ($2\alpha = 77°$, $\phi = 20°$, $A = B = 5.6088\ \lambda$, vertical polarization).

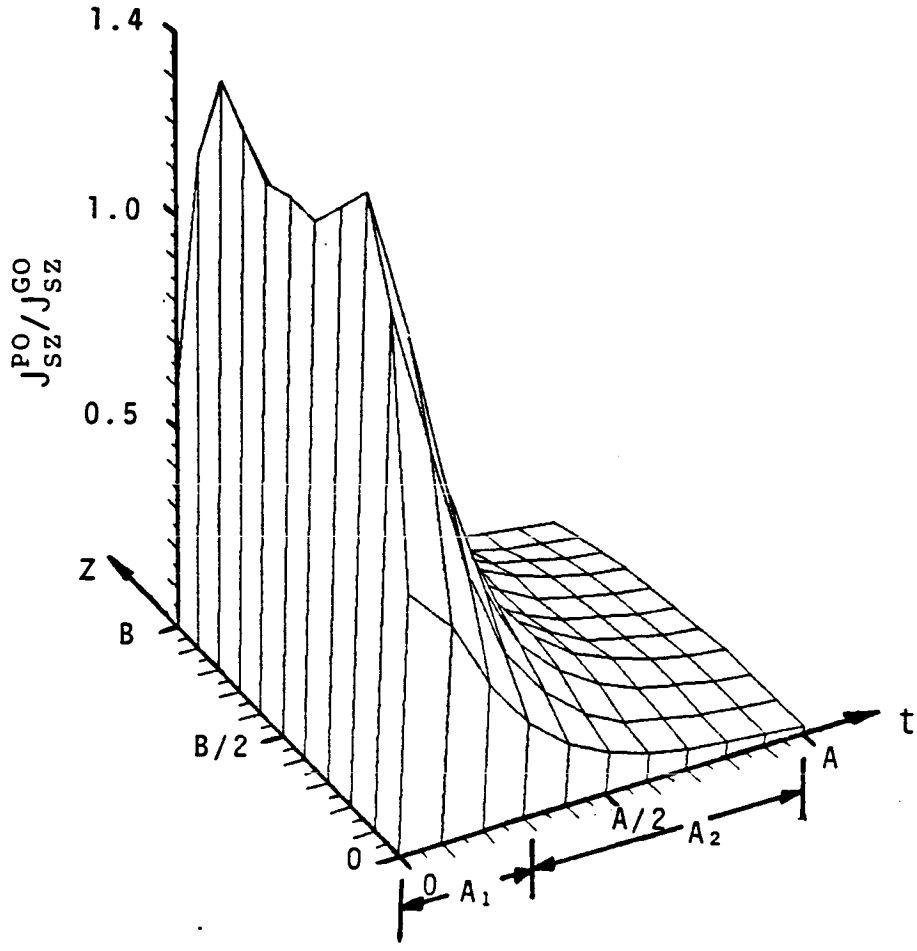

Fig. 6-8. Normalized physical optics surface current density on plate II due to the fields radiated by the physical optics surface current density on plate I. ($2\alpha = 77°$, $\phi = 20°$, A = B = 5.6088 λ, vertical polarization).

boundary between the illuminated and non-illuminated portions of Plate II which would exist if geometrical optics theory was used for the first reflection.

Using geometrical optics, the left portion A_1 would be illuminated and would have a uniform physical optics current density (normalized to unity) while the right portion, A_2, would be in shadow and would have zero physical optics current density. It should be noted that the boundary of the geometrical optics illuminated portion, indicated by the dashed vertical line, seems to fall quite near the 0.500 contour line. This indicates that at the boundary the physical optics current density on Plate II due to the physical optics reflection from Plate I is very nearly one-half the current density which would exist on Plate II if the geometrical theory was used for the reflection from Plate I. Whereas the geometrical optics theory predicts a sharp discontinuity in the normalized current density from unity to zero at this boundary, the physical optics theory predicts a continuous current distribution crossing this shadow boundary at a normalized current density amplitude of 0.5.

The expression for the current density J_{sz}^{PO} used to produce these contour and three-dimensional plots is derived in Appendix B and is presented by (B-17) as a function of the x, y, and z coordinates of a surface element on the plate. The current density for the vertically polarized case is everywhere z-directed on the plates of the dihedral corner reflector.

6.4 Backscatter Components

The components of the backscattered field from the dihedral

corner reflector, using the notation of Chapter 5, and using strictly physical optics theory for the double reflected fields, is illustrated in Figs. 6-9, 6-10 and 6-11 for the right, obtuse and acute angle dihedrals. The total radar cross section is subdivided into individual components which are plotted in separate graphs in these figures. The groups are chosen so as to combine mutually symmetric or reciprocal components. For these computations the dihedral plate dimensions were A = B = 5.6088λ and the incident field was vertically polarized at a frequency of 9.4 GHz. The radar cross section, as a function of the dihedral orientation over the first 90° on each side of the forward region is illustrated. In each figure, the last graph (numbered eight) gives the total backscatter cross section as the sum of all the individual components. These final cross section calculations will be compared with experimental results in the next chapter.

These figures are interpreted using the same numbering conventions constructed for the geometrical analysis of Figs. 5-5 through 5-10. For example, graph 1 illustrates the cross section of the combined fields of the two single reflections, C2 and C4, from the two plates of the dihedral corner reflector. Likewise, graph 2 illustrates the combined cross section due to the single diffracted fields from the outside plate edges C1 and C5.

It was found that not as many backscattered terms were needed in the PTD analysis, as in the GTD analysis, to achieve continuity of the cross section pattern. It is very interesting to note that while the corresponding backscatter terms predicted by the physical and geometrical theories are strikingly different, the total cross section

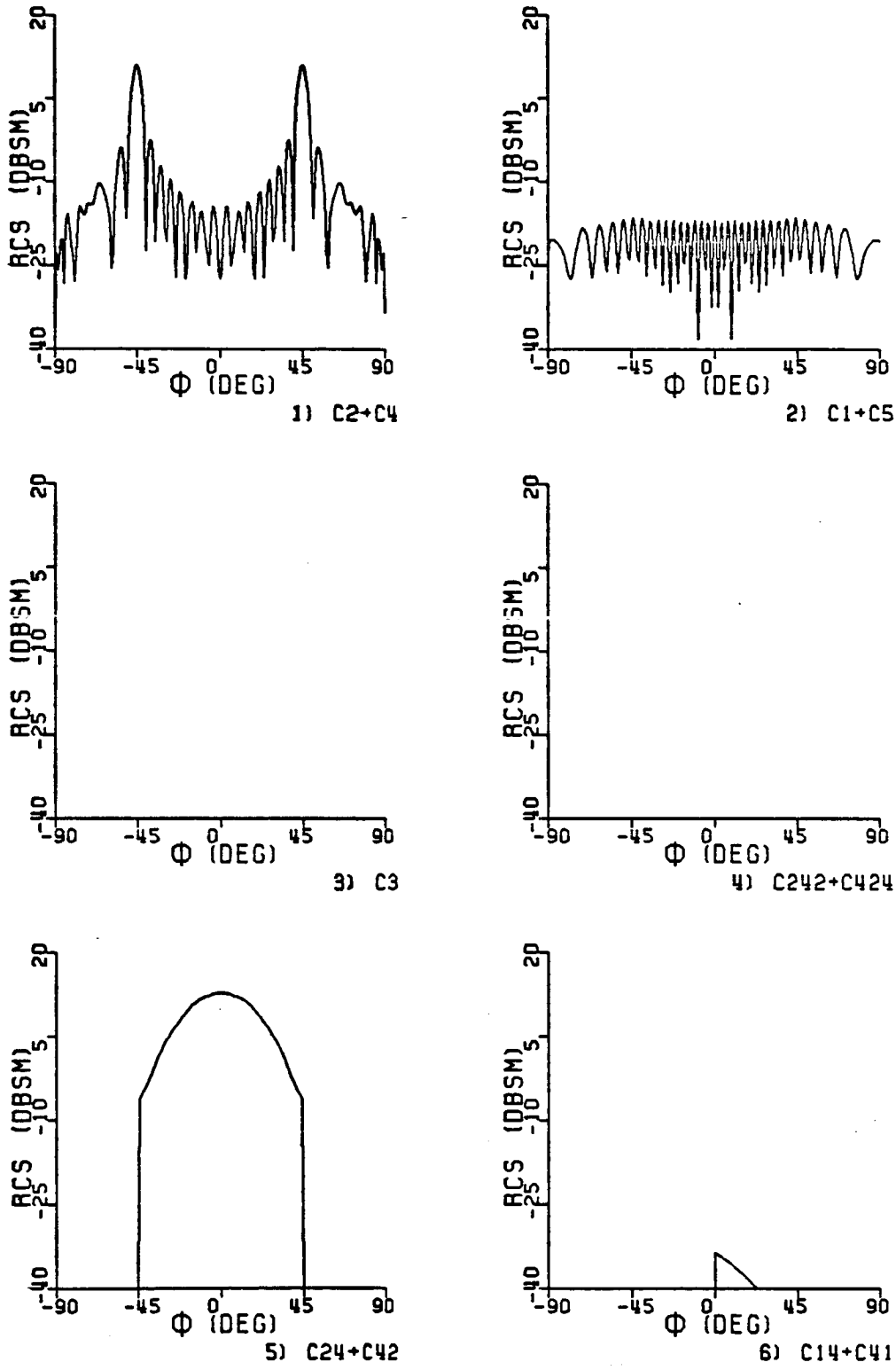

Fig. 6-9. Components of the radar cross section of a 90° dihedral corner reflector using physical optics and physical diffraction (A = B = 5.6088 λ, vertical polarization, f = 9.4 GHz).

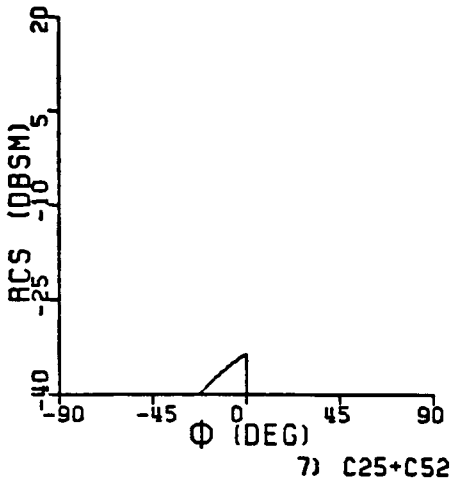

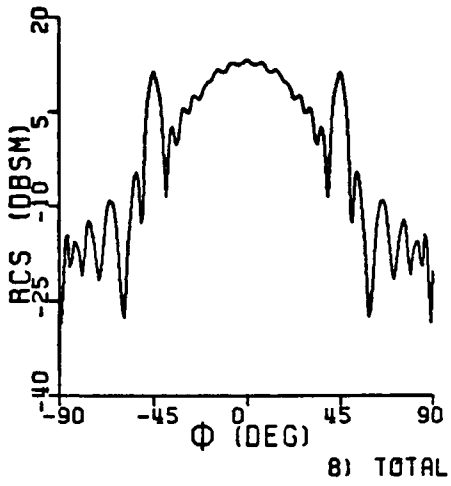

Fig. 6-9. (continued)

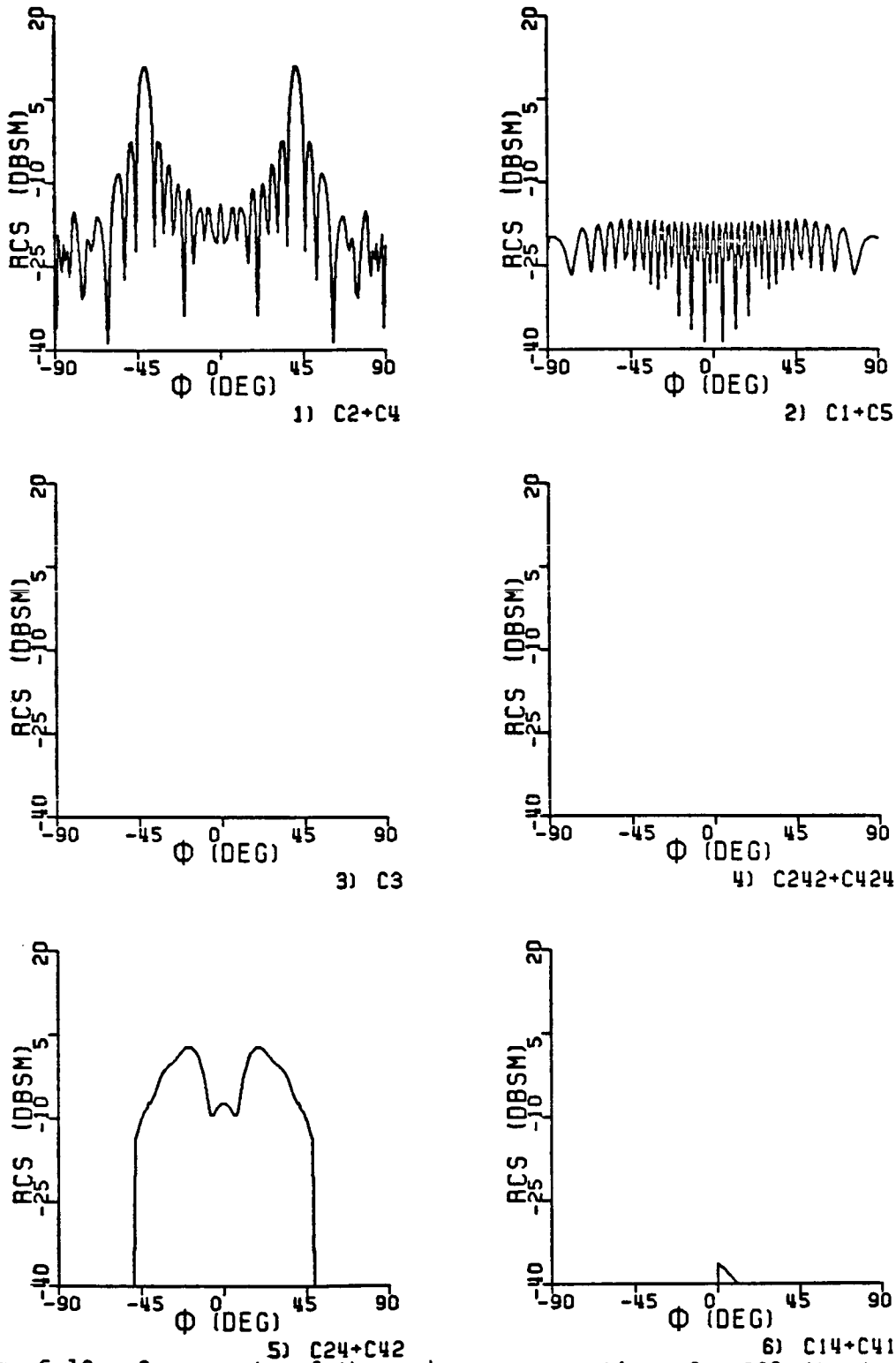

Fig. 6-10. Components of the radar cross section of a 98° dihedral corner reflector using physical optics and physical diffraction (A = B = 5.6088 λ, vertical polarization, f = 9.4 GHz).

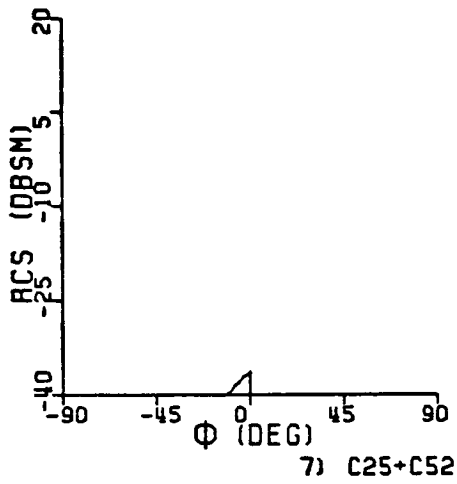

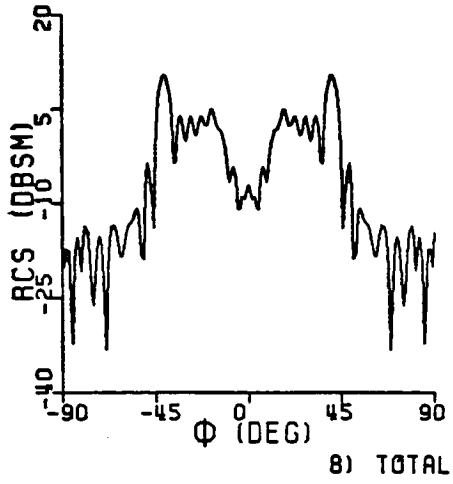

Fig. 6-10. (continued)

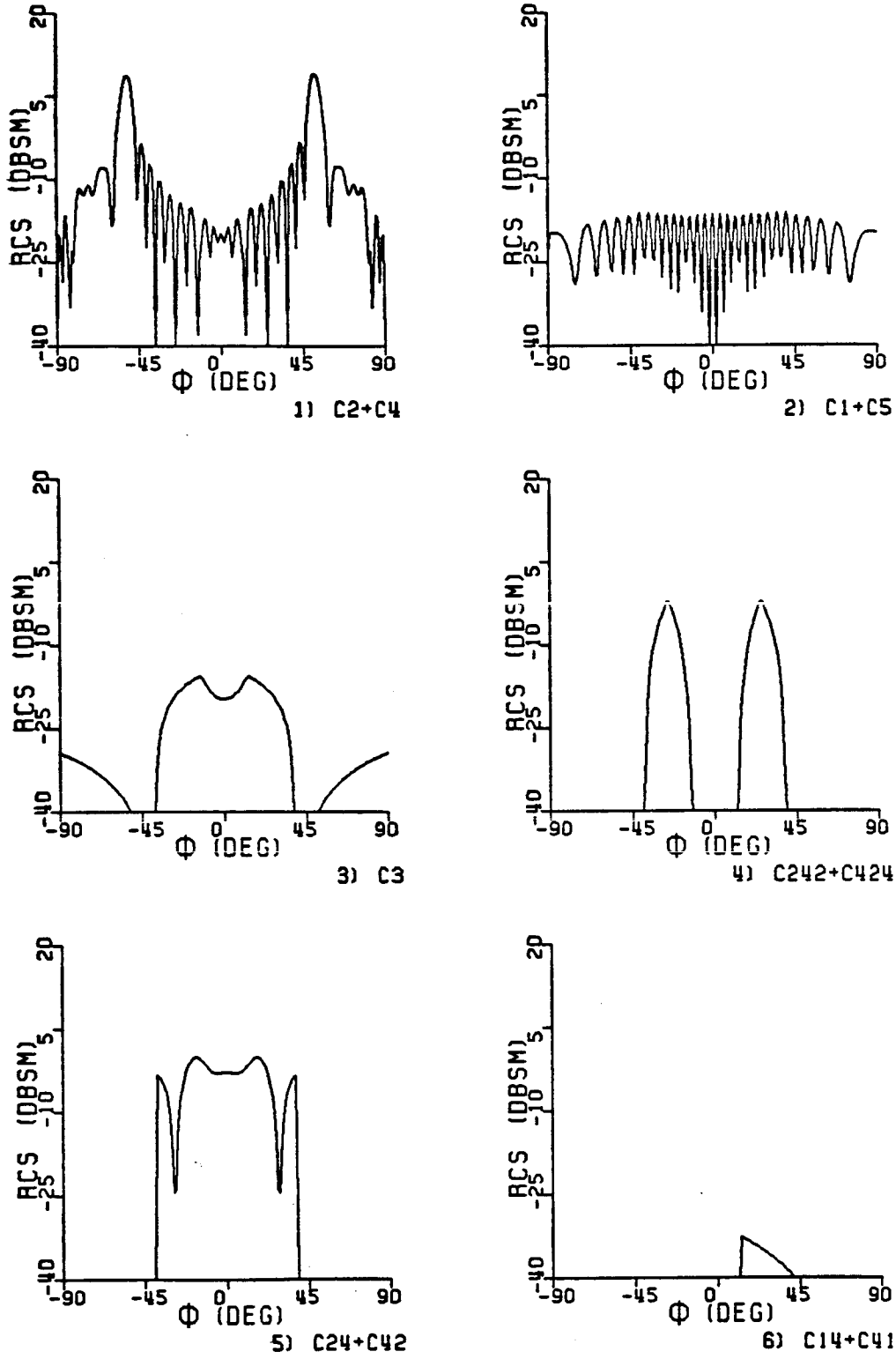

Fig. 6-11. Components of the radar cross section of a 77° dihedral corner reflector using physical optics and physical diffraction (A = B = 5.6088 λ, vertical polarization, f = 9.4 GHz).

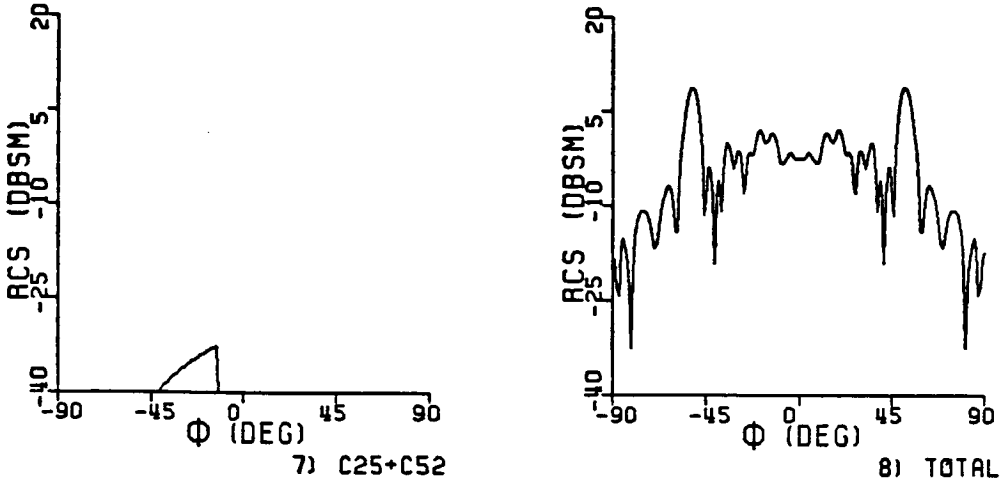

Fig. 6-11. (continued)

found as the sum of all the individual components are remarkably similar.

Since the backscatter cross section patterns from the physical theory compared well with experiment using only the terms illustrated in Figs. 6-9, 6-10 and 6-11, higher order diffractions were not considered. It is likely that the inclusion of higher order terms would tend to refine the results to an even closer agreement with experiment. However, there does seem to be some contention among authors about the method of application of the physical theory of diffraction when used to determine double and higher order diffracted fields [26]-[28].

CHAPTER 7

COMPARISON WITH EXPERIMENTAL RESULTS

7.1 Configuration

The theories of geometrical optics and geometrical diffraction, and the theories of physical optics and physical diffraction can be judged in terms of their accuracy by comparison of analytical and experimental results.

The specific dihedral corner reflectors, for which limited experimental results were available, were constructed of two square plates each with sides of 5.6088 λ. These experimental measurements, reported in [20], were conducted at 9.4 GHz using vertically polarized fields (i.e. the electric field vector was parallel to the longitudinal axis of the dihedral corner reflector). The backscatter cross section, as a function of azimuthal angle in a plane perpendicular to the dihedral corner longitudinal axis, was available for reflectors with 90°, 77° and 98° interior angles.

The measured radar cross section for the 90° dihedral corner reflector, shown as the solid curve in Fig. 7-1, is characterized by a large return in the forward region due to a large specular double reflected field. It is this large cross section, which is relatively smoothly varying over a wide angular range, that makes the dihedral so desirable as a radar calibration and testing target [30]-[32]. The 90° corner reflector, in addition, has a large cross section at $\phi = \pm 45°$ since a large singly reflected specular field exists whenever the direction of observation is normal to one of the dihedral corner

reflector's faces. The measured radar cross section of the 98° dihedral corner reflector, shown by the solid curve in Fig. 7-2, is characterized by the same large single reflection lobes near angles at which the observation direction is normal to a face of the reflector; however the large double reflected field is noticeably absent. This characteristic decrease in the double reflected field along surface junctions was the motivation for Knott's work in RCS reduction [8]. The measured radar cross section of the 77° dihedral corner reflector, shown by the solid curve in Fig. 7-3, is characterized by a large but rapidly fluctuating magnitude in the forward region. The two sharp nulls in this region would eliminate this dihedral as a useful target for radar testing and calibration, because lost detection by a radar system could be caused solely by a misalignment of the calibration target. Nonetheless, study of the acute angle dihedral corner reflector is an important test of the analytical theory, since for this corner reflector, the higher order reflections and diffractions become important.

7.2 Geometrical Optics

The backscatter cross section of the dihedral corner reflector found using the geometrical optics theory is compared with experimental results in Figs. 7-1, 7-2 and 7-3. The methods discussed in Chapter 5 were used to locate specular points on each surface, if they existed, and for each specular reflection point a source image could be defined. The analytical results here were calculated at a distance of 200λ which satisfied the far field criterion. The geometrical optics cross section has a very large return over the very small angle where a specular point due to single reflection exists on a dihedral face. The 90° dihedral

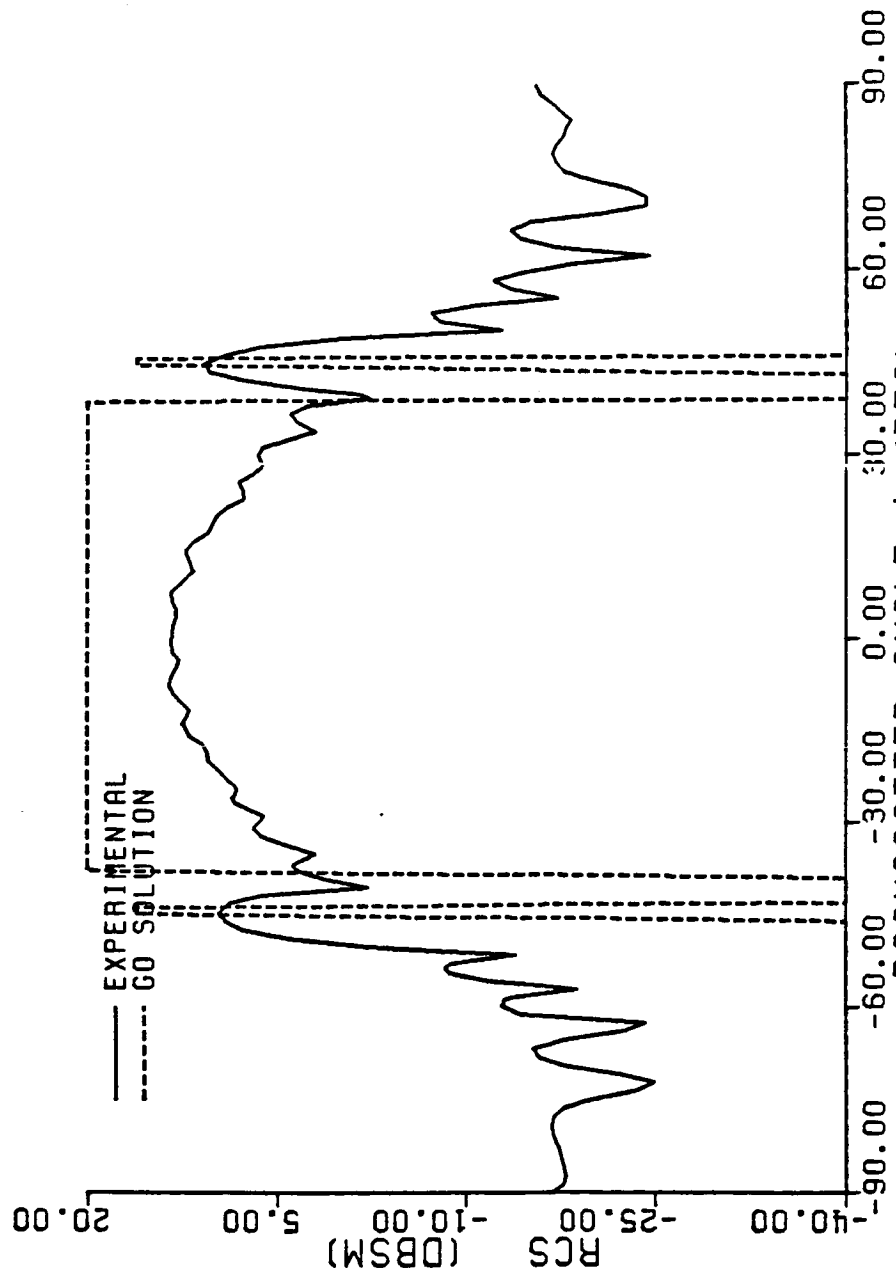

Fig. 7-1. Experimental and geometrical optics radar cross sections for the 90° dihedral corner reflector (A = B = 5.6088 λ, vertical polarization, f = 9.4 GHz).

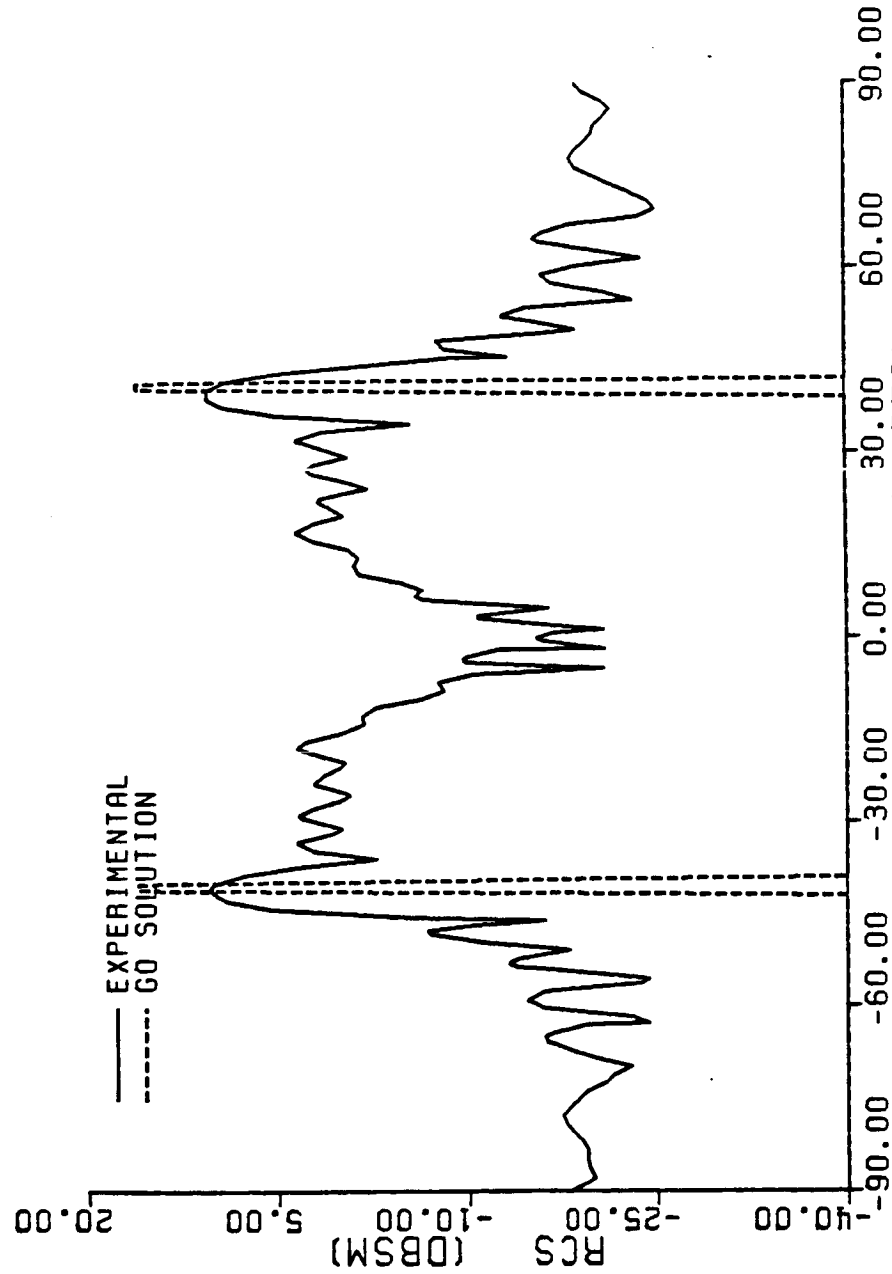

Fig. 7-2. Experimental and geometrical optics radar cross sections for the 98° dihedral corner reflector (A = B = 5.6088 λ, vertical polarization, f = 9.4 GHz).

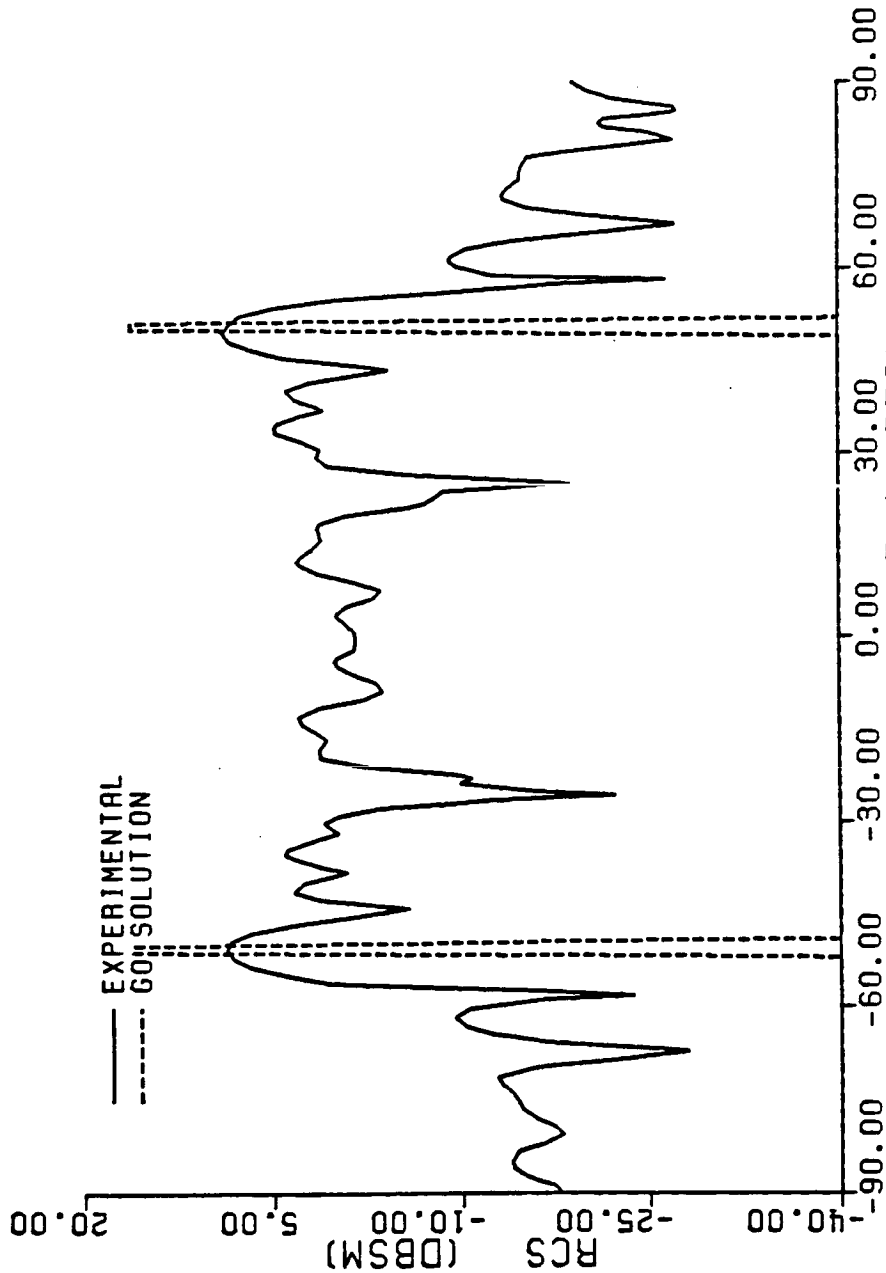

Fig. 7-3. Experimental and geometrical optics radar cross sections for the 77° dihedral corner reflector (A = B = 5.6038 λ, vertical polarization, f = 9.4 GHz).

corner, in addition, has a double reflected field which is very large over $-\pi/4 < \phi < \pi/4$. As discussed in Chapter 5, the cross sections of flat plates, due to geometrical optics alone, is a function of the distance of observation and will increase without bound as the distance of observation increases. For this reason, if the observation distance is increased beyond 200 λ, the geometrical optics single reflected cross section will increase in magnitude, but will decrease in angular extent, approaching an infinite cross section over zero angle. The double reflected field would also increase without bound in the 90° dihedral case but would exist over the same angular extent of $-\pi/4 < \phi < \pi/4$ for far distances.

From these illustrations it is apparent that the theory of geometrical optics by itself is a poor method of finding the radar cross section of an object composed of flat plates. The theory predicts infinite cross section whenever a specular point exists on a flat plate of the structure and zero cross section when no such point exists. Furthermore the cross section is strongly dependent on the distance from the target. However, even though geometrical optics is inappropriate for flat surface structures such as this, it should be noted that geometrical optics has found useful application in the past for analysis of bodies which are composed solely of curved surfaces without abrupt boundaries.

7.3 Geometrical Diffraction

The addition of geometrical diffraction terms to the geometrical optics terms significantly improves the accuracy of the analytical results when compared with experiment. The discontinuities in the

diffraction coefficients of GTD produce discontinuities in the backscattered field, which remove the discontinuities inherent in the geometrical optics backscattered fields. And, equally important, the backscattered fields found using the combination of geometrical optics and the geometrical diffraction are nearly invariant with distance of observation provided the distance is large in comparison to the target size. The cross section must be independent of distance for it to be a useful parameter in the radar range equation of (2-5), since the basic motivation behind introducing cross sections as target parameters is to separate the effects of radar distance and configuration from the target specification.

In Figs. 7-4, 7-5 and 7-6 the radar cross section of the dihedral corner reflector found using the combination of geometrical optics and geometrical diffraction is compared with experiment for the 90°, 98° and 77° corner reflector. Again the distance of observation was 200 λ for these comparisons, but the cross section is relatively independent of distance, provided the distances are large. Computationally, however, it is best to choose a distance which is not too much larger than that given by the far field criterion, because as the distance increases, the accuracy required in the calculations of ψ and ψ_0 of the diffraction coefficients increases. Even at 200 λ, considerable care must be taken to avoid any approximations, especially when determining ψ and ψ_0. Seemingly insignificant inaccuracies in these angles can yield large errors in the radar cross section near shadow and reflection boundaries.

The theory of geometrical diffraction, along with geometrical

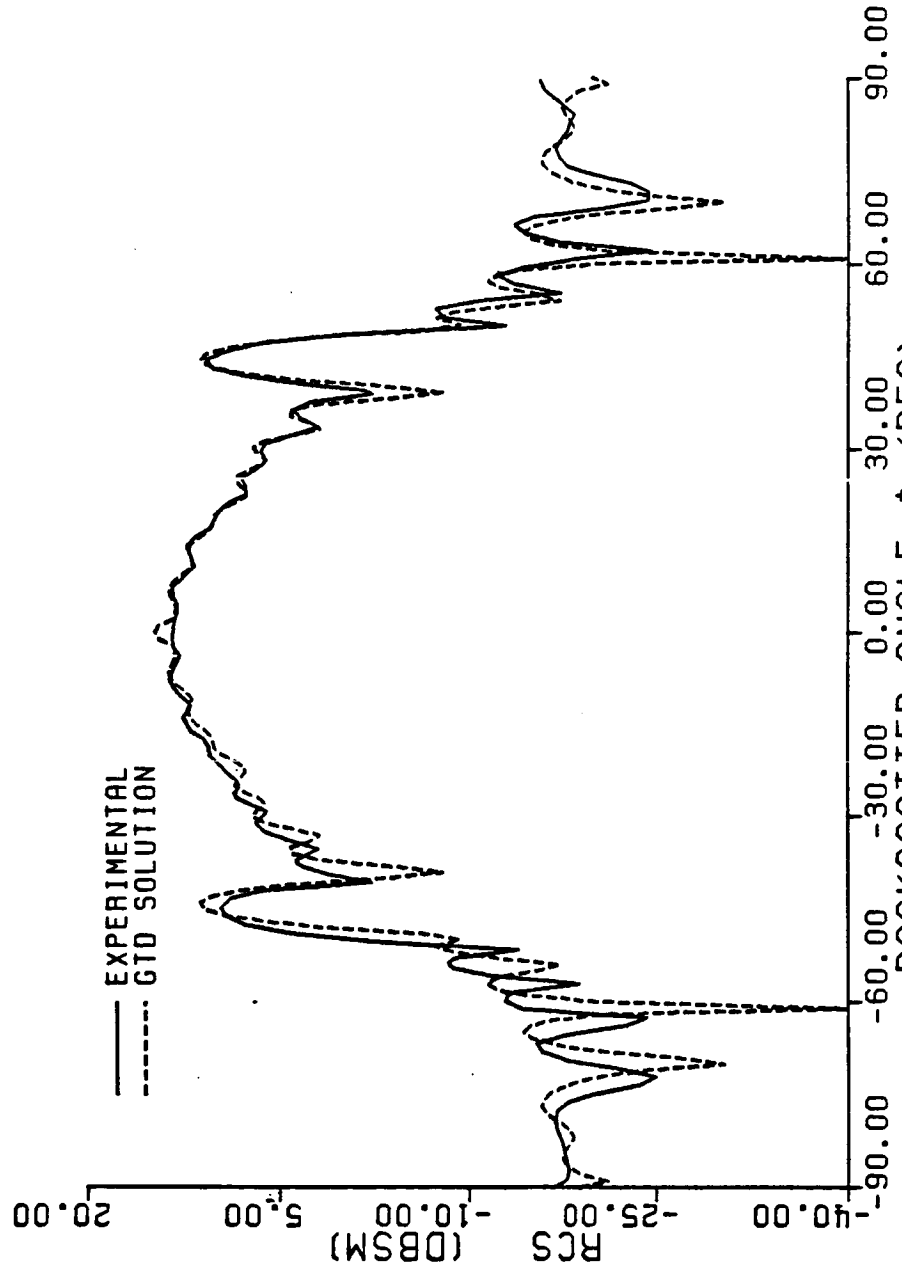

Fig. 7-4. Experimental and geometrical theory of diffraction cross sections for the 90° dihedral corner reflector ($A = B = 5.6088\ \lambda$, vertical polarization, f = 9.4 GHz).

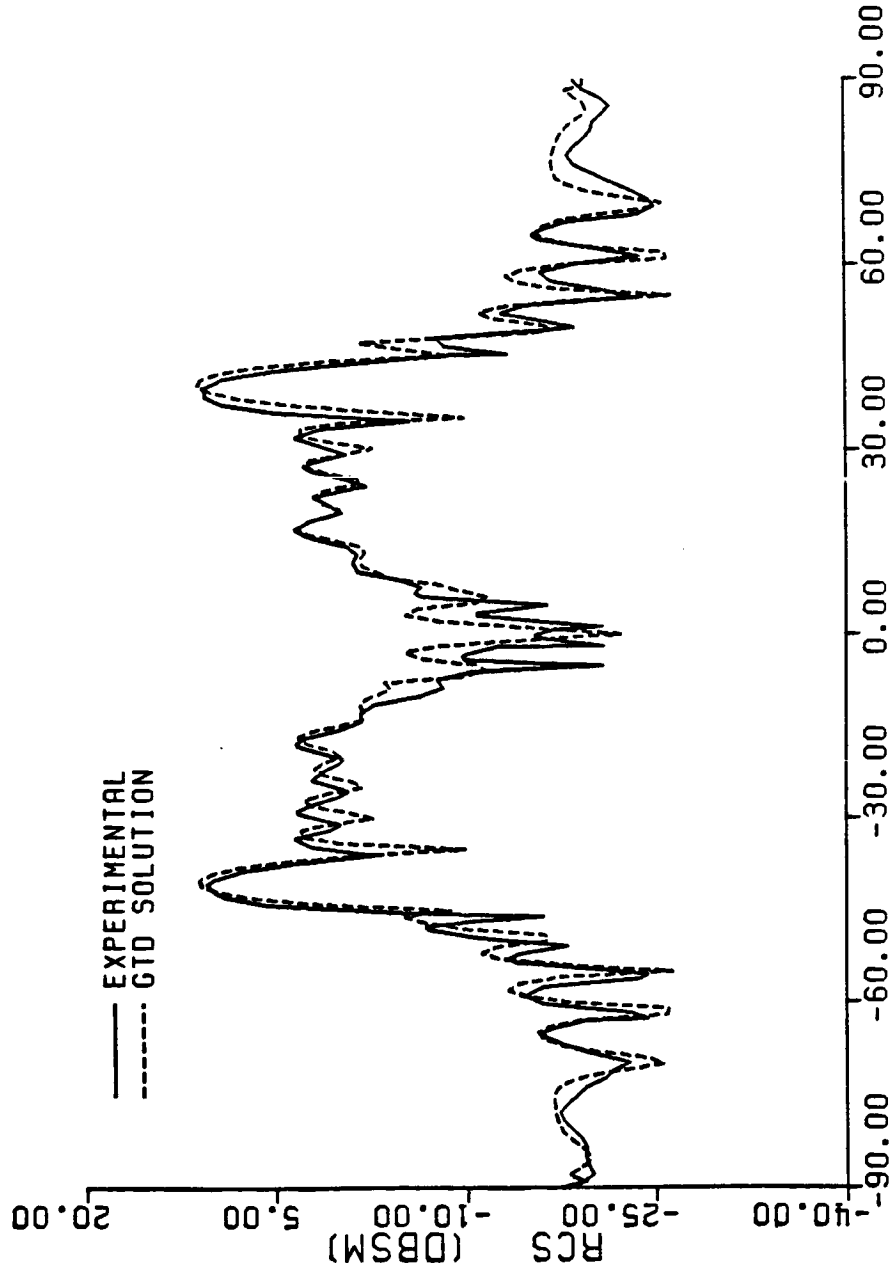

Fig. 7-5. Experimental and geometrical theory of diffraction cross sections for the 98° dihedral corner reflector (A = B = 5.6088 λ, vertical polarization, f = 9.4 GHz).

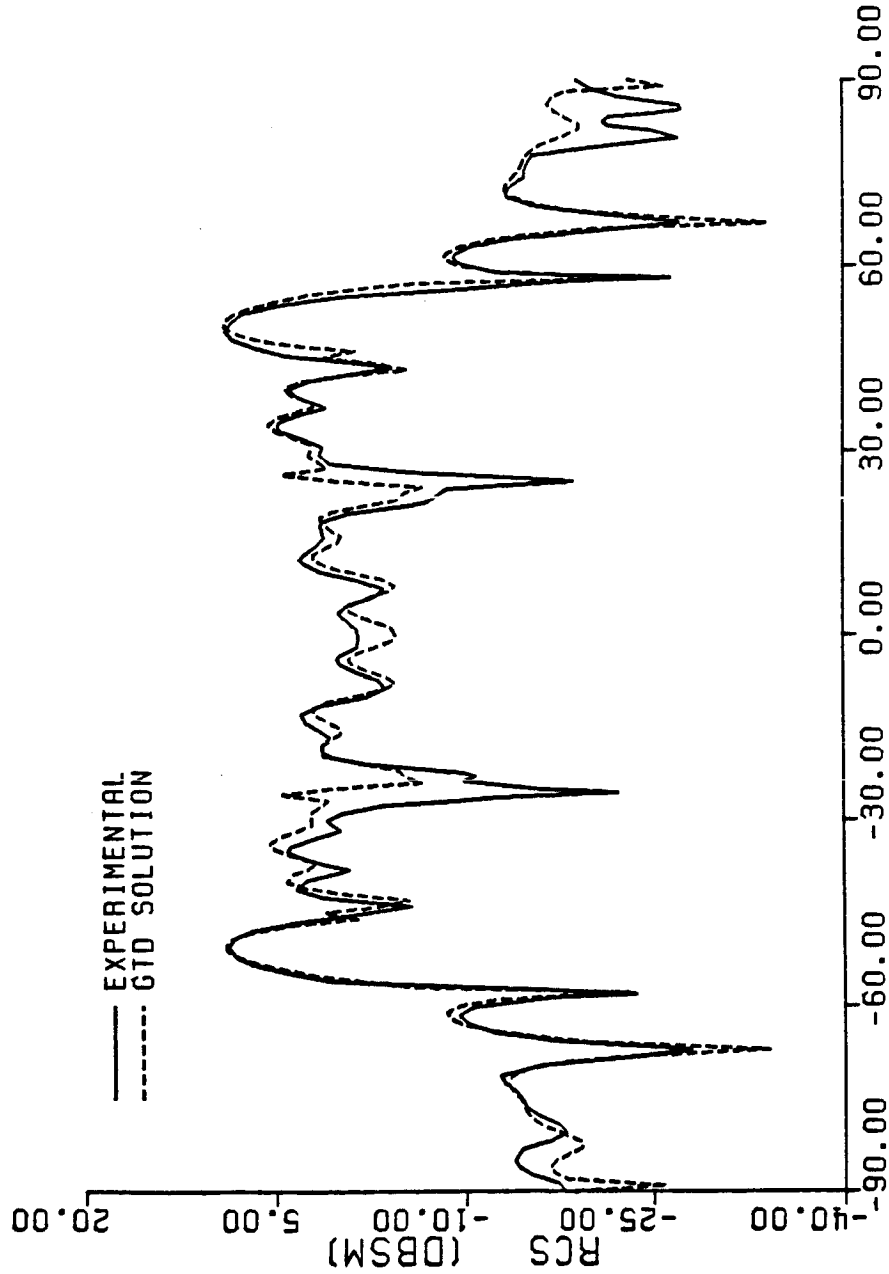

Fig. 7-6. Experimental and geometrical theory of diffraction cross sections for the 77° dihedral corner reflector ($A = B = 5.6088\ \lambda$, vertical polarization, f = 9.4 GHz).

optics, performs well at predicting the experimental cross section pattern. The theory matches many of the major and minor lobes of the experimental curves quite accurately. It should be remembered that to achieve this quality of accuracy, especially for the acute angle dihedral, up to third order reflections and diffractions have been considered. For the vertically polarized case, for which experimental results were available, many of the multiple reflection terms from edge to edge are zero. For the horizontally polarized case more of these multiple diffractions become important.

7.4 Physical Optics

The theory of physical optics is applied to the dihedral corner and compared with experiment for the right, obtuse and acute corner in Figs. 7-7, 7-8 and 7-9. The physical optics terms were found using the methods of Chapter 6 in which a surface current density is introduced in proportion to the incident tangential magnetic field. The single reflected fields are evaluated in terms of this induced surface current density. The double reflected fields are determined using the method of Knott [18] in which all double reflected components are determined by considering geometrical optics (image) reflection at each first reflection, and physical optics reflection (in terms of the incident geometrical optics field) at the second reflection. The advantage of this method is that all the integrations associated with finding the reflected physical optics fields can be performed in closed form to avoid costly numerical integrations.

For the obtuse and right angle dihedral corner, the physical optics analysis approximated in this manner gives good results in most

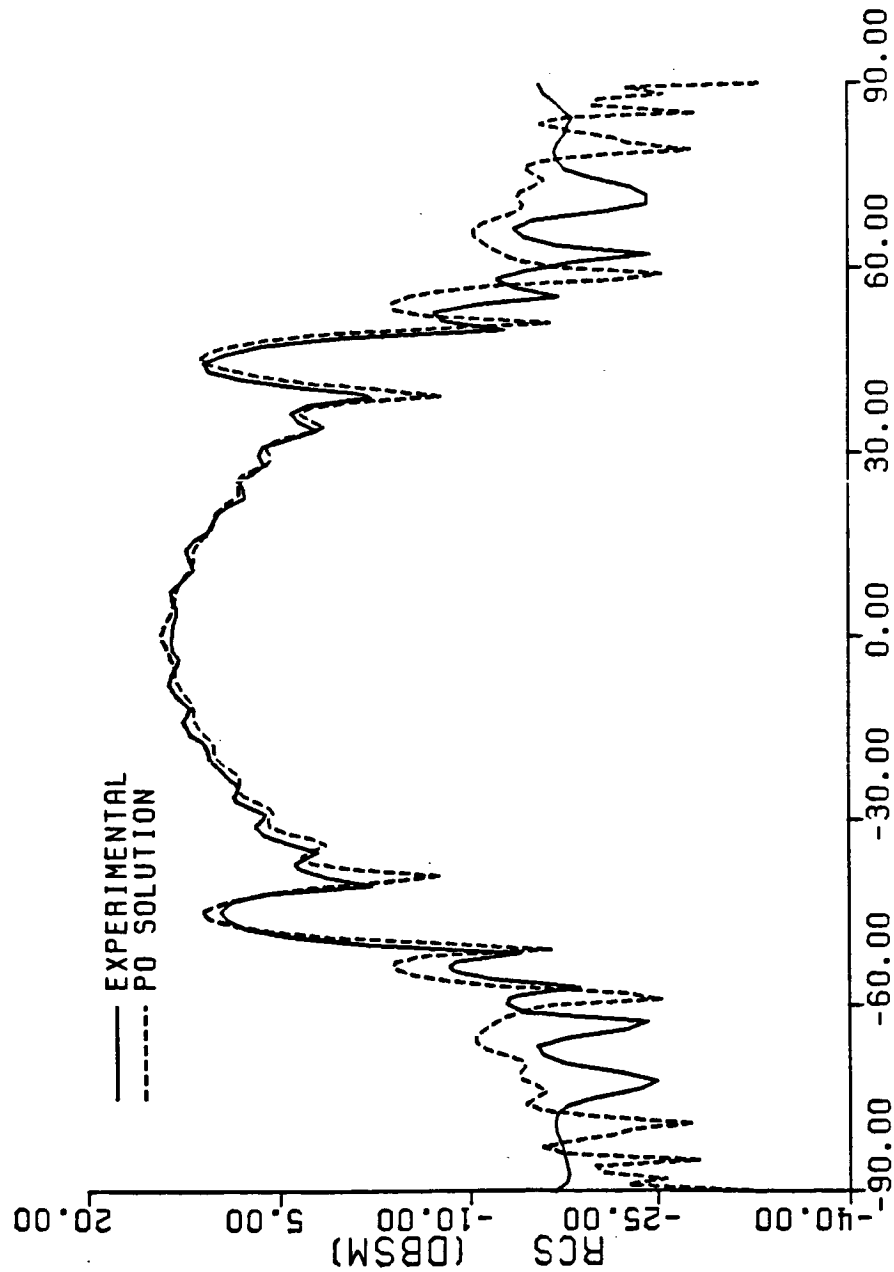

Fig. 7-7. Experimental and physical optics radar cross sections for the 90° dihedral corner reflector (A = B = 5.6088 λ, vertical polarization, f = 9.4 GHz).

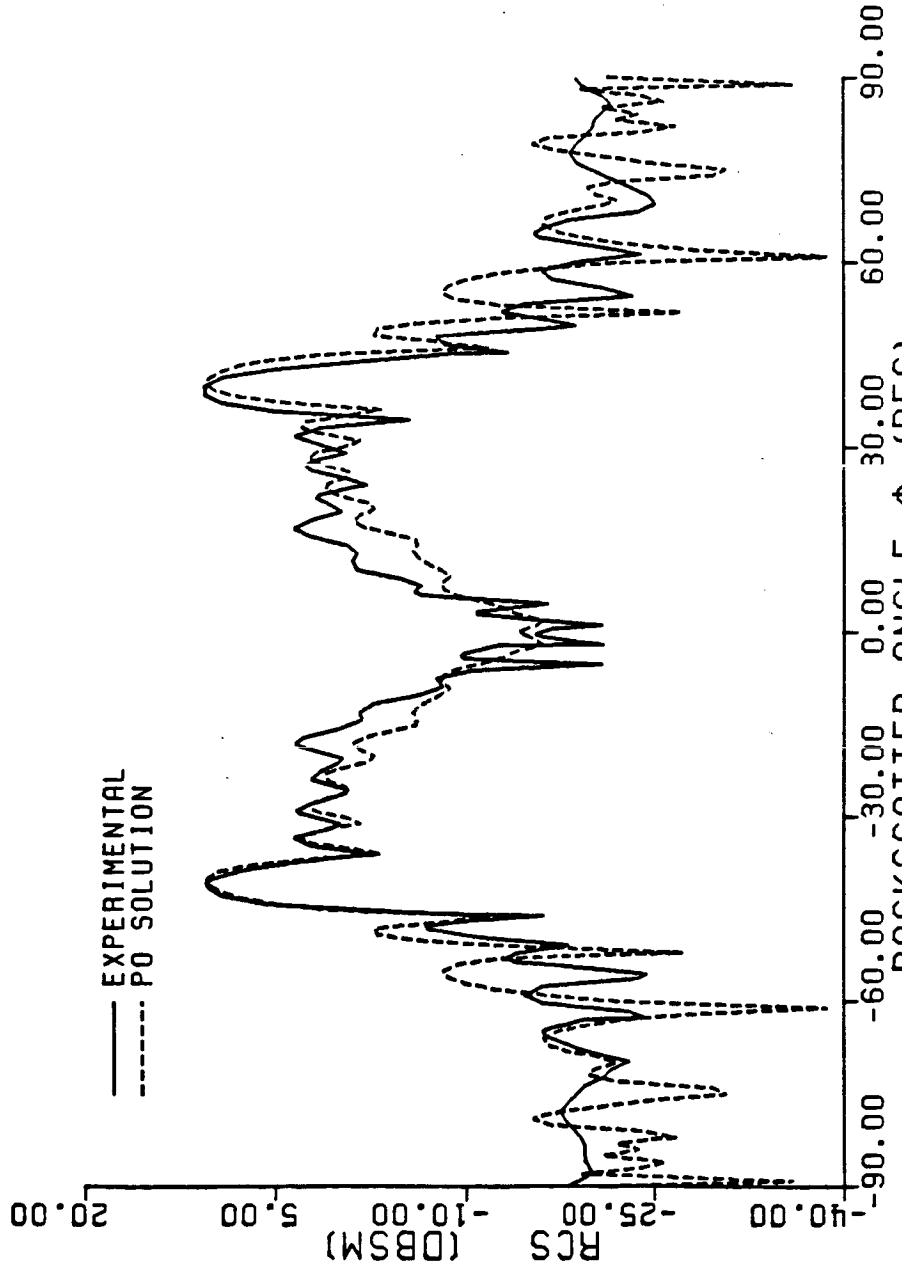

Fig. 7-8. Experimental and physical optics radar cross sections for the 98° dihedral corner reflector (A = B = 5.6088 λ, vertical polarization, f = 9.4 GHz).

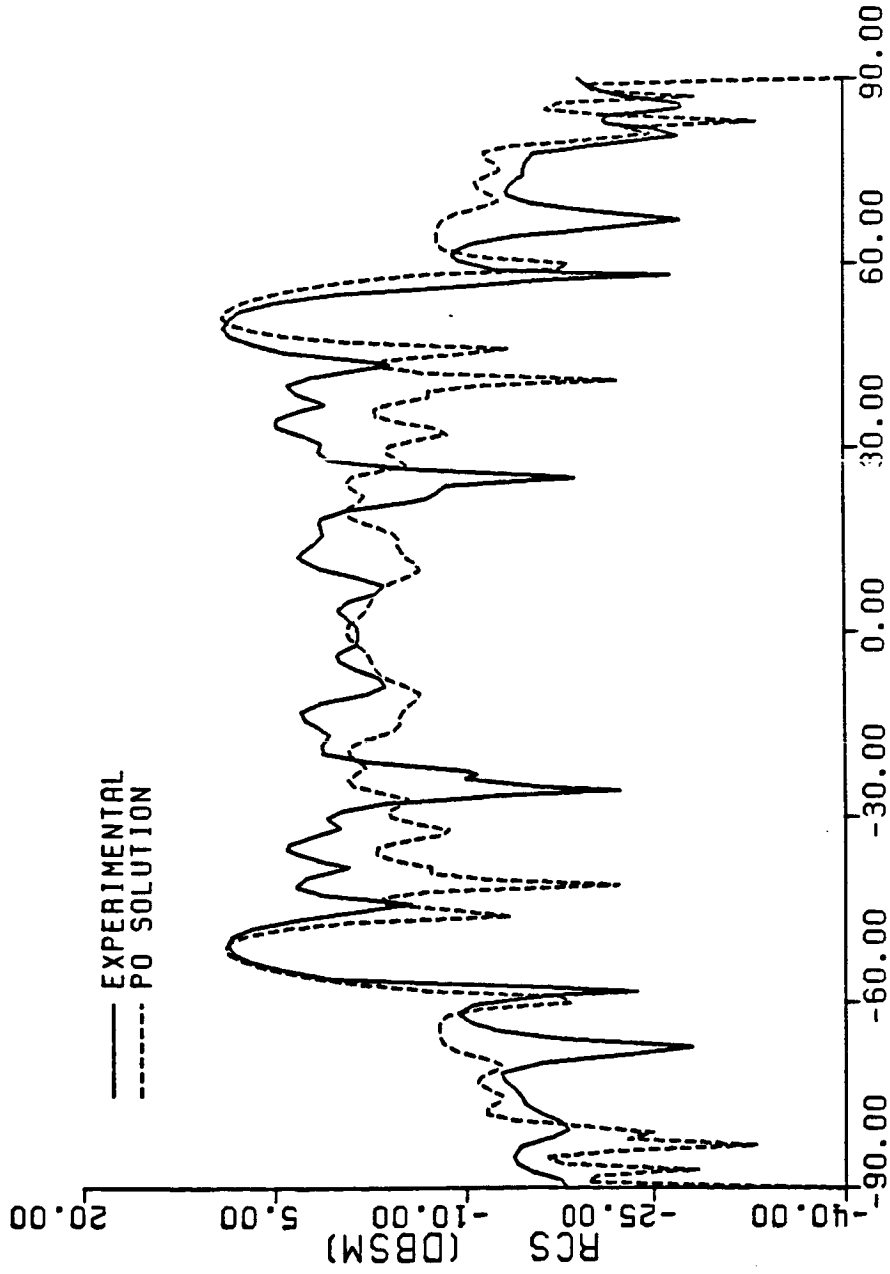

Fig. 7-9. Experimental and physical optics radar cross sections for the 77° dihedral corner reflector (A = B = 5.6088 λ, vertical polarization, f = 9.4 GHz).

regions. The theory is certainly more accurate than geometrical optics by itself, but it is not as accurate as the combination of geometrical optics and geometrical diffraction.

The acute angle dihedral, unfortunately, has significant inaccuracies in the analytical cross section when compared with experimental data. The results are acceptable near the single specular reflection lobes but are inconsistent with experiment elsewhere. This method of using a combination of geometrical optics and physical optics for double reflected fields does not appear to yield satisfactory results for acute angle dihedral corner reflectors which induce strong multiple reflections.

7.5 Physical Diffraction

The addition of physical diffraction terms to the physical optics field of the right, obtuse, and acute dihedral corner reflectors is compared with experimental results in Figs. 7-10, 7-11, and 7-12. The physical diffraction fields tend to be smaller than the physical optics fields, but they give some improvement to the cross section pattern in comparison to the experimental results.

The diffraction terms included in the analysis of these cross section patterns were all those examined in Chapter 4. The diffracted fields were found using the methods of [16] whereby all diffracted fields could be obtained in closed form and numerical integrations were unnecessary. Double and triple reflected fields were included in these figures and all initial reflections were performed geometrically using image theory whereas the final reflection was performed physically and in closed form.

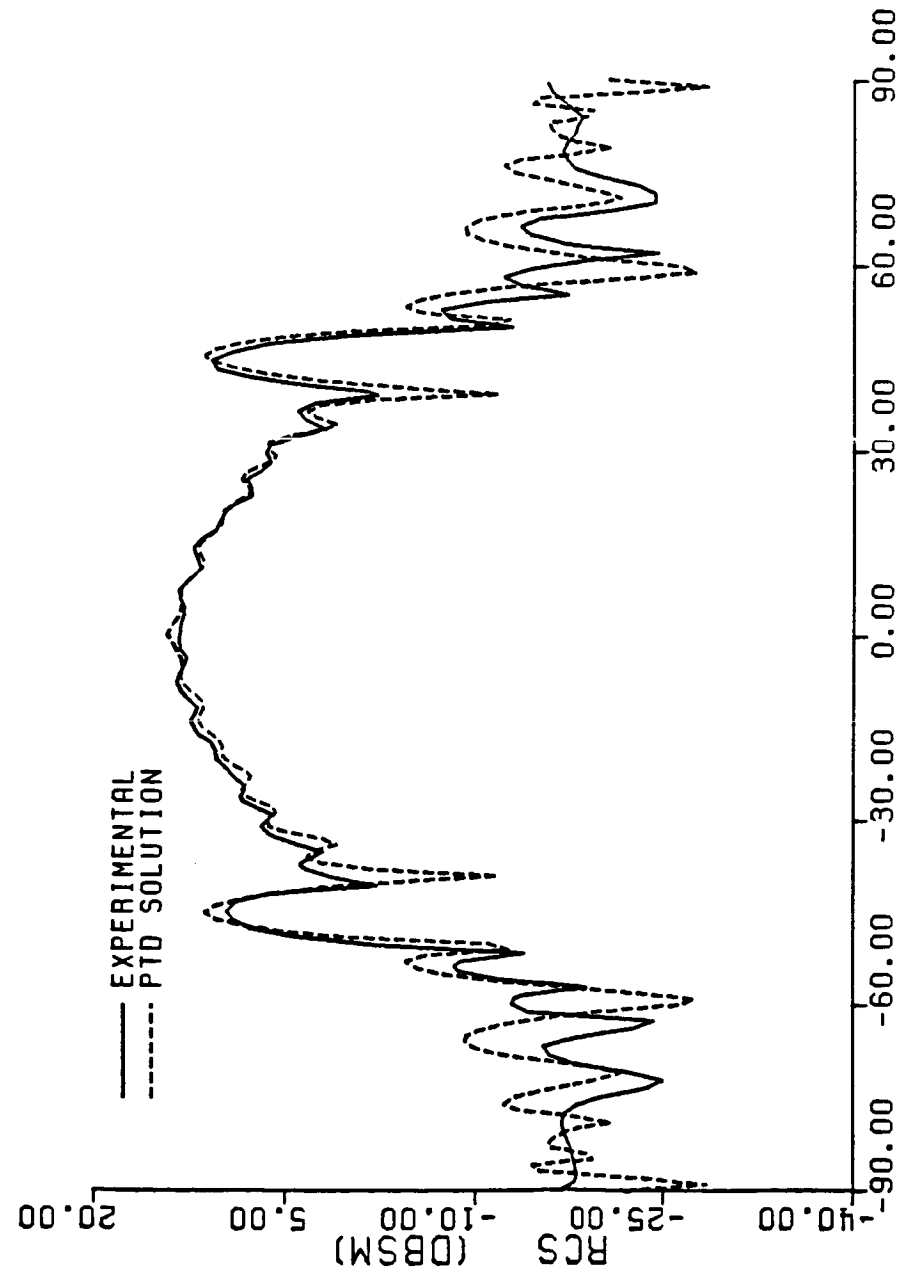

Fig. 7-10. Experimental and physical theory of diffraction cross sections for the 90° dihedral corner reflector using a combination of geometrical and physical optics for the double reflected field (A = B = 5.6088 λ, vertical polarization, f = 9.4 GHz).

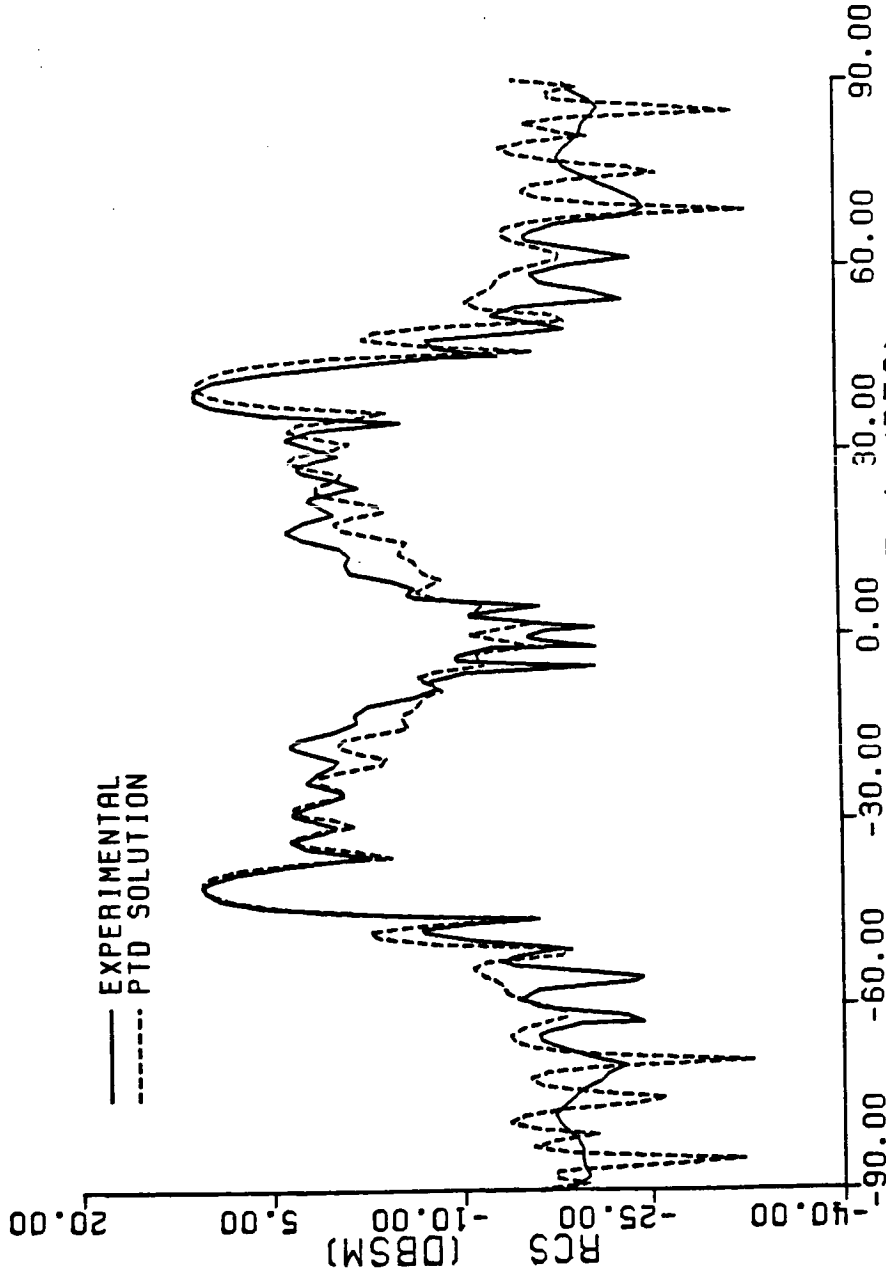

Fig. 7-11. Experimental and physical theory of diffraction cross sections for the 98° dihedral corner reflector using a combination of geometrical and physical optics for the double reflected field (A = B = 5.6088 λ, vertical polarization, f = 9.4 GHz).

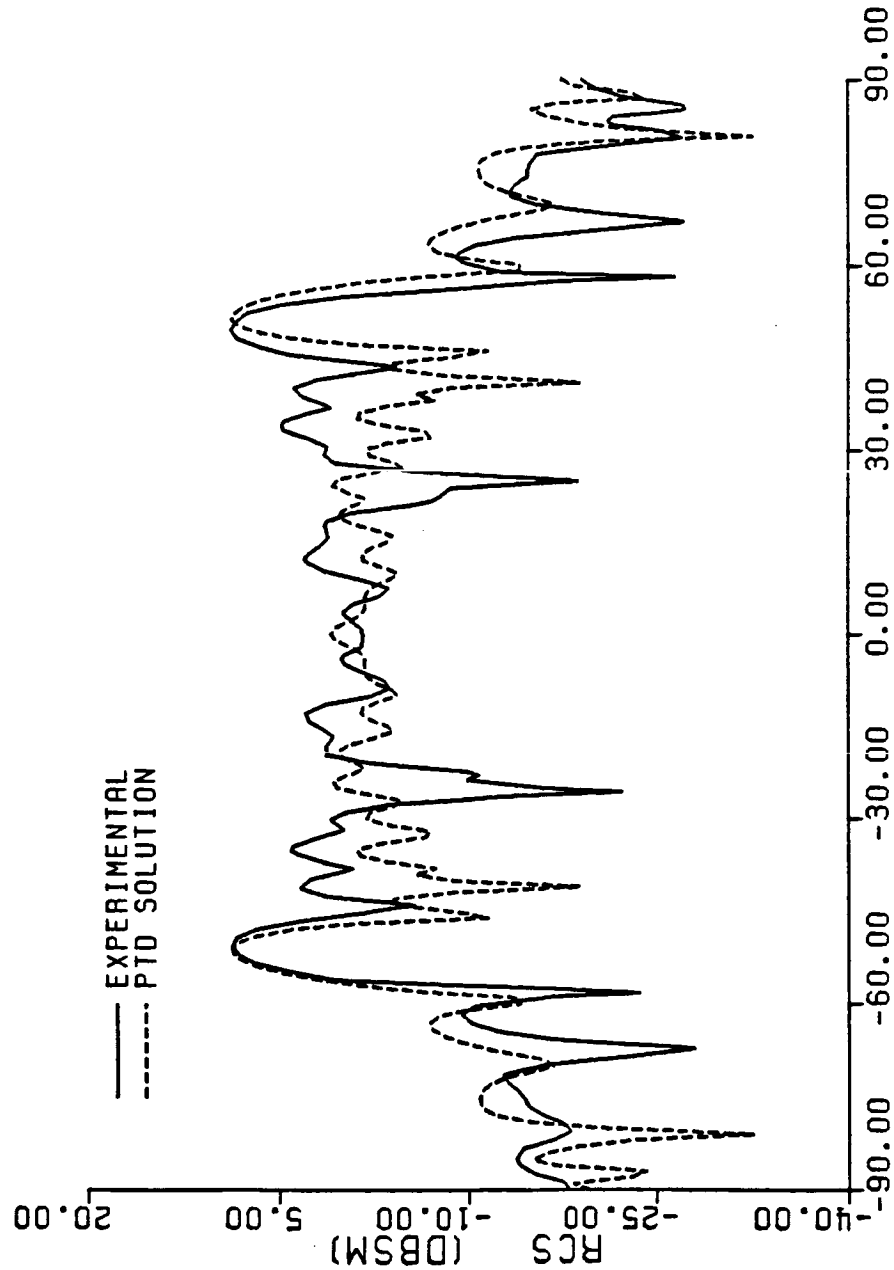

Fig. 7-12. Experimental and physical theory of diffraction cross sections for the 77° dihedral corner reflector using a combination of geometrical and physical optics for the double reflected field (A = B = 5.6088 λ, vertical polarization, f = 9.4 GHz).

In Fig. 7-12 it is apparent that even the inclusion of physical diffraction to the backscatter analysis is insufficient to bring the analytical results satisfactorily close to experiment for the acute dihedral corner reflector. The inaccuracy seems to lie in the approximate method by which the double reflected field was obtained, and it is this component which can be improved by choosing an alternate technique.

In order to improve the analytical results for the dihedral corner reflector, the double reflected field is reevaluated using the strict physical optics method of Section 6.3 and Appendix B. The resulting cross section pattern with the inclusion of this superior reflection computation is illustrated in Figs. 7-13, 7-14 and 7-15. The only change between these and the previous figures was the reevaluation of the double-reflected field by the improved technique. The significant improvement for the 77° dihedral corner reflector cross section is evident. To achieve this accuracy, the analysis was much more complex, and it involved a complicated and time-consuming numerical evaluation of a quadruple integral. For more complex geometries the formulation of a corresponding integration may be an insurmountable task.

7.6 Comparison of Scattering Theories

The radar cross sections determined using geometrical optics and geometrical diffraction, and the radar cross sections determined using physical optics and physical diffraction, can be readily extended for comparison on the back side of the dihedral so that the full 360° azimuthal plane may be examined. Although the dihedral corner reflector

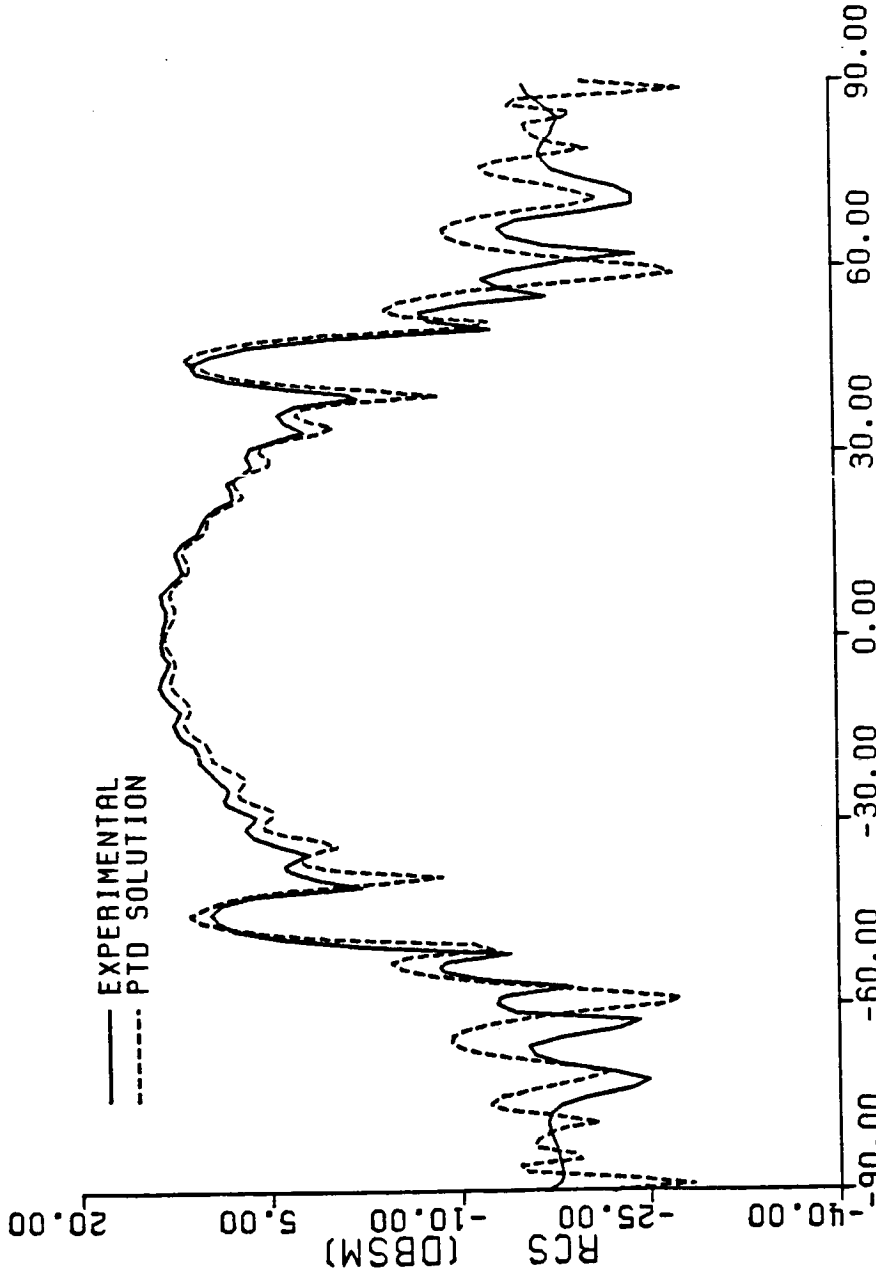

Fig. 7-13. Experimental and physical theory of diffraction cross sections for the 90° dihedral corner reflector using strictly physical optics for the double reflected field (A = B = 5.6088 λ, vertical polarization, f = 9.4 GHz).

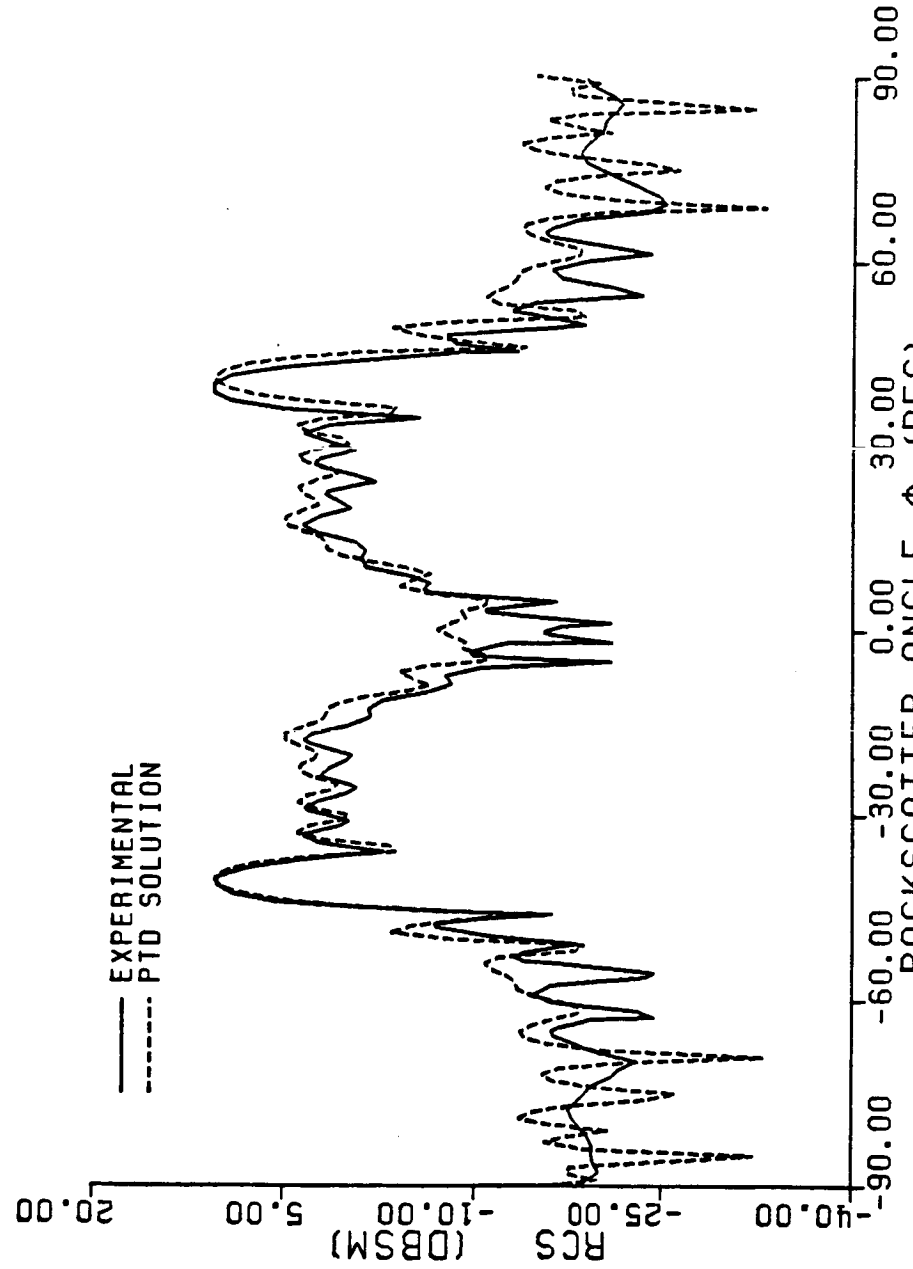

Fig. 7-14. Experimental and physical theory of diffraction cross sections for the 98° dihedral corner reflector using strictly physical optics for the double reflected field (A = B = 5.6088 λ, vertical polarization, f = 9.4 GHz).

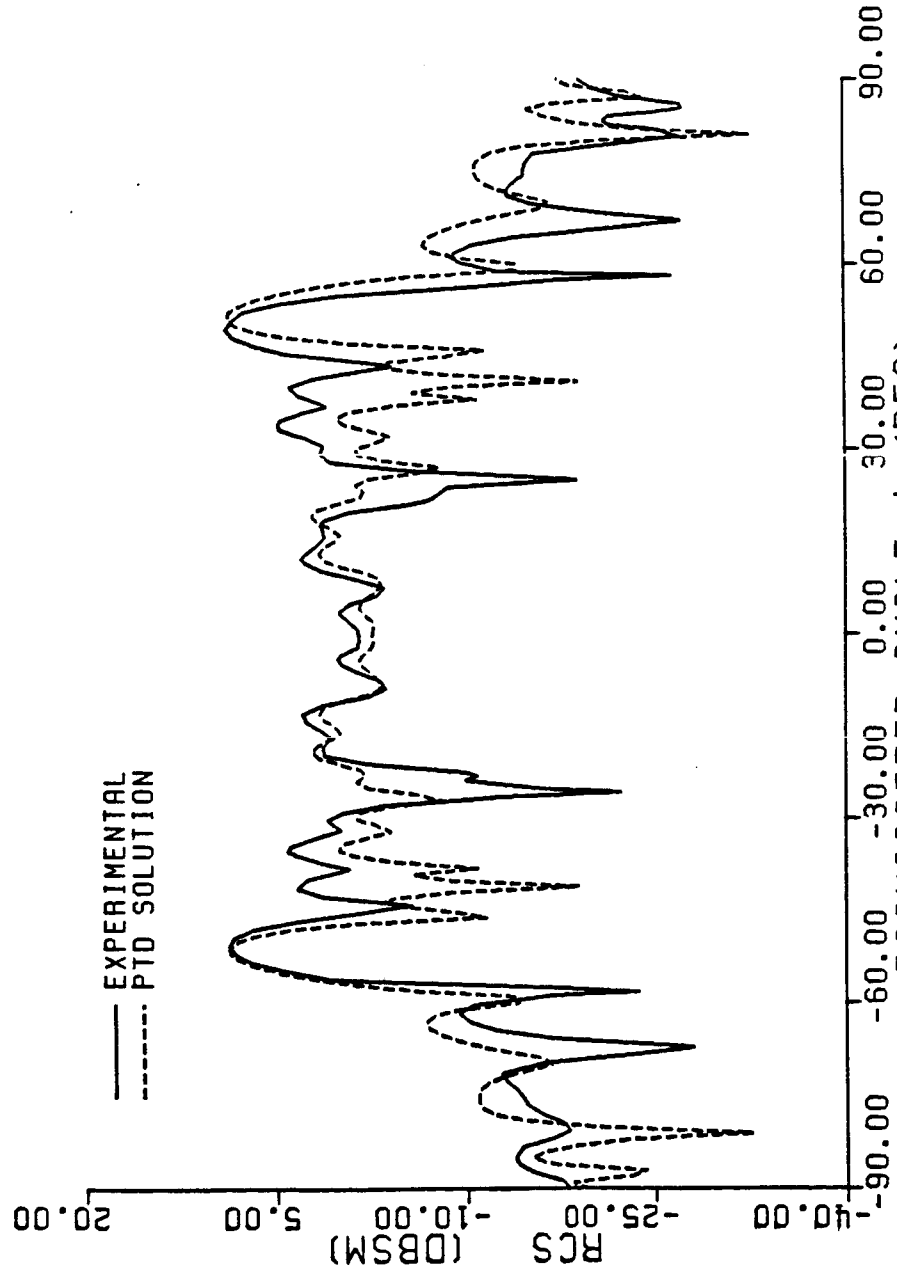

Fig. 7-15. Experimental and physical theory of diffraction cross sections for the 77° dihedral corner reflector using strictly physical optics for the double reflected field (A = B = 5.6088 λ, vertical polarization, f = 9.4 GHz).

is intended for use in the forward region only, where the double reflections are dominant, the analysis on the back side allows the method of GTD and PTD to be evaluated for the exterior corners. Exterior corners will exist on more complex structures such as ships, aircraft or other objects.

Although experimental results were not available for the back regions of the dihedral corner reflector, the geometrical and physical theories can be compared against each other in Figs. 7-16, 7-17 and 7-18 for the three dihedrals of interest. These figures show that the geometrical theory and the physical theory are nearly identical for the back side of the dihedral corner reflector. The theories would be expected to provide nearly equivalent results for general scattering from arbitrary exterior corners.

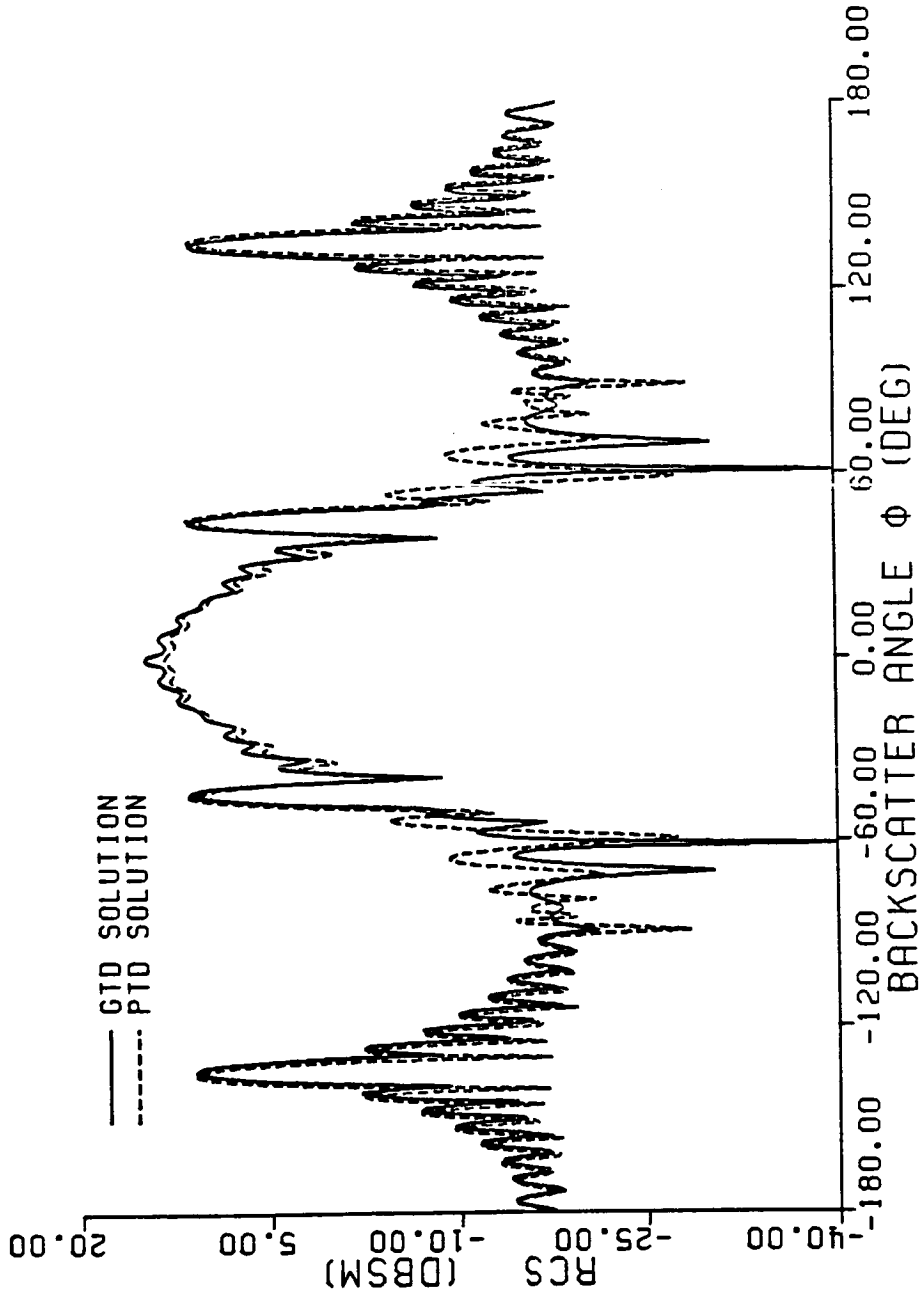

Fig. 7-16. Comparison of physical and geometrical cross sections for the 90° dihedral corner reflector (A = B = 5.6088 λ, vertical polarization, f = 9.4 GHz).

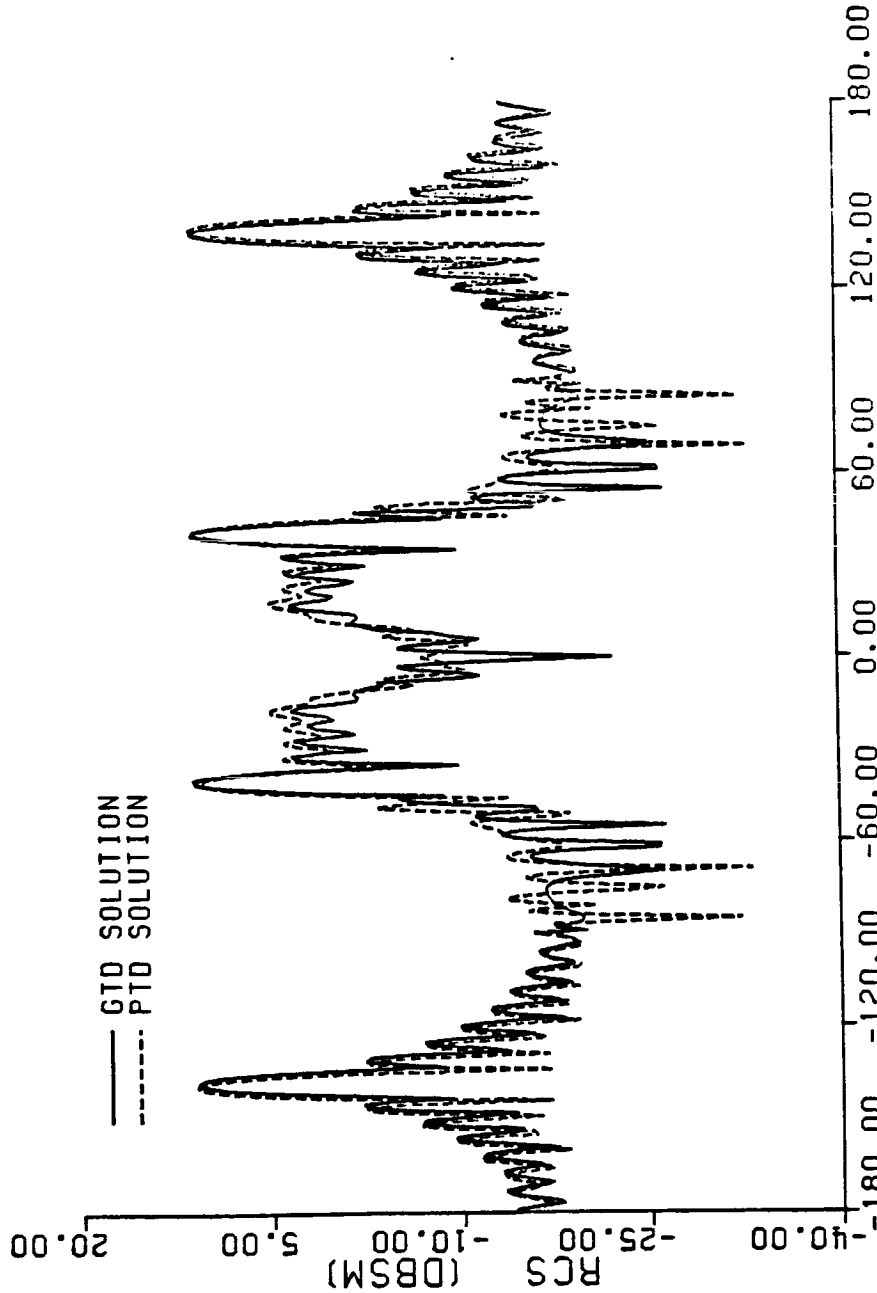

Fig. 7-17. Comparison of physical and geometrical cross sections for the 98° dihedral corner reflector (A = B = 5.6088 λ, vertical polarization, f = 9.4 GHz).

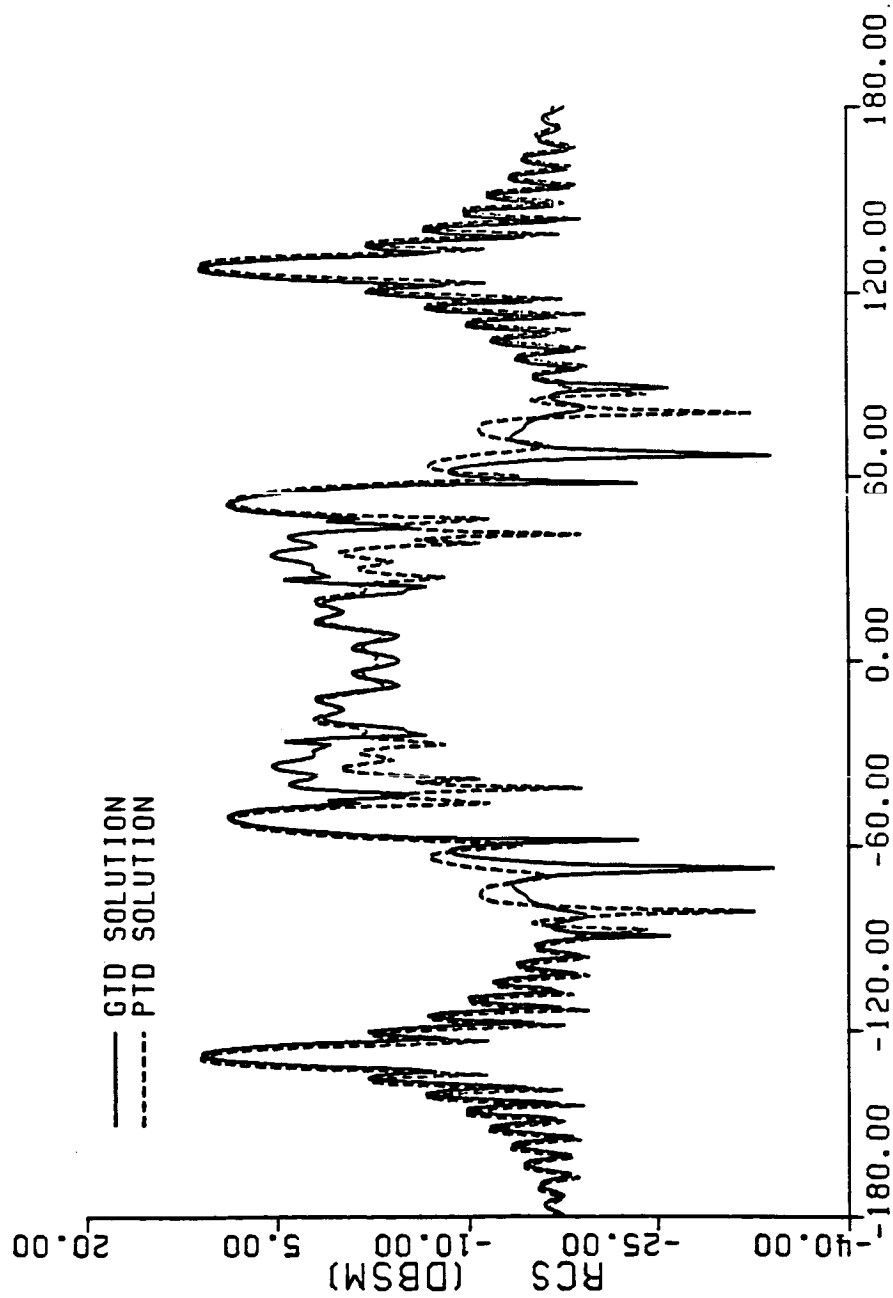

Fig. 7-18. Comparison of physical and geometrical cross sections for the 77° dihedral corner reflector (A = B = 5.6088 λ, vertical polarization, f = 9.4 GHz).

CHAPTER 8

CONCLUSION

The combination of Geometrical Optics (GO) and the Geometrical Theory of Diffraction (GTD) and the combination of Physical Optics (PO) and the Physical Theory of Diffraction (PTD) have been used to predict the radar cross section of a dihedral corner reflector, and the analytical results were shown to agree quite well with experimental data.

The geometrical theory and the physical theory share certain advantages over other analytical techniques, such as the Moment Method, in that both theories provide insight into the mechanisms of reflection and diffraction. They identify specific points or regions on a conducting body which contribute to the total radar cross section at a particular aspect. In this respect, they can give a better understanding of electromagnetic scattering from conducting surfaces and edges.

Upon examining the comparison of the theories with the experimental results for the dihedral corner reflector, the combination of geometrical optics with the geometrical theory of diffraction and the combination of physical optics with the physical theory of diffraction would be expected to provide nearly the same degree of accuracy over a considerable range of aspect angles. The geometrical theory does, however, seem to have some advantage in predicting the fine details of the dihedral cross section pattern especially near the minor lobes of a given pattern. The physical theory does not predict the minor lobes as well.

Considering only the geometrical optics and physical optics theories, and hence neglecting edge diffraction, the geometrical optics theory alone is unable to provide a reasonable first order approximation to the cross section pattern, while the physical optics theory alone may be satisfactorily accurate. In the geometrical theory, the diffraction mechanisms are mandatory, at least for targets formed of planar surfaces, to obtain satisfactory results. In the physical theory, the diffraction mechanisms tend to be required only to add refinements to the cross section pattern.

When applied to targets formed of planar surfaces, the geometrical theory contains many discontinuities in the reflection and diffraction terms which must be carefully considered to ensure continuity of the total field. Angles and distances used to find diffraction coefficients must be accurately obtained for an observation point lying in the far field. In particular, the conventional "far-field" approximation cannot be used in all except the least complex geometries, such as the flat plate. For a planar reflecting surface, the diffracted fields become infinite as the aspect direction nears the normal to the flat surface. The sum of the diffracted fields however will be finite as normal incidence is approached (as is shown in Appendix A), provided that two mutually parallel edges exist which are perpendicular to the plane of observation. If two mutually parallel edges do not exist (as in an arbitrary polygonal shape), the shape must be subdivided into rectangular strips as an approximation. In addition, if two mutually parallel edges do not exist because the view of one of the edges is obstructed by the presence of another object in the aspect

line-of-sight, then an edge diffraction should be imposed at the obstruction shadow boundary to ensure continuity in the total field near normal incidence. When considering third order (or higher) reflection/diffraction mechanisms, it has been shown that symmetrically reciprocal diffraction terms must be included twice in the total cross section to achieve a continuous cross section pattern.

When applied to targets formed of planar surfaces, the physical theory contains few discontinuities and can be used with the conventional "far field" approximations commonly utilized in electromagnetic theory. Indeed if the far field approximations are used, the incident field will be a plane wave and the surface and line integrations associated with physical optics and the physical theory of diffraction can be performed in closed form provided the object is composed solely of flat surface bounded by straight edges. To allow this closed form integration solution for multiple reflections, only the last reflection should be performed using physical optics induced currents while all preceding reflections should be performed geometrically in terms of images to preserve the planar nature of the incident field. This approximate method was found to be acceptably accurate for the obtuse and right dihedral corner reflectors, but was inadequate for the acute dihedral corner reflector. The solution for the acute dihedral corner reflector, using strictly physical optics for all the reflections associated with the double reflected field, is tractable, but for other more general geometries the solution is not as readily obtained. This alternate method does provide an improvement in accuracy, but it is not deemed appropriate for a general method for

analyzing backscattered fields from complex targets formed of flat surfaces. A comparison of the current distributions on the dihedral plates, as obtained by these two methods, has been included. When considering higher order diffractions, several authors have debated on the method of application of the physical theory of diffraction when compared with more exact analytical solutions.

The techniques developed to analyze the scattering from a dihedral corner reflector in the principle azimuthal plane should be extended to include oblique incidence directions. Some GTD approaches which might prove successful are using equivalent currents, subdividing a target into rectangular segments, utilizing the semi-heuristic corner diffraction coefficient, or using Michaeli's generalized diffraction coefficients. Some PTD approaches which could be utilized include the equivalent currents method and Mitzner's incremental length diffraction coefficients.

Other corner reflectors of interest for further study include the triangular and square corner reflectors, each of which is composed of three flat plates. Also, in the past years, enthusiasm has developed in studying objects which are covered with dielectric or lossy materials. These are just a few of the topics open for study in electromagnetic scattering and each individual subject will surely open even newer domains of inquiry.

REFERENCES

[1] J. B. Keller. "Geometrical theory of diffraction", J. Opt. Soc. Amer., vol. 52, pp. 116-130, Feb. 1962.

[2] R. G. Kouyoumjian, and P. H. Pathak, "A uniform geometrical theory of diffraction for an edge in a perfectly conducting surface", Proc. IEEE, vol. 62, no. 11, pp. 1448-1461, Nov. 1974.

[3] P. H. Pathak and R. G. Kouyoumjian, "An analysis of the radiation from apertures in curved surfaces by the geometrical theory of diffraction", Proc. IEEE, vol. 62, no. 11, pp. 1438-1461, Nov. 1974.

[4] C. E. Ryan and L. Peters, "Evaluation of edge-diffracted fields including equivalent currents for the caustic regions", IEEE Trans. Ant. Prop., vol. AP-17, pp. 292-299, May 1969.

[5] E. F. Knott and T. B. A. Senior, "Equivalent currents for a ring discontinuity", IEEE Trans. Ant. Prop., vol. AP-21, pp. 693-695, Sept. 1973.

[6] G. A. Deschamps, "Ray techniques in electromagnetics", Proc. IEEE, vol. 60, no. 9, pp. 1022-1035, Sept. 1972.

[7] S. W. Lee, "Electromagnetic reflection from a conducting surface: Geometrical optics solution", IEEE Trans. Ant. Prop., vol. AP-23, no. 2, pp. 184-191, March 1975.

[8] C. A. Balanis, Antenna Theory: Analysis and Design, New York: Harper and Row, pp. 65-67, 118, 307-316, 502-522, 1982.

[9] A. Michaeli, "Equivalent edge currents for arbitrary aspects of observation", IEEE Trans. Ant. Prop., vol. AP-32, no. 3, pp. 252-258, March 1984.

[10] A. Michaeli, "Correction to 'Equivalent edge currents for arbitrary aspects of observation'", IEEE Trans. Ant. Prop., vol. AP-33, no. 2, p. 227, Feb. 1985.

[11] P. Y. Ufimtsev, "Method of edge waves in the physical theory of diffraction", 1962, translated by U.S. Air Force Foreign Technology Division, Wright-Patterson AFB, Ohio, Sept. 1971.

[12] P. I. Ufimtsev, "Approximate computation of the diffraction of plane electromagnetic waves at certain metal bodies", Sov. Phy.-Tech. Phys., pp. 1708-1718, 1957.

[13] P. I. Ufimtsev, "Secondary diffraction of electromagnetic waves by a strip", Sov. Phys.-Tech. Phys., vol. 3, pp. 535-548, 1958.

[14] K. M. Mitzner, "High frequency bistatic scattering from a polygonal plate", presented at the 1973 URSI Meet., Boulder, CO, Aug. 21-24, 1973.

[15] R. F. Harrington, Time-Harmonic Electromagnetic Fields, New York: McGraw-Hill, pp. 127-128, 1961.

[16] H. B. Tran, T. J. Kim, "Monostatic and bistatic radar cross section analysis", High Frequency Electromagnetic Scattering Theory, vol. I, 1982.

[17] R. A. Ross, "Radar cross section of rectangular flat plates as a function of aspect angle", IEEE Trans. Ant. Prop., vol. AP-14, no. 3, pp. 329-335, May 1966.

[18] E. F. Knott, "RCS reduction of dihedral corners", IEEE Trans. Ant. Prop., vol. AP-25, no. 3, pp. 406-409, May 1977.

[19] M. A. Plonus, "Radar cross section of curved plates using geometrical and physical diffraction techniques", IEEE Trans. Ant. Prop., vol. AP-26, no. 3, pp. 488-493, May 1978.

[20] C. L. Yu and J. Huang, "Air target analytical model", Internal Report, Naval Weapons Center, China Lake, CA.

[21] F. A. Sikta, W. D. Burnside, T. Chu, L. Peters, "First-order equivalent current and corner diffraction scattering from flat plate structures", IEEE Trans. Ant. Prop., vol. AP-31, no. 4, pp. 584-589, July 1983.

[22] A. Michaeli, "Comments on 'First-order equivalent current and corner diffraction scattering from flat plate structures'", IEEE Trans. Ant. Prop., vol. AP-32, no. 9, pp. 1011-1012, Sept. 1984.

[23] F. A. Sikta, "UTD analysis of electromagnetic scattering by flat plate structures", Ph.D. dissertation, Ohio State University, 1981.

[24] A. Michaeli, "A closed form physical theory of diffraction solution for electromagnetic scattering by strips and 90° dihedrals", Radio Science, vol. 19, no. 2, pp. 609-616, March-April 1984.

[25] E. F. Knott, "A progression of high-frequency RCS prediction techniques", Proc. IEEE., vol. 73, no. 2, pp.

252-264, Feb. 1985.

[26] T. B. A. Senior and P. L. E. Uslenghi, "Comparison between Keller's and Ufimtsev's theories for the strip", IEEE Trans. Ant. Prop., vol. AP-19, no. 4, pp. 557-558, July 1971.

[27] E. F. Knott and T. B. A. Senior, "Comparison of three high-frequency diffraction techniques", Proc. IEEE, vol. 62, no. 11, pp. 1468-1474, Nov. 1974.

[28] P. Y. Ufimtsev, "Comments on 'Comparison of three high-frequency diffraction techniques'", Proc. IEEE., vol. 63, no. 12, pp. 1734-1737, Dec. 1975.

[29] E. F. Knott, "The relationship between Mitzner's ILDC and Michaeli's equivalent currents", IEEE Trans. Ant. Prop., vol. AP-33, no. 1, pp. 112-114, Jan. 1985.

[30] J. W. Crispin, Jr., and K. M. Siegel, Methods of Radar Cross-Section Analysis, New York: Academic Press, pp. 237-280, 1968.

[31] G. T. Ruck, Radar Cross Section Handbook, New York: Plenum Press, pp. 588-611, 1970.

[32] E. F. Knott, J. F. Shaeffer, and M. T. Tuley, Radar Cross Section, Dedham, MA: Artech House, pp. 174-196, 1985.

[33] J. R. Riley, "Radar cross section of insects", Proc. IEEE., vol. 73, no. 2, pp. 228-232, Feb. 1985.

[34] K. M. Siegel, "Far field scattering from bodies of revolution", Appl. Sci. Res. sec. B, vol. 7, p. 315, 1958.

[35] T. B. A. Senior and P. L. E. Uslenghi, "Experimental detection of the edge-diffraction cone", Proc. IEEE, vol. 60, no. 11, p. 1448, Nov. 1972.

[36] J. Boersma, "Computation of Fresnel Integrals", J. Math. Comp., vol. 14, p. 380, 1960.

[37] Diffraction Coefficient Computer Program, Ohio State University ElectroScience Laboratory, G. 9, pp. 591-594.

[38] R. F. Millar, "An approximate theory of the diffraction of an electromagnetic wave by an aperture in a plane screen", IEE Monograph, no. 152R, Oct. 1955.

[39] R. F. Millar, "The diffraction of an electromagnetic wave by a circular aperture", IEE Monograph, no. 196R, Sept. 1956.

[40] R. F. Millar, "The diffraction of an electromagnetic wave by a large aperture", IEE Monograph, no. 213R, Dec. 1956.

[41] R. T. Brown, "Treatment of singularities in the physical theory of diffraction", IEEE Trans. Ant. Prop., vol. AP-32, no. 6, pp. 640-641, June 1984.

APPENDIX A

CONTINUITY OF FLAT SURFACE BACKSCATTER CROSS SECTION NEAR NORMAL INCIDENCE USING THE GEOMETRICAL THEORY OF DIFFRACTION

APPENDIX A

CONTINUITY OF FLAT SURFACE BACKSCATTER CROSS SECTION NEAR NORMAL INCIDENCE USING THE GEOMETRICAL THEORY OF DIFFRACTION

The diffracted fields from a conducting edge become infinite as one approaches normal incidence to one of the flat surfaces that make up the edge whenever Keller's diffraction coefficients are employed. Ross [17] has shown, however, that the total diffracted field by two edges in a flat plate are continuous, even though each diffraction individually is discontinuous. In this appendix, the fields are shown to be continuous for a flat surface of arbitrary edge wedge angle less then 270°, provided the two edges are parallel.

The geometry of interest is shown in Fig. A-1. Two edges of arbitrary edge parameters n_1 and n_2 diffract an incident wave from the direction $\phi = \Psi_1 = \pi - \Psi_2$. The incident field can be written as

$$E^i = E_0 e^{+jk(x\cos\Psi_1 + y\sin\Psi_1)} \tag{A-1}$$

where the polarization is intentionally unspecified and can be either of the two principle polarizations. A general polarization can always be decomposed into components of these two polarizations. The plate width is w.

The diffracted field from edge 1, given either soft or hard polarization of the incident field is

$$E^{d_1}_{s,h}(s) = E^i(Q_1)\, D_{s,h}(\Psi_1, \Psi_1, n_1)\, \frac{e^{-jks_1}}{\sqrt{s_1}} \tag{A-2}$$

$$E^{d_2}_{s,h}(s) = E^i(Q_2)\, D_{s,h}(\Psi_2, \Psi_2, n_2)\, \frac{e^{-jks_2}}{\sqrt{s_2}} \tag{A-3}$$

When using far field techniques

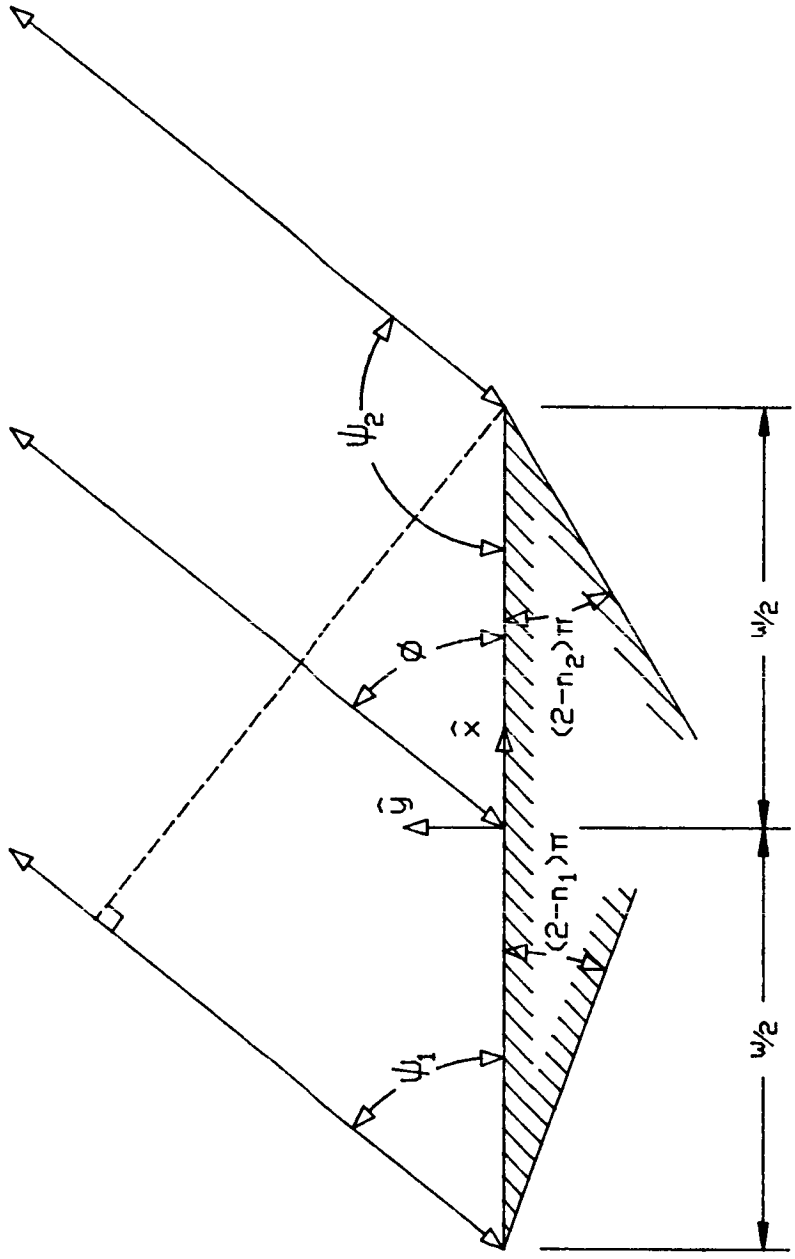

Fig. A-1. A flat conducting surface with parallel edges of arbitrary angles.

$$E^i(Q_1) \cong E_0 e^{-jk\frac{w}{2}\cos\psi_1} \tag{A-4}$$

$$E^i(Q_2) \cong E_0 e^{+jk\frac{w}{2}\cos\psi_1} \tag{A-5}$$

$$\frac{e^{-jks_1}}{\sqrt{s_1}} \cong \frac{e^{-jk(s+\frac{w}{2}\cos\psi_1)}}{\sqrt{s}} \tag{A-6}$$

$$\frac{e^{-jks_2}}{\sqrt{s_2}} \cong \frac{e^{-jk(s+\frac{w}{2}\cos\psi_1)}}{\sqrt{s}} \tag{A-7}$$

The total diffracted field is

$$E_{s,h}(s) = E^{d_1}_{s,h}(s) + E^{d_2}_{s,h}(s) \tag{A-8}$$

$$= \left\{E_0\frac{e^{-jks}}{\sqrt{s}}\right\}\left[D_{s,h}(\psi_1,\psi_1,n_1)e^{-jkw\cos\psi_1} + D_{s,h}(\psi_2,\psi_2,n_2)e^{+jkw\cos\psi_1}\right]$$

where

$$D_{s,h}(\psi,\psi,n) = \frac{e^{-j\pi/4}\sin\frac{\pi}{n}}{n\sqrt{2\pi k}}\left[\frac{1}{\cos(\frac{\pi}{n})-1} \mp \frac{1}{\cos(\frac{\pi}{n})-\cos(\frac{2\psi}{n})}\right] \tag{A-9}$$

The difficulties occur when $\psi = \frac{\pi}{2}$ (normal incidence) in both diffraction coefficients. Other discontinuities can occur, for instance at normal incidence to the second surface bounded by the edge, but each diffraction discontinuity must be compensated by an opposing diffraction on the shared surface.

The total field can be expressed as

$$E_{s,h}(s) = \left\{E_0\frac{e^{-jks}}{\sqrt{s}}\right\}\left[\frac{e^{-j\pi/4}}{\sqrt{2\pi k}}\right]\left[D_a \mp D_b\right] \tag{A-10}$$

where the upper sign is chosen for soft polarization and the lower sign is chosen for hard polarization, and

$$D_a = \frac{\frac{1}{n_1}\sin\frac{\pi}{n_1}}{\cos(\frac{\pi}{n_1})-1} e^{-jkw\cos\phi} + \frac{\frac{1}{n_2}\sin\frac{\pi}{n_2}}{\cos(\frac{\pi}{n_2})-1} e^{+jkw\cos\phi} \qquad \text{(A-11)}$$

$$D_b = \frac{\frac{1}{n_1}\sin\frac{\pi}{n_1}\ (e^{-jkw\cos\phi})}{\cos(\frac{\pi}{n_1})-\cos(\frac{2\phi}{n_1})} + \frac{\frac{1}{n_2}\sin\frac{\pi}{n_2}\ (e^{+jkw\cos\phi})}{\cos(\frac{\pi}{n_2})-\cos(\frac{2\pi-2\phi}{n_2})} \qquad \text{(A-12)}$$

Adding over a common denominator, $D_b = f_1/f_2$ where

$$f_1 = \frac{1}{n_1}\sin(\frac{\pi}{n_1})\left[\cos(\frac{\pi}{n_2})-\cos(\frac{2\pi-2\phi}{n_2})\right]e^{-jkw\cos\phi} \qquad \text{(A-13)}$$

$$+ \frac{1}{n_2}\sin(\frac{\pi}{n_2})\left[\cos(\frac{\pi}{n_2})-\cos(\frac{2\phi}{n_1})\right]e^{jkw\cos\phi}$$

$$f_2 = \left[\cos(\frac{\pi}{n_1})-\cos(\frac{2\phi}{n_1})\right]\left[\cos(\frac{\pi}{n_2})-\cos(\frac{2\pi-2\phi}{n_2})\right] \qquad \text{(A 14)}$$

but

$$f_1 = f_2 = 0 \qquad \text{at} \quad \phi = \pi/2.$$

Therefore

$$D_b = \frac{f_1}{f_2} = \frac{0}{0} \qquad \text{and } D_b \text{ is indeterminate at } \phi = \frac{\pi}{2}$$

Using L'Hopital's Rule for indeterminate ratios,

$$\left.\frac{df_1}{d\phi}\right|_{\phi=\frac{\pi}{2}} = 0 \qquad \left.\frac{df_2}{d\phi}\right|_{\phi=\frac{\pi}{2}} = 0 \qquad \text{(A-15)}$$

$$\left.\frac{d^2f_1}{d\phi^2}\right|_{\phi=\frac{\pi}{2}} = (-j8ka)(\frac{1}{n_1}\sin\frac{\pi}{n_1})(\frac{1}{n_2}\sin\frac{\pi}{n_2}) \qquad \text{(A-16)}$$

$$\left.\frac{d^2f_2}{d\phi^2}\right|_{\phi=\frac{\pi}{2}} = -8(\frac{1}{n_1}\sin\frac{\pi}{n_1})(\frac{1}{n_2}\sin\frac{\pi}{n_2}) \qquad \text{(A-17)}$$

So that

$$\left.D_b\right|_{\phi=\frac{\pi}{2}} = \left.\frac{f_1''}{f_2''}\right|_{\phi=\frac{\pi}{2}} = jka \qquad \text{(A-18)}$$

The result then, for the diffracted fields from a flat surface at

normal incidence, for the soft or hard polarization is

$$E_{s,h}(s)\Big|_{\phi=\frac{\pi}{2}} = E_0 \frac{e^{-jks}}{\sqrt{s}} \left[\frac{e^{-j\pi/4}}{\sqrt{2\pi k}}\right] \left[\mathcal{D}_a \mp \mathcal{D}_b\right] \qquad \text{(A-19)}$$

where

$\mathcal{D}_a$ is given by (A-11)

$\mathcal{D}_b$ is given by (A-18)

As long as the edge parameters are in the range $2 \geq n > \frac{1}{2}$, that is the edge angles are $0° < WA < 270°$, the parameters $\mathcal{D}_a$ and $\mathcal{D}_b$ will be continuous everywhere and in particular near $\phi = \frac{\pi}{2}$.

APPENDIX B

QUADRUPLE INTEGRATION TECHNIQUE TO DETERMINE THE PHYSICAL OPTICS DOUBLE REFLECTED FIELDS

APPENDIX B

QUADRUPLE INTEGRATION TECHNIQUE TO DETERMINE THE PHYSICAL OPTICS DOUBLE REFLECTED FIELDS

If the theory of physical optics is used to determine the double reflected field from a dihedral corner reflector, a quadruple integration arises which must be evaluated numerically. This procedure is more difficult and more costly to implement than the approximate technique developed by Knott [18] but it yields more accurate results when compared with experiment. This Appendix derives the quadruple integral expression required to find the backscattered fields for the vertically polarized case.

The dihedral geometry is shown in Fig. B-1 where A is the width and B is the height of both dihedral plates. The interior angle of the dihedral is 2α and the direction of the incidence field is ϕ. Two normal vectors $\hat{n}_s$ and $\hat{n}_t$ are defined perpendicular to the reflecting surfaces. The procedure to find the double reflected field components which reflect first from Plate I and then from Plate II begins by using the physical optics approximation of the induced currents on Plate I. The reflected field can be found everywhere and in particular on the surface of Plate II where a surface current density is induced. The field radiated from Plate II is the desired double reflected field.

For the geometry shown in Fig. B-1, let the incident field be

$$\bar{E}^i = \hat{a}_z E_0 e^{jk(x\cos\phi+y\sin\phi)} \tag{B-1}$$

$$\bar{H}^i = (\hat{a}_y\cos\phi-\hat{a}_x\sin\phi)\, H_0 e^{jk(x\cos\phi+y\sin\phi)} \tag{B-2}$$

$$\text{where } E_0 = \eta H_0 \tag{B-3}$$

The unit normal vectors are

$$\hat{n}_s = \hat{a}_x\sin\alpha + \hat{a}_y\cos\alpha \tag{B-4}$$

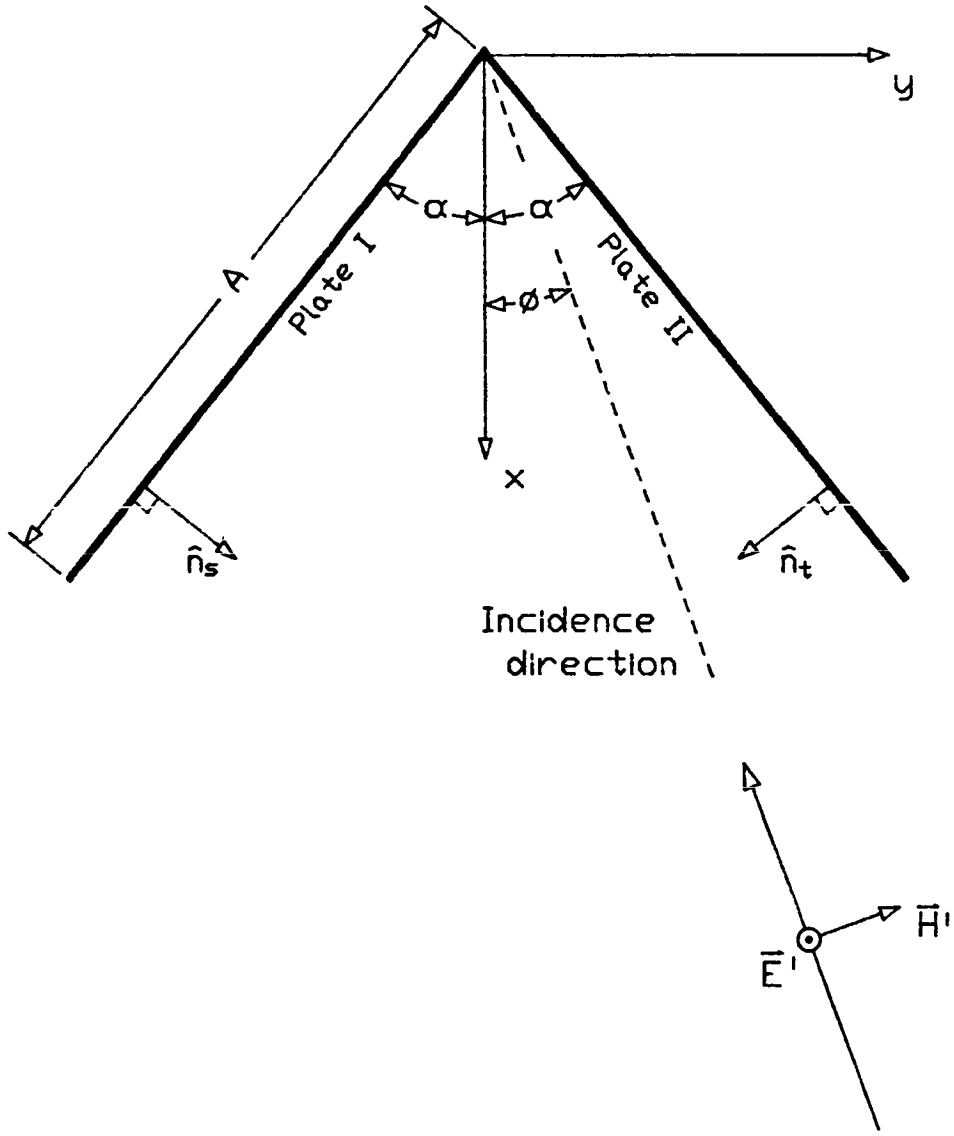

Fig. B-1. Double-reflected physical optics field using physical optics theory for both the first and second reflections.

$$\hat{n}_t = \hat{a}_x \sin\alpha - \hat{a}_y \cos\alpha \tag{B-5}$$

On plate I: $y = -x\tan\alpha$ (B-6)

On plate II: $y = x\tan\alpha$ (B-7)

The incident field at plate I is

$$\bar{H}^i\Big|_I = (\hat{a}_y \cos\phi - \hat{a}_x \sin\phi)\, H_0 e^{jk(x\cos\phi - x\tan\alpha\sin\phi)} \tag{B-8}$$

By the physical optics approximation

$$\bar{J}_s\Big|_I = 2\hat{n}_s \times \bar{H}^i\Big|_I = 2(\hat{a}_x\sin\alpha + \hat{a}_y\cos\alpha) \times \bar{H}^i\Big|_I$$

$$= 2H_0 \hat{a}_z \sin(\phi+\alpha) e^{jkx(\cos\phi - \tan\alpha\sin\phi)} \tag{B-9}$$

Then the vector potential $\bar{A}_I$ is

$$\bar{A}_I = \frac{\mu}{4\pi} \int\int \bar{J}_s(x',y',z')\Big|_I \frac{e^{-jkR}}{R}\, dA_I' \tag{B-10}$$

$$\text{where } dA_I' = \frac{dx'dz'}{\cos\alpha} \tag{B-11}$$

$$\bar{A}_I = \frac{\mu}{2\pi} H_0 \frac{\sin(\phi+\alpha)}{\cos\alpha} \times$$

$$\int_0^B \int_0^{A\cos\alpha} e^{jkx'(\cos\phi - \tan\alpha\sin\alpha)} \frac{e^{-jkR}}{R}\, dx'dz' \tag{B-12}$$

and $$R^2 = (x-x')^2 + (y+x'\tan\alpha)^2 + (z-z')^2$$

The reflected field from plate I is

$$\bar{H}_I^s = \frac{1}{\mu} \nabla \times \bar{A}_I = \frac{1}{\mu}\left[\hat{a}_x \frac{\partial A_z}{\partial y} - \hat{a}_y \frac{\partial A_z}{\partial x} \right] \tag{B-13}$$

$$\bar{H}_I^s = \frac{H_0}{2\pi} \frac{\sin(\phi+\alpha)}{\cos\alpha} \int_0^B \int_0^{A\cos\alpha} \bar{K}_1(x,y,z,x',y',z')\, dx'dz' \tag{B-14}$$

where

$$\bar{K}_I(x,y,z,x',y',z') = e^{jkx'(\cos\phi - \tan\alpha\sin\phi)} \frac{e^{-jkR}}{R} \times$$

$$\left(\frac{1}{R} + jk\right)\left[\hat{a}_y\left[\frac{x-x'}{R}\right] + \hat{a}_x\left[\frac{y+x'\tan\alpha}{R}\right]\right] \qquad \text{(B-15)}$$

On Plate II, therefore, the current density is

$$\bar{J}_s\Big|_{II} = 2\hat{n}_s \times \bar{H}_1^s\Big|_{II} = 2\left[\hat{a}_x\sin\alpha - \hat{a}_y\cos\alpha\right] \times \bar{H}_1^s\Big|_{II} \qquad \text{(B-16)}$$

$$= \hat{a}_z \frac{H_0}{\pi} \frac{\sin(\phi+\alpha)}{\cos\alpha} \int_0^B\int_0^{A\cos\alpha} \left[\hat{a}_x\sin\alpha - \hat{a}_y\cos\alpha\right] \times$$

$$\bar{K}_1(x,y,z,x',y',z')\, dx'dz' \qquad \text{(B-17)}$$

$$\triangleq J_{sz}^{PO}$$

The vector potential $\bar{A}_{II}$ due to current density $\bar{J}_s\Big|_{II}$ is

$$\bar{A}_{II} = \frac{\mu}{4\pi}\int\int \bar{J}_s(x',y',z')\Big|_{II} \frac{e^{-jkR_1}}{R_1}\, dA_{II}' \qquad \text{(B-18)}$$

where $$R_1 \cong r - \frac{x'\cos(\alpha-\phi)}{\cos\alpha} \qquad \text{(B-19)}$$

and $$dA_{II}' = \frac{dx'dz'}{\cos\alpha} \qquad \text{(B-20)}$$

The desired double reflected field, found using strictly the physical optics approximation is

$$\bar{E}^s = -j\omega\bar{A}_{II} =$$

$$= \left[-j\frac{E_0}{2\pi\lambda}\frac{\sin(\phi+\alpha)}{\cos^2\alpha}\hat{a}_z\right] \times \qquad \text{(B-21)}$$

$$\left[\int_0^B\int_0^{A\cos\alpha}\int_0^B\int_0^{A\cos\alpha} K(x',z',x'',z'')dx''dz''dx'dz'\right]\frac{e^{-jkr}}{r}$$

where $K(x',z',x'',z'') = \left[\frac{2x'}{R'}\sin\alpha\right]\left[\frac{1}{R'} + jk\right] \times$

$$\left[e^{jkx''\frac{\cos(\alpha+\phi)}{\cos\alpha}}\right]\left[e^{jkx'\frac{\cos(\alpha-\phi)}{\cos\alpha}}\right]\frac{e^{-jkR'}}{R'} \qquad \text{(B-22)}$$

and $$(R')^2 = (x'-x'')^2 + (x'+x'')^2\tan^2\alpha + (z'-z'')^2 \qquad \text{(B-23)}$$